



Universiteit
Leiden
The Netherlands

Chemokines in Ewing sarcoma

Sand, L.G.L.

Citation

Sand, L. G. L. (2016, October 27). *Chemokines in Ewing sarcoma*. Retrieved from <https://hdl.handle.net/1887/43794>

Version: Not Applicable (or Unknown)

License: [Licence agreement concerning inclusion of doctoral thesis in the Institutional Repository of the University of Leiden](#)

Downloaded from: <https://hdl.handle.net/1887/43794>

Note: To cite this publication please use the final published version (if applicable).

Cover Page



Universiteit Leiden

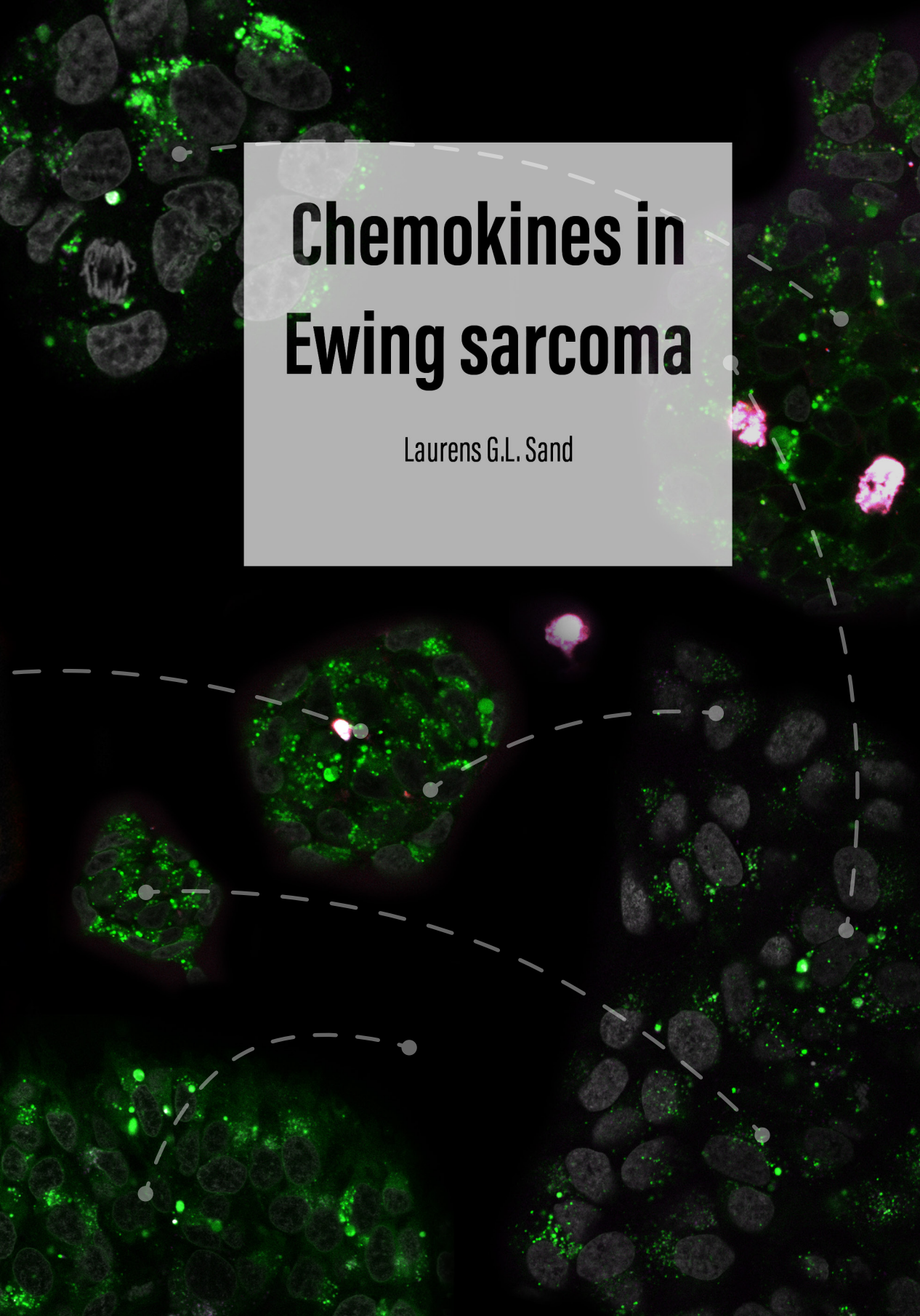


The handle <http://hdl.handle.net/1887/43794> holds various files of this Leiden University dissertation

Author: Sand, Laurens

Title: Chemokines in Ewing sarcoma

Issue Date: 2016-10-27

The background of the cover is a fluorescence microscopy image of Ewing sarcoma cells. The cells are stained with a green fluorescent marker, likely a chemokine receptor, and a red fluorescent marker, likely a nuclear stain like DAPI. The cells are arranged in a cluster, and the green signal is distributed throughout the cytoplasm and nucleus. The red signal highlights the nuclei. A dashed white line with circular markers at the end of each segment is overlaid on the image, tracing a path through the cells. The title and author's name are centered in a white rectangular box.

Chemokines in Ewing sarcoma

Laurens G.L. Sand

Chemokines in Ewing sarcoma

Cover design by: L.G.L. Sand & Proefschriftmaken.nl
Layout by: L.G.L. Sand
Printed by: Proefschriftmaken.nl || Uitgeverij BOXPress
ISBN: 978-94-6295-499-1

The studies described in this thesis were financially supported by the National organization for Scientific Research (NWO) grant NWO-TOP GO 854.10.012

Publication of this thesis was financially supported by the Department of Pathology, Leiden University Medical Center Leiden and Pfizer

Copyright 2016 Laurens Sand
All rights reserved. No part of this thesis may be reproduced in any form or by any means, without prior permission of the author.

Chemokines in Ewing sarcoma

Proefschrift

ter verkrijging van de graad van Doctor aan de Universiteit Leiden,
op gezag van Rector Magnificus prof.mr. C.J.J.M. Stolker,
volgens besluit van het College voor Promoties
te verdedigen op donderdag 27 oktober
klokke 13.45 uur

door

Laurens Gerard Leo Sand

geboren te Breda
in 1988

Promotor: Prof.dr. P.C.W. Hogendoorn

Copromotor: Dr. K. Szuhai

Leiden promotiecommissie: Prof. dr. H.J. Tanke
Prof. dr. O. Delattre (Institut Curie)
Prof. dr. C.A.M. Marijnen
Prof. dr. A.J. Gelderblom
Prof. dr. T. Schmidt (Leiden Institute of
Physics)

Voor mijn vriendin en familie

Contents

| | | |
|------------------|---|-----|
| Chapter 1 | General Introduction | 9 |
| Chapter 2 | Sequencing overview of Ewing sarcoma: a journey across genomic, epigenomic and transcriptomic landscapes <i>Int. J. Mol. Sci. 2015, 16(7), 16176-16215</i> | 17 |
| Chapter 3 | Expression of CCL21 in Ewing sarcoma is associated with development of metastases and a candidate target for immunotherapy. <i>Cancer Immunol. Immunother. 2016, 65(8), 995-1002</i> | 49 |
| Chapter 4 | CXCL14, CXCR7 expression and CXCR4 splice variant ratio associate with survival and metastases in Ewing sarcoma patients <i>Eur. J. Cancer 2015, 51(17), 2624-2633</i> | 63 |
| Chapter 5 | Novel splice variants of CXCR4 identified by transcriptome sequencing in Ewing sarcoma and validated in other cell lines and tissues <i>Biochem. Biophys. Res. Commun. 2015, 466(1), 89-94</i> | 83 |
| Chapter 6 | Fluorescently labeled CXCR4 targeting peptide as alternative to antibody staining in Ewing sarcoma <i>In submission</i> | 95 |
| Chapter 7 | Evaluation of CXCR4 specific endocytosis using an activatable peptide <i>In preparation</i> | 107 |
| Chapter 8 | Summary and future directions | 123 |
| | Nederlandse samenvatting | 130 |
| | Curriculum Vitae | 134 |
| | List of publications | 135 |
| | Abbreviations | 137 |

Chapter 1

General introduction

EWING SARCOMA

Ewing sarcoma (EWS) is a malignant round cell tumor occurring predominantly in bone in children and young adolescents and to a lesser extent in soft tissue and occasionally organ based [1]. EWS is the third most common primary bone sarcoma with an incidence of three per million in this patient group [2]. It is slightly more common in male than female (1.4:1) and majority of patients are Caucasians [3]. It was first recognized by Lücke in 1866 and afterwards reported by Hildebrand and Marckwald at the end of the nineteenth century [4,5].

Ewing designated new attention to the tumor, popularized it by giving it the entity 'diffuse endothelioma of bone' as a descriptive name and in detail described the morphology as little differentiated round cell tumor which was highly vascularized [6]. The use of intensive chemotherapy, radiotherapy and surgery increased the three year event free survival in patients diagnosed with a localized disease to 75.4% [7]. However, 15% to 30% of the patients have metastases at diagnosis and, together with patients with a recurrent disease, have a poor survival of about 30% [8,9].

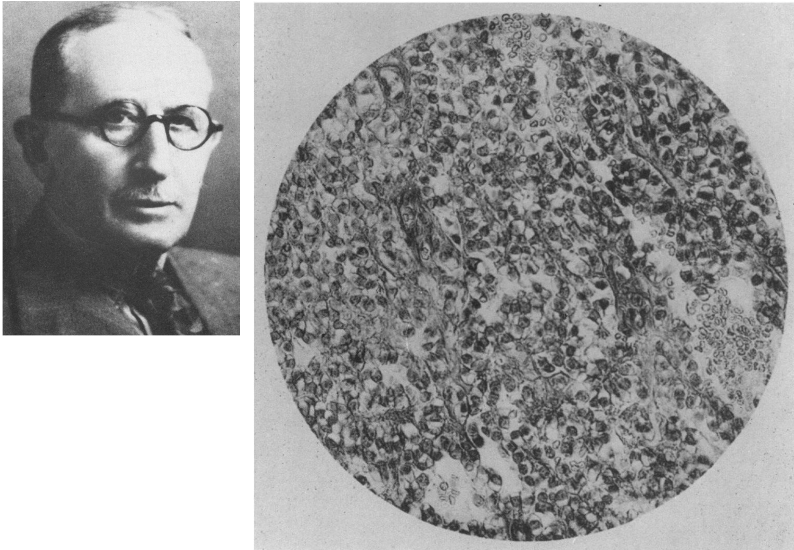


Figure 1: James Ewing and a by him published image of an Ewing sarcoma demonstrating blood sinuses lined by tumor cells, adapted from Ewing J. [6].

CLASSIFICATION OF EWING SARCOMA

Since EWS shows very little differentiation with the exception of some degree of neurogenic differentiation in some cases, the cellular origin of tumor still remains enigmatic. Based on clinical presentation, several clinical entities have been described such as peripheral primitive neuroectodermal tumor (PNET) and Askin tumor. However, in the latest WHO classification all separate clinical entities are unified to EWS characterized by its pathognomonic chromosomal translocation [1]. The translocation fuses at the 5' end the *EWSR1* gene, located on chromosome 22, with a gene of the ETS transcription factor family at the 3' end. The most common 3' end partner is, with 85%, the on chromosome 11 located gene *Friend leukemia*

virus integration site 1 (FLI1), followed by the *ETS-related gene (ERG)* on chromosome 21 with 10% [10,11]. More sporadic 3' end partners are *ETV1*, *ETV4* and *FEV* [1]. The incidentally detected *FUS-ERG* fusion gene in a EWS patient demonstrates that, like the 3' end partner gene the 5' end partner is interchangeable [12]. Gene fusion involving non-ETS gene or genes neither TET nor ETS genes with histopathological features of EWS have been recently reported involving *EWSR1-NFTAC2*, *BCOR-CCNB3* or *CIC-DUX4* genes. These entities are collectively being grouped as Ewing-like sarcoma [13-15].

TUMOR MICROENVIRONMENT OF EWING SARCOMA

The *EWSR1-ETS* fusion gene is, besides the genetic marker of EWS, also the oncogenic driver [16]. The *EWSR1*, a housekeeping gene, has an RNA binding domain on the 3' end and a transactivation domain at the 5' end with yet not well-defined functions. The 3' end of the *ETS* gene included the fusion contains a DNA binding domain and acts as a transcription factor. The chimera protein has a preferential binding to GGAA repeats modulating gene expression of nearby genes [17,18]. The fusion protein interferes with various fundamental cellular processes including expression, splicing and protein signaling resulting in a malignant, aggressive growth and highly vascularized phenotype [19-21]. Such a phenotype is often the result of an extensive interplay between the tumor cell and its microenvironment. The tumor microenvironment consists of extracellular matrix, blood vessels, stromal cells, monocytes and leukocytes [22]. The tumor microenvironment is crucial for the tumor to metastasize and for blood vessel growth (angiogenesis) [23]. Main players in facilitating the interaction within the tumor microenvironment are chemokines with at least four major features: 1) attraction of endothelial cells and pericytes leading to angiogenesis; 2) paracrine or autocrine stimulation signaling leading to tumor cell proliferation and 3) increased tumor cell migration and invasion and 4) influence of the immune response.

CHEMOKINES

Chemokines are small chemoattractive proteins, which vary from eight to ten kDa in their molecular weight. Based on the presence of four conserved cysteine residues they can be divided in subfamilies depending on their cysteine pattern as CXC, CC, CX₃C and XC chemokines [24]. The CXC subfamily can be further subclassified as ELR⁻ and ELR⁺ (glutamic acid-leucine-arginine) amino acid motif containing chemokines where ELR⁺ (CXCL1, 2, 3, 5, 6 and 8) are angiogenic and ELR⁻ chemokines (CXCL9, CXCL10 and CXCL11) are angiostatic [24,25]. Besides angiostatic, CXCL9 and CXCL10 are T-cell attractants and protein expression levels of CXCL9 and CXCL10 in EWS correlated with increased number of cytotoxic T-cells and a better patient survival [26]. Immunotherapy to stimulate the attraction of immune cells and to improve the immune response in EWS were successfully applied in *in vitro* studies providing a promising ground for novel immunotherapy approaches for EWS patients [27-29].

CXCR4 SIGNALING

Most chemokines and receptors are expressed by specific cells and are involved in some of the four major processes in the tumor microenvironment; angiogenesis, proliferation, metastasis and immune system recognition. Stromal derived factor 1 (SDF-1/CXCL12) and its receptor CXCR4 are exceptions since they are widely distributed across the body and involved

in the regulation of all four main tumor microenvironmental processes. [30,31]. Moreover, overexpression of CXCR4 receptors in tumors is frequently associated with increased metastatic propensity and poor clinical outcome [31-33]. Various downstream signaling pathways of CXCR4 mediate its diverse functions (**Figure 1**). CXCL12 binding to CXCR4 leads to activation of the receptor which then activates an associated G protein leading to the activation of the migration associated protein kinase C and cofilin pathway and the proliferation stimulating PI3K-Akt and RAS-MAPK-ERK pathways [30,34]. After ligand binding, CXCR4 is phosphorylated at the C-terminus and recruits Beta-arrestins. Depending on the type of recruited beta-arrestin, these either desensitize the G protein activation or transduce the activation signal towards RAF-MEK-ERK pathway [35]. The desensitization of CXCR4 activation is followed by internalization of the receptor leading to either recirculation or degradation [36,37]. Endocytosis and recycling of the receptor are vital for proper functioning of CXCR4 [38]. Recent reports suggest that the internalization of the receptor and its downstream signaling are connected to each other [39,40].

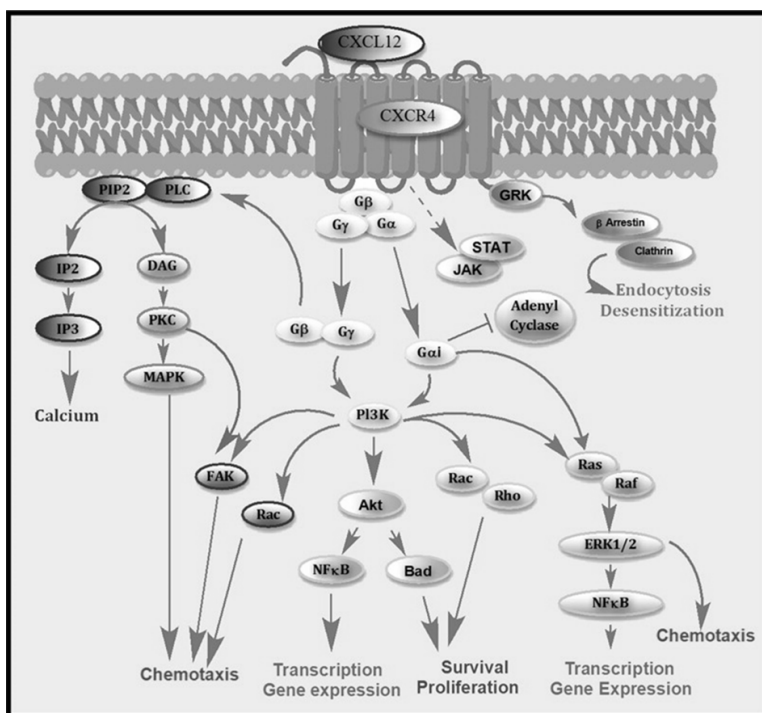


Figure 2: CXCR4 downstream signaling, adapted from Lauren E. Woodard and Sridhar Nimmagadda *et al.* [41].

WHOLE TRANSCRIPTOME ANALYSIS OF CHEMOKINES

The chemokine field is still in development and novel chemokines and chemokine receptors have recently been identified [42-44]. In addition, alternative splicing of chemokines and chemokine receptors forms novel isoforms with other or additional functions [45-48]. Whole transcriptome sequencing, next generation sequencing of the RNA, of tumors elicits the identification of novel splice variants. Whole transcriptome sequencing is an unbiased approach

since it uses adapters to sequence the complete RNA, both coding and non-coding. When analyzing the mapped paired-end novel splice variants and their sequence can be determined. In addition it can be used to quantify the splice variants expressed.

AIM OF THE STUDY AND OUTLINE OF THIS THESIS

The aim of this study was in depth investigation on the presence of chemokines and their role in the tumor microenvironment of EWS and the clinical usability of the chemokines as predictive and/or prognostic markers in EWS.

Detailed characterization of EWS and the effect of the fusion protein on the tumor cellular processes at DNA, RNA and protein level is needed to unravel the interactions with its tumor microenvironment. When this interplay is better defined it might lead to identification of new therapeutic targets and predictive and prognostic candidate markers. Recent advances in the sequencing has helped to fulfill this characterization of EWS at genome, epigenome and transcriptome level. In **Chapter 2** a comprehensive compilation/overview is given of all the reported sequencing studies in EWS. The results of these studies were put in clinical perspective by linking them with treatment efficacy of existing therapies against EWS. In addition, novel potential targeted therapies and immunotherapies were reported which were identified or strengthened by the sequencing results.

The role of chemokines in the immune microenvironment in EWS was partially studied previously by us. We extended the understanding of EWS its immune microenvironment with the role of the T-cell attracting chemokine CCL21 in EWS (**Chapter 3**). CCL21 is, besides its T-cell attracting ability, of interest since CCL21 activation-based immunotherapy is tested in a clinical trial for non-small cell lung cancer.

The highest expressed chemokine receptor in EWS found so far is CXCR4. In **Chapter 4** we focused on the role of the CXCR4 network in EWS by investigating the *in vitro* and *in vivo* expression of the *CXCR4-CXCR7 axis* genes and of the two described isoforms *CXCR4-1* and *CXCR4-2*. The obtained levels were correlated to clinical parameters in two independent cohorts.

Since the EWSR1-ETS fusion protein alters splicing, alternative splicing of CXCR4 was analyzed by whole transcriptome sequencing. This has led to identification of the 2 new CXCR4 isoforms (**Chapter 5**). Detailed characterization of the function of the two novel isoforms were performed and presented.

CXCR4 has various signaling pathways and CXCR4 localization and protein dynamics is important in regulating its activity. Earlier EWS studies demonstrated contradictory results between RNA and protein expression in metastases. Since only cell membrane located CXCR4 is able to be bound and activated by a ligand, we studied the CXCR4 cell membrane expression in EWS by using a peptide-based method (**Chapter 6**). With this method CXCR4 cell membrane expression in EWS cell lines could be determined qualitatively and quantitatively. As the receptor was internalized upon binding the peptide, we synthesized and validated *in vitro* and *in vivo* a CXCR4 endocytosis tracker based on the previous used peptide combined with a FRET (Förster resonance energy transfer) dimer, to track the internalized receptor and study the endocytosis of CXCR4 (**Chapter 7**). In the FRET dimer Cy5 and Cy3 fluorophores were connected by a disulfide bond which can be reduced intracellularly. Reduction disrupts the FRET ability of the dimer and the resulting difference in fluorescence intensity can be measured.

In **Chapter 8** the results are summarized and the future perspectives are discussed.

REFERENCES

- 1 De Alava, E., Lessnick, S. L. & Sorensen, P. H. in *WHO Classification of Tumors of Soft Tissue and Bone* (eds C.D.M. Fletcher, J.A. Bridge, P. C. W. Hogendoorn, & F. Mertens) 306-9 (IARC, 2013).
- 2 Esiashvili, N., Goodman, M. & Marcus, R. B., Jr. Changes in incidence and survival of Ewing sarcoma patients over the past 3 decades: Surveillance Epidemiology and End Results data. *J Pediatr Hematol Oncol* **30**, 425-30, (2008).
- 3 Jawad, M. U. *et al.* Ewing sarcoma demonstrates racial disparities in incidence-related and sex-related differences in outcome. *Cancer* **115**, 3526-36, (2009).
- 4 Lücke, A. Beiträge zur Geschwulstlehre. *Virchows Arch Pathol Anat Physiol Klin Med* **35**, 524-39, (1866).
- 5 Hildebrand, Z. C. Ueber das tubuläre Angiosarkom oder Endotheliom des Knochens. *Dtsch Z Chir* **31**, 262-81, (1890).
- 6 Ewing, J. Diffuse endothelioma of bone *Proc New York Path Soc* **21**, 17-24, (1921).
- 7 Le Deley, M.-C. *et al.* Impact of EWS-ETS Fusion Type on Disease Progression in Ewing's sarcoma/peripheral primitive neuroectodermal tumor: Prospective Results From the Cooperative Euro-EWING 99 Trial. *J Clin Oncol* **28**, 1982-8, (2010).
- 8 Ladenstein, R. *et al.* Primary disseminated multifocal Ewing sarcoma: results of the Euro-EWING 99 trial. *J Clin Oncol* **28**, 3284-91, (2010).
- 9 Duchman, K. R., Gao, Y. & Miller, B. J. Prognostic factors for survival in patients with Ewing's sarcoma using the surveillance, epidemiology, and end results (SEER) program database. *Cancer Epidemiol* **39**, 189-95, (2015).
- 10 van Doorninck, J. A. *et al.* Current Treatment Protocols Have Eliminated the Prognostic Advantage of Type 1 Fusions in Ewing sarcoma: A Report From the Children's Oncology Group. *J Clin Oncol* **28**, 1989-94, (2010).
- 11 Tirode, F. *et al.* Genomic Landscape of Ewing sarcoma Defines an Aggressive Subtype with Co-Association of STAG2 and TP53 Mutations. *Cancer Discov* **4**, 1342-53, (2014).
- 12 Shing, D. C. *et al.* FUS/ERG Gene Fusions in Ewing's Tumors. *Cancer Res* **63**, 4568-76, (2003).
- 13 Graham, C., Chilton-MacNeill, S., Zielenska, M. & Somers, G. R. The CIC-DUX4 fusion transcript is present in a subgroup of pediatric primitive round cell sarcomas. *Hum Pathol* **43**, 180-9, (2012).
- 14 Szuhai, K. *et al.* The NFATc2 Gene Is Involved in a Novel Cloned Translocation in a Ewing sarcoma Variant That Couples Its Function in Immunology to Oncology. *Clin Cancer Res* **15**, 2259-68, (2009).
- 15 Pierron, G. *et al.* A new subtype of bone sarcoma defined by BCOR-CCNB3 gene fusion. *Nat Genet* **44**, 461-6, (2012).
- 16 Stoll, G. *et al.* Systems biology of Ewing sarcoma: a network model of EWS-FLI1 effect on proliferation and apoptosis. *Nucleic Acids Res* **41**, 8853-71, (2013).
- 17 Guillon, N. *et al.* The Oncogenic EWS-FLI1 Protein Binds *In Vivo* GGAA Microsatellite Sequences with Potential Transcriptional Activation Function. *PLoS One* **4**, e4932, (2009).
- 18 Riggi, N. *et al.* EWS-FLI1 Utilizes Divergent Chromatin Remodeling Mechanisms to Directly Activate or Repress Enhancer Elements in Ewing sarcoma. *Cancer Cell* **26**, 668-81, (2014).
- 19 Selvanathan, S. P. *et al.* Oncogenic fusion protein EWS-FLI1 is a network hub that regulates alternative splicing. *Proc Natl Acad Sci U S A* **112**, E1307-E16, (2015).
- 20 Erkizan, H. V. *et al.* RNA helicase A activity is inhibited by oncogenic transcription factor EWS-FLI1. *Nucleic Acids Res* **43**, 1069-80, (2015).
- 21 Erkizan, H. V., Uversky, V. N. & Toretsky, J. A. Oncogenic Partnerships: EWS-FLI1 Protein Interactions Initiate Key Pathways of Ewing's sarcoma. *Clin Cancer Res* **16**, 4077-83, (2010).
- 22 Allen, M. & Louise Jones, J. Jekyll and Hyde: the role of the microenvironment on the progression of cancer. *J Pathol* **223**, 163-77, (2011).
- 23 Rousfos, E. T., Condeelis, J. S. & Patsialou, A. Chemotaxis in cancer. *Nat Rev Cancer* **11**, 573-87, (2011).
- 24 Vandercappellen, J., Van Damme, J. & Struyf, S. The role of CXC chemokines and their receptors in cancer. *Cancer Lett* **267**, 226-44, (2008).
- 25 Bizzarri, C. *et al.* ELR+ CXC chemokines and their receptors (CXC chemokine receptor 1 and CXC chemokine receptor 2) as new therapeutic targets. *Pharmacol Ther* **112**, 139-49, (2006).
- 26 Berghuis, D. *et al.* Pro-inflammatory chemokine-chemokine receptor interactions within the Ewing sarcoma microenvironment determine CD8+ T-lymphocyte infiltration and affect tumour progression. *J Pathol* **223**, 347-57, (2011).
- 27 Verhoeven, D. H. J. *et al.* NK cells recognize and lyse Ewing sarcoma cells through NKG2D and DNAM-1 receptor dependent pathways. *Mol Immunol* **45**, 3917-25, (2008).
- 28 Pahl, J. W. *et al.* Antibody-dependent cell lysis by NK cells is preserved after sarcoma-induced inhibition

- of NK cell cytotoxicity. *Cancer Immunol Immunother* **62**, 1235-47, (2013).
- 29 Evans, C. H. *et al.* EWS-FLI-1-targeted cytotoxic T-cell killing of multiple tumor types belonging to the
Ewing sarcoma family of tumors. *Clin Cancer Res* **18**, 5341-51, (2012).
- 30 Domanska, U. M. *et al.* A review on CXCR4/CXCL12 axis in oncology: No place to hide. *Eur J Cancer* **49**,
219-30, (2013).
- 31 Lippitz, B. E. Cytokine patterns in patients with cancer: a systematic review. *Lancet Oncol* **14**, e218-e28,
(2013).
- 32 Kim, S. *et al.* Inhibition of the CXCR4/CXCL12 chemokine pathway reduces the development of murine
pulmonary metastases. *Clin Exp Metastasis* **25**, 201-11, (2008).
- 33 Brennecke, P. *et al.* CXCR4 antibody treatment suppresses metastatic spread to the lung of intratibial hu-
man osteosarcoma xenografts in mice. *Clin Exp Metastasis* **31**, 339-49, (2014).
- 34 Yoder, A. *et al.* HIV Envelope-CXCR4 Signaling Activates Cofilin to Overcome Cortical Actin Restriction
in Resting CD4 T Cells. *Cell* **134**, 782-92, (2008).
- 35 Busillo, J. M. *et al.* Site-specific Phosphorylation of CXCR4 Is Dynamically Regulated by Multiple Kinases
and Results in Differential Modulation of CXCR4 Signaling. *J Biol Chem* **285**, 7805-17, (2010).
- 36 Cronshaw, D. G., Nie, Y., Waite, J. & Zou, Y.-R. An Essential Role of the Cytoplasmic Tail of CXCR4 in
G-Protein Signaling and Organogenesis. *PLoS One* **5**, e15397, (2010).
- 37 Kumar, A., Kremer, K. N., Dominguez, D., Tadi, M. & Hedin, K. E. Ga13 and Rho Mediate Endosomal
Trafficking of CXCR4 into Rab11+ Vesicles upon Stromal Cell-Derived Factor-1 Stimulation. *The Journal*
of Immunology **186**, 951-8, (2011).
- 38 Gómez-Moutón, C. *et al.* Filamin A interaction with the CXCR4 third intracellular loop regulates endo-
cytosis and signaling of WT and WHIM-like receptors. *Blood* **125**, 1116-25, (2015).
- 39 Bamidele, A. O. *et al.* IQGAP1 promotes CXCR4 chemokine receptor function and trafficking via EEA-1+
endosomes. *The Journal of Cell Biology* **210**, 257-72, (2015).
- 40 Malik, R., Soh, U. J. K., Trejo, J. & Marchese, A. Novel Roles for the E3 Ubiquitin Ligase Atrophin-inter-
acting Protein 4 and Signal Transduction Adaptor Molecule 1 in G Protein-coupled Receptor Signaling.
The Journal of Biological Chemistry **287**, 9013-27, (2012).
- 41 Woodard, L. E. & Nimmagadda, S. CXCR4-Based Imaging Agents. *J Nucl Med* **52**, 1665-9, (2011).
- 42 Burns, J. M. *et al.* A novel chemokine receptor for SDF-1 and I-TAC involved in cell survival, cell adhe-
sion, and tumor development. *The Journal of Experimental Medicine* **203**, 2201-13, (2006).
- 43 Maravillas-Montero, J. L. *et al.* Cutting Edge: GPR35/CXCR8 Is the Receptor of the Mucosal Chemokine
CXCL17. *The Journal of Immunology* **194**, 29-33, (2015).
- 44 Sarmiento, J. *et al.* Diverging Mechanisms of Activation of Chemokine Receptors Revealed by Novel
Chemokine Agonists. *PLoS One* **6**, e27967, (2011).
- 45 Lasagni, L. *et al.* An Alternatively Spliced Variant of CXCR3 Mediates the Inhibition of Endothelial Cell
Growth Induced by IP-10, Mig, and I-TAC, and Acts as Functional Receptor for Platelet Factor 4. *The*
Journal of Experimental Medicine **197**, 1537-49, (2003).
- 46 Yu, L. *et al.* Identification and expression of novel isoforms of human stromal cell-derived factor 1. *Gene*
374, 174-9, (2006).
- 47 Gupta, S. K. & Pillarisetti, K. Cutting Edge: CXCR4-Lo: Molecular Cloning and Functional Expression of
a Novel Human CXCR4 Splice Variant. *J Immunol* **163**, 2368-72, (1999).
- 48 De Jong, E. K. *et al.* Expression of CXCL4 in microglia in vitro and in vivo and its possible signaling
through CXCR3. *J Neurochem* **105**, 1726-36, (2008).

Chapter 2

Sequencing overview of Ewing sarcoma: a journey across genomic, epigenomic and transcriptomic landscapes

L.G.L. Sand, K. Szuhai and P.C.W. Hogendoorn

International Journal of Molecular Sciences, 2015, 16, 16176-215

ABSTRACT

Ewing sarcoma is an aggressive neoplasm occurring predominantly in adolescent Caucasians. At the genome level, a pathognomonic *EWSR1-ETS* translocation is present. The resulting fusion protein acts as a molecular driver in the tumor development and interferes, amongst others, with endogenous transcription and splicing. The Ewing sarcoma cell shows a poorly differentiated, stem-cell like phenotype. Consequently, the cellular origin of Ewing sarcoma is still a hot discussed topic. To further characterize Ewing sarcoma and to further elucidate the role of *EWSR1-ETS* fusion protein multiple genome, epigenome and transcriptome level studies were performed. In this review, the data from these studies were combined into a comprehensive overview. Presently, classical morphological predictive markers are used in the clinic and the therapy is dominantly based on systemic chemotherapy in combination with surgical interventions. Using sequencing, novel predictive markers and candidates for immuno- and targeted therapy were identified which were summarized in this review.

KEYWORDS

bone neoplasm; bone tumor; Ewing sarcoma; soft tissue tumor; targeted therapy; epigenetics; tumor microenvironment; immunotherapy; next generation sequencing; splicing

INTRODUCTION

Ewing sarcoma (EWS) is a high-grade sarcoma occurring predominantly in the bones of children and young adolescents, in which it is the third most common primary bone sarcoma, following osteosarcoma and chondrosarcoma. In adults, it occurs less frequently, but at this age, soft tissue and organ related involvement is more common [1,2]. At the cellular level, EWS has a poorly differentiated, stem cell-like phenotype with some degree of neurogenic features. These were partly represented by earlier classification as peripheral primitive neuroectodermal tumors (PNET). In the current World Health Organization (WHO) classification, however, PNET and a clinical variant of EWS known as Askin tumor, arising in the chest wall, are all classified as EWS based on the presence of a unifying pathognomonic chromosomal translocation¹. This translocation forms a chimera gene fusing the *EWSR1* gene with a member of the *ETS* transcription factor family. Of the *EWSR1-ETS* translocations, *EWSR1-FLI1* is the most common with 85% of the cases. Other partners of *EWSR1* are *ERG* (10%), *ETV1*, *ETV4* and *FEV* [2]. No difference in survival was observed between the different translocation types [2]. There is an increasing body of evidence from tumors with histopathological appearance of EWS without the involvement of *EWSR1* and/or *ETS*. The clinical relevance of this Ewing-like tumor family from classical EWS is yet unknown and is studied [3-5]. The incidence of EWS is three per million and around a nine-fold more in Caucasians compared to Africans [6]. A suggested genetic explanation for this is the presence of intronic Alu elements (retrotransposons) located near the breakpoint region. In the African population, an allele which lacks the majority of the Alu elements has been identified with an allele frequency of 8% [7]. Alu elements are potentially more preferred during recombination and their increase could increase the chance of a translocation to occur [8]. The lack of Alu repeats may contribute, but it cannot be the leading mechanism behind the observed difference in tumor incidence. Furthermore, a similar occurrence in Alu distribution was not observed in other *EWSR1* translocation positive sarcomas, like clear cell sarcoma [9]. A large genome-wide association

study (GWAS) on EWS identified no single-nucleotide polymorphism (SNP) association at the *EWSR1* and *ETS* breakpoints. However, they did find three SNPs; rs9430161 on chromosome 1 upstream *TARDBP* (Tat activating regulatory DNA-binding protein), rs224278 on chromosome 10 upstream *EGR2* (early growth response 2) and rs4924410 at locus 15q15, which were associated with EWS with odds ratio of 2.2, 1.7 and 1.5, respectively. *EGR2* is a target of *EWSR1-FLI1* and *TARDBP* was proposed to be structurally and functionally similar to *EWSR1* [10]. Further validation is required for the SNP at 15q15, since multiple genes are located in close proximity of it. The SNPs on chromosome 10 and 1 were more frequent present in Caucasians compared to Africans and could thereby be a factor in the differences in incidence of EWS in different racial patient populations [10]. Recently, another possible cause of the epidemiologic difference in the occurrence of EWS has been proposed. The *EWSR1-ETS* chimeric protein binds to GGAA microsatellites which differ in distribution between Caucasians and Africans. Caucasians have a higher frequency of repeats of 20–30 GGAA elements compared to Africans, which have a higher frequency of repeats longer than 30 elements. In a reporter gene assay, the highest *EWSR1-FLI1* expression was observed when the GGAA microsatellite consisted of 20–30 motifs and this was concordant with the EWS target gene expression in relation to GGAA microsatellite length in EWS cell lines [11,12]. This suggests that the expression inducible capability of *EWSR1-ETS* can be larger in Caucasians compared to Africans.

RELATION BETWEEN *EWSR1-ETS* AND THE CELL OF ORIGIN OF EWS

There is an ongoing debate on the identification of the cell of origin of EWS. Expression of the fusion protein leads to more stem cell-like phenotypes and expressions of neuro-ectodermal markers [13]. In addition, *EWSR1* is expressed in many tissues, its function is poorly understood and the *EWSR1* gene is involved in translocations in multiple other tumors [14–17]. Multiple cells of origin have been suggested, such as mesenchymal stem and neural crest cells [13,18,19]. In order to shed some light on this debate, the effect of induced expression of the chimeric protein in non-tumorigenic cells was investigated. It was expected that the translocation had a large impact on cell homeostasis and interfered at multiple levels in endogenous processes. To study the impact of this gene chimera, primary human fibroblasts were transfected with an *EWSR1-FLI1* construct and that led to a TP53 dependent growth arrest. This points towards the need of additional (secondary) changes to be able to transform [20]. Likewise, in other studies, which used *EWSR1-ETS* transfected adult human mesenchymal stem cells (MSCs), an additional mutation was needed for the cells to form tumors; while transformation was possible using unmodified pediatric MSCs [18,21,22]. Animal models containing inducible *EWSR1-FLI1* constructs led to phenotypically varying tumors from malignant peripheral nerve sheath tumors to myeloid/erythroid leukemia [23,24]. These observations directed towards a hypothesis that certain epigenetic changes might be needed to result in an *EWSR1-ETS* driven tumor and that this partly dictates the phenotype of the tumor. The presently hypothesized cells of origin are MSCs and neural crest cells. This is based on their capability to endure expression of *EWSR1-ETS* gene chimera without additional mutations, and the finding that transient *EWSR1-ETS* expression leads to a tumor similar to EWS at the level of expressed cellular markers and micro-array expression data [22,25]. Recently, a new mouse model has been created to mimic EWS using specific selected cells of the embryonic superficial zone of the long bones. In these animals, EWS-like tumors developed without any additional gene modifications. This might be a leap forward in creating a mouse model for

EWS [19]. To gain further insight into the tumor specific genetic changes multiple massive parallel sequencing studies were performed at the genome, the transcriptome and the epigenome level (**Table 1**). By combining the results of these studies, researchers may identify landscape marks in the EWS OMIC atlas explaining some of the mechanisms behind the behavior of Ewing sarcoma with the aim to identify new, targeted therapeutic targets. These targets can be validated by combining functional studies and testing. In addition, this might shed light on the cell of origin and secondary events necessary for tumor formation and changes that are related to a more therapy resistant or more aggressive phenotype.

Table 1: Next generation sequencing studies in Ewing sarcoma

| Sequence level | Study | Method | Platform | Material | Data accessibility |
|----------------|-----------------------------|------------------------------------|------------------------|---|--------------------|
| | Brohl <i>et al.</i> [26]. | whole genome paired-end sequencing | Complete genomics | 6 germline control paired samples | not accessible |
| | | targeted genomic sequencing | Iontorrent | 65 tumor samples and 36 cell lines | only mutations |
| | Tirode <i>et al.</i> [27] | whole genome paired-end sequencing | Illumina His-seq2000 | 112 germline control tumor samples | raw data |
| Genome | Crompton <i>et al.</i> [28] | whole genome paired-end sequencing | Illumina His-seq2000 | 7 germline control tumor samples | analyzed data |
| | | whole exome paired-end sequencing | | 26 germline control tumor samples, 66 tumor samples, 4 paired relapses, 11 cell lines | analyzed data |
| | Lawrence <i>et al.</i> [29] | whole exome sequencing | Illumina His-seq2000 | 20 germline control tumor samples | not accessible |
| | Jiang <i>et al.</i> [30] | targeted exome sequencing | FoundationOne platform | 28 tumor samples | only mutations |

| Sequence level | Study | Method | Platform | Material | Data accessibility |
|----------------|----------------------------|--------------------------|--------------------|---|-----------------------|
| | | H3K27ac ChIP-seq | | | |
| | | H3K4me3 ChIP-seq | | A673, SKNMC cell line, pediatric mesenchymal stem cells and 4 primary tumor samples | |
| | | H3K27me3 ChIP-seq | | | |
| | | FLI1 ChIP-seq | Illumina | | raw data |
| | | p300 ChIP-seq | HiSeq2000 | A673, SKNMC cell line | |
| | Riggi <i>et al.</i> [31] | GABPA ChIP-seq | | | |
| | | ELF1 ChIP-seq | | | |
| | | WDR5 ChIP-seq | | A673, SKNMC cell line and pediatric mesenchymal stem cells | |
| | | ATAC-seq | Illumina HiSeq2500 | SKNMC cell line and mesenchymal stem cell | raw data |
| | | DNA methylation RRBS | | | |
| | | DNA methylation WGBS | | | |
| | | ATAC-seq | | | |
| | | H3K4me3 ChIP-seq | | | |
| | Tomazou <i>et al.</i> [32] | H3K27me3 ChIP-seq | Illumina HiSeq2000 | A673 cell line | raw and analyzed data |
| | | H3K27ac ChIP-seq | | | |
| | | H3K56ac ChIP-seq | | | |
| | | H3K9me3 ChIP-seq | | | |
| | | H3K4me1 ChIP-seq | | | |
| | | H3K36me3 ChIP-seq | | | |
| | | RRBS | | | |
| | | FOXp2 ChIP-seq | | | |
| | ENCODE[33] | POLR2AphosphoS5 ChIP-seq | ND | SKNMC cell line | raw and analyzed data |
| | | H3K4me3 ChIP-seq | | | |

| Sequence level | Study | Method | Platform | Material | Data accessibility |
|-----------------------------|------------------------------------|---|-----------------------------|--|---|
| Epigenome | Guillon <i>et al.</i> [34] | FLI1 ChIP-seq | Illumina 1G | A673, SKNMC cell line | not accessible |
| | Bilke <i>et al.</i> [35] | FLI1 ChIP-seq E2F3 ChIP-seq | Illumina genome analyzer I | A673 cell line | raw data |
| | Wei <i>et al.</i> [36] | FLI1 ChIP-seq | Illumina genome analyzer | SKNMC cell line | raw data |
| | Brohl <i>et al.</i> [26] | whole transcriptome TruSeq paired-end sequencing | Illumina Hiseq2000 | 31 cell lines and 58 tumor samples | not accessible |
| | Crompton <i>et al.</i> [28] | whole transcriptome TruSeq paired-end sequencing | Illumina Hiseq2000 | 20 tumor samples, 3 paired relapses, 9 cell lines | analyzed data |
| Transcriptome | Sankar <i>et al.</i> [37] | whole transcriptome TruSeq sin- gle-end sequencing | Illumina Hiseq2000 | A673 and TTC-466 cell line | analyzed data raw data raw data raw data |
| | Marques Howarth <i>et al.</i> [38] | 3' SEQ | Illumina Genome Analyzer II | pediatric multipotent cells | raw data |
| | Raggi <i>et al.</i> [31] | whole transcriptome TruSeq paired-end sequencing | Illumina Hiseq2000 | A673 cell line | raw data |
| | Tomazou <i>et al.</i> [32] | whole transcriptome sequencing | Illumina Hiseq2000 | A673, SKNMC cell line | raw data |
| | Selvanathan <i>et al.</i> [39] | whole transcriptome paired-end sequencing | Illumina Hiseq2000 | 7 cell lines | not accessible |
| Erikizan <i>et al.</i> [40] | RIP-seq | FLI1 CLIP-seq | Illumina Hiseq2000 | TC32 cell line | raw and analyzed data |
| | | BruDRB-seq | Illumina Hiseq2000 | Otogenetics | not accessible |

GENOME MAP

To identify possible secondary genetic and genomic alterations related to the development of EWS and its biology, several groups performed genome-wide studies such as: whole genome sequencing (WGS), whole exome sequencing (WES) and whole transcriptome sequencing (WTS) [26-28]. These three types of studies included WGS of 123 tumor samples in parallel with the normal tissue derived germline controls, WES of 92 tumors of which 26 with paired normal control and 11 cell lines and WTS of 92 tumors and 42 cell lines resulting in data about structural rearrangements and variations, somatic mutations and expression profiles.

For a long time, EWS was known as a genetically stable tumor with rarely occurring additional mutations. Only a few genomic changes such as *TP53* mutations or *CDKN2A/CDKN2B* deletions were observed in a minority of samples in retrospective studies and they were reported to be associated with an inferior outcome in a multivariate analysis [29,30]. The search for secondary mutations that provide a permissive genetic background, and might explain how the EWSR1-ETS chimera protein transforms cells, remained unsuccessful for over twenty years after the initial identification of the *EWSR1-FLI1* fusion gene [43]. The goal of the genome sequencing studies was to identify the missing link in this area. Both WGS and WES studies detected only a very low number of somatic mutations (0.65–0.15 per Mb) although different statistics for analysis were used [27,28]. Similarly, the low number of single nucleotide variations (SNV) in EWS has been reported in an earlier study and was, when compared to other tumors, one of the lowest [29]. Possible causes for the low number of SNVs could be related to the pathognomonic gene fusion acting as a direct tumor driver, and to the young age of onset of the tumor with possible fewer gained environmental mutations. Rhabdomyosarcoma (RMS) consists of both fusion gene positive and negative subtypes and the fusion positive subtype contained significant less mutations compared to the fusion negative subtype [44]. The number of mutations detected in fusion positive RMS was similar to EWS. The number of additional mutations correlated with age in both the RMS and EWS, confirming an age related factor [28,44]. Another retrospective study confirmed that the increased number of somatic mutations was in a univariate analysis correlated to shorter survival time [27]. This might partly explain why an increased age is correlated with inferior prognosis in EWS, but it could also be due decreased tolerance to chemotherapy [45,46]. In biopsies, the most common kind of mutation detected was a C to T transition, which was linked to the common event of deamination of methylated cytosines [28]. The number of mutations was, as expected, increased in post-chemotherapy samples and an association between the increased numbers of novel mutations with a poor patient outcome was observed [28]. In theory, these clones might already have been present but remained undetected due to tumor heterogeneity. Alternatively, these mutations were caused by the treatment resulting in a drug resistance phenotype. This would be very interesting for understanding treatment response prediction. Overall, EWS is from a global genomic perspective a relatively stable tumor with low number of somatic mutations, implying a functional mutation recognition and repair mechanism.

Structural and Copy Number Variant Map

All *bona fide* EWS contained an *EWSR1-ETS* translocation and these were detected in all tumors and cell lines tested [26–28]. In the study by Brohl *et al.* [26], however, seven cases were identified with cellular phenotype similarly to EWS but without an *EWSR1-ETS* translocation, supported by the fact that these samples cluster separately based on RNA expression

profile. This observation supports the notion of the existence of a Ewing-like tumor with clinical- and histo-morphological appearances similarly to EWS but carrying other, specific translocations such as, *BCOR-CCNB3*, *EWSR1-NFATc2*, *FUS-NFATc2* and *CIC-FOXO4* and *CIC-DUX4* [3–5]. As these entities are rare, follow-up studies have to show if these groups should be further stratified based on the genes involved or might be lumped as one clinical entity, Ewing-like sarcoma. None of the sequenced EWS samples detected an additional, commonly occurring translocation co-existing with *EWSR1-ETS*.

Although EWS tumors with a complex karyotype occur in a minority of cases, there are some common chromosomal alterations. These are gain of chromosome 1q, 8, 12 and loss of 9p21 and 16q [47–50]. Gain of chromosome 1q and chromosome 16q loss were strongly co-associated caused by an unbalanced translocation *der(16)t(1;16)* [47,51–53]. The frequency of 1q gain was, in various studies, associated with a dismal prognosis and was higher in chemotherapeutic treated tumors [27,28,47,48,54,55]. The responsible factor for this association was investigated by Mackintosh *et al.* who compared samples with and without 1q gain and 16 loss. At chromosome 1q, they identified increased expression of the gene Cell Division Cycle Protein 2 (*CTD2*), also known as Denticleless E3 Ubiquitin Protein Ligase Homolog (*DTL*), as the suspected factor [48]. *DTL* is, like *TP53*, involved in DNA damage repair and could therefore have an effect on tumor progression [56]. The chromosome 1q gain is not a EWS specific aberration, as it is one of the most frequently observed secondary changes in many tumor entities and even in Scultured embryonic stem cells [57]. The large heterochromatic regions at 1q12 might be responsible for the frequent translocation breakpoint leading to gain of the long arm of chromosome 1 [58–60]. As was observed with 1q, gain of chromosome 8 and 12 was present in many other tumors summarized by the progenetix website [61]. According to this website, these chromosome gains might be linked to pluripotency and proliferation. Chromosome 12 gain has also been observed in cultured human embryonic stem cells [62]. The oncogene associated with the increased tumorigenicity for chromosome 12 gain is not clear since next to *NANOG* it contains many genes including known oncogenes *CDK4*, *ERBB3*, *GLI1* and *MDM2*. For chromosome 8 gain, the increased expression of the oncogene *MYC* may be the attributing factor; however, EWS without the gain of chromosome 8 show similarly high expression of *MYC* [63–66]. Homozygous loss of 9p21 is, with about 12%, less common in EWS but could have a large impact since a well-known cell cycle regulator *CDKN2A/CDKN2B* is in this locus. Huang *et al.* [41] demonstrated in a retrospective study of 60 patients that the loss of *CDKN2A/CDKN2B* has a negative effect on the overall survival. Recently, Tirode *et al.* [27] analyzed 300 EWS samples and did not observe a significant difference in overall survival of patients with or without *CDKN2A/CDKN2B* loss. This underlines the importance of large sample size in studies of EWS, when trying to predict the effect of genomic alternations on prognosis. However, no data on chemotherapeutic response was presented of these patients, which has been reported to be significantly worse in patients with a *CDKN2A/CDKN2B* loss [27]. Loss of heterozygosity (LOH) is detected in earlier studies in a minority of the patients and was investigated using micro-satellite instability markers and identification markers, but no overlapping chromosomal regions were detected [67,68]. A recent study examined LOH in only six EWS samples by using SNP microarrays and showed some overlapping chromosomal regions with the ones reported earlier [69]. These were 17p and 11p and may be relevant to verify since *TP53* is located at the 17p chromosomal region. In several tumors inactivation of *TP53* has been reported due to point mutations or, less frequently, homozygous deletion, or deletion in combination with point mutation due to LOH. Intriguingly, in EWS inactivation of *TP53* caused by deletion was found as a rarely occurring

event in earlier studies and was not even reported in any of recent large genomic landscape studies [26–28,41,48,49,70].

Mutation Map

Although EWS contains few SNVs, their distribution over the genome is quite specific. The most commonly affected genes found in the genomic landscape studies were *STAG2* and *TP53* with an occurrence in patients of respectively 9%–21.5% and 5.2% to 7% and both were in a retrospective study in a univariate analysis associated with poor prognosis [26,27,72]. The most commonly mutated gene *STAG2* was only recently reported for the first time in EWS [73]. The distribution of the mutations is striking, with a quarter of the cases having a mutation at R216X, which is a possible CpG site and might be linked to a *STAG2*-DNA methylation pattern (see **Figure 1A**). The mutated *STAG2* status correlated only with an increase in structural variants and no other of the tested parameters [27,28]. This observation may be related to the function of *STAG2*, as it is a subunit of the cohesin complex and involved in chromatin modeling, chromatin cohesion, repair of stalled replication forks and double-strand breaks (DSBs) [74–77]. *STAG2* or other mutations in the cohesin complex were observed also in other tumors, including glioblastoma, myeloid malignancies, colon cancer and bladder cancer [72,73,78,79]. In colon cancer and glioblastoma, cohesin complex mutations were associated, like in EWS, with an increase in structural variants and aneuploidy [73,79]. In contrast, in myeloid malignancies this was not observed and in bladder cancer an inverse association was reported [80,81]. However, in myeloid malignancies, like in EWS, cohesin mutations were associated with poor prognosis [78]. In addition, when one of the cohesin complex genes was mutated in myeloid leukemia cell lines, less cohesin was bound to the chromatin [80]. Since cohesin is a key regulator of the chromatin structure and consequently influences gene expression, a reduction in the cohesin bound to the chromatin could affect the global gene expression [74,80,82]. *TP53* is the second most common mutated gene in EWS and is one of the most common mutated genes in all tumors [83]. The frequency of *TP53* mutations is slightly lower compared to earlier reports with an average of 10%. The two most frequent detected *TP53* mutations were the p.C176F and p.R273X of which p.R273X has been reported earlier [84]. In the International Agency for Research on Cancer (IARC) database, p.R273X is, like in EWS, a hot spot mutation. Yet, the most frequent *TP53* mutation in EWS p.C176F is remarkably not listed as a hot spot in the IARC database. In addition, the IARC database hot spot mutation p.R248Q is detected in only one tumor sample and only in one cell line, although it has been reported more frequent in earlier studies. This suggests that more samples are needed for a clear *TP53* mutation pattern (see **Figure 1B**) [26–28,83,85]. Mutations of *STAG2* and *TP53* showed a trend for co-occurrence with a synergistic negative effect on prognosis when both mutations were present. They are both involved in the checkpoint and repair processes, which may be further abrogated when both genes are mutated [27]. A trend for mutual exclusivity of *TP53* mutation and the loss of *CDKN2A* with only a few exceptions were present. Moreover, *CDKN2A* loss and *STAG2* mutation were mutual exclusive [27,28]. This indicates that *CDKN2A* and *STAG2* may be involved in complementary essential processes such as cell cycle and chromatin remodeling. Having a mutation in both genes may be lethal or redundant for EWS tumors [27,28,41,42,86,87]. To correct errors that may be caused by the relatively low numbers of cases analyzed, validation of these data in a bigger study is necessary.

Other somatic gene mutations in EWS, described in three large genomic studies, were low and not recurrent. All three studies reported a different process to be most influenced by

these somatic mutations. Tirode *et al.* [27] found mutations in several epigenetic regulators with *EZH2* as the most frequent mutated gene (3/112 cases), whereas Crompton *et al.* [28] reported mutations in other ETS transcription factors, including *ERF* (3/46 cases). Brohl *et al.* [26] reported mutations in the DNA repair pathway, in specific, with the deleterious polymorphism K3326X in *BRCA2* (4/55 cases) and a mutation in *RAD51* (1/55 case). An earlier study identified only four mutations in 75 EWS tumors with a hotspot array of 275 recurrent mutations across 29 genes which were not reported by these large genomic studies [88]. A recent study in chemotherapy-treated EWS tumors observed mutations which had implications for further targeted therapy response, such as *KRAS* [30].

Genome-wide sequencing of EWS was expected to show a common secondary event that would help to understand and model Ewing sarcoma and its onset. However, no common secondary event was identified. Overall, EWS was found to be a relatively stable tumor with a low frequency of mutations, which were scattered across the genome and acted dominantly on cell cycle processes. This suggests that these mutations occur during tumor progression and may be used as a marker for tumor progression but are not associated with the onset of EWS. Consequently, this may indicate the involvement of other factors in the onset of EWS pointing to disturbances at the epigenetic level as potential candidate.

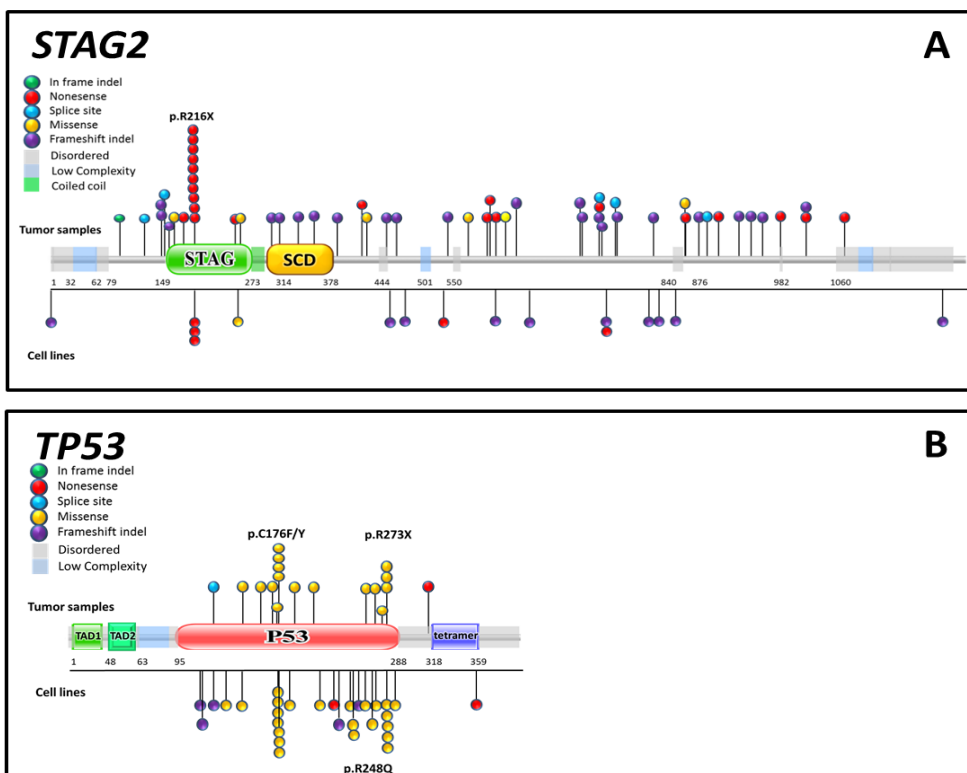


Figure 1: Mutation overview of reported STAG2 and TP53 in Ewing sarcoma. Overview of published mutations on *STAG2* and *TP53* from next generation sequencing data divided in five mutation subtypes based on data collected from 472 tumors and 54 cell lines. (A) Overview of the *STAG2* mutations (B) Overview of the *TP53* mutations. Amino acid sequence of the proteins is presented with different protein domains annotated in boxes and every sphere represents a reported mutation.

EPIGENOME MAP

Epigenetic modification involves both histone and DNA modifications such as acetylation or methylation of histone proteins and methylation of CpG islands. The DNA accessibility for transcription factors and polymerases, and thereby transcription, is partly regulated by these modifications. Classical sequencing reactions are not suited for the detection of epigenetic changes, therefore additional treatments have to be applied to detect these modifications. Examples of treatments to detect DNA methylation are MeDIP-seq, methylated DNA immunoprecipitation sequencing and WGBS, whole-genome bisulfite sequencing [89,90]. More complex approaches should be used to detect modifications influencing histone composition, such as ChIP-seq, chromatin immunoprecipitation sequencing; ChIP-exo, chromatin immunoprecipitation-exonuclease, or the detection of DNase-I sensitive sites [31,91,92]. As these approaches are complex reactions and not uniformly applied in different laboratories, comprehensive epigenome mapping of tumors are rarely published, although the ENCODE project, specifically set up for this, has generated a general overview [31,33,91,92]. Many parts of the epigenome in tumors however have been reported, since it is thought to have great therapeutic potential [93–96]. Recently an epigenome overview has been published by Tomazou *et al.* [32] covering the epigenome and transcriptome of EWS cell line A673 with inducible EWSR1-FLI1 knockdown construct. Four separate clusters of histone marks were detected with different effects upon knockdown of EWSR1-FLI1 [32]. Furthermore unique EWS open chromatin structures at distant enhancer and super-enhancers sites were detected, suggesting an important role for epigenomic regulation [32]. This might be related to the earlier described binding of the EWSR1-ETS fusion protein to GGAA containing microsatellite elements at enhancer sites and thereby affecting expression of downstream located genes (see **Figure 2A**) [31,97,98]. However, experimental evidence is lacking here. Binding to GGAA elements is an ETS specific effect and acts specifically on genes which do not contain a TATA box promoter [99]. Examples of such genes are *CAV1*, *NROB1* and *FCGRT*. The binding of EWSR1-FLI1 to GGAA microsatellites might lead to multimer formation which is needed to attract sufficient number of chromatin remodelers necessary for the sustained expression [31,34,98]. An important attracted chromatin remodeler for this sustained expression is p300 that acetylates histone 3 lysine H3K27 (H3K27ac). Monomeric EWSR1-FLI1 binding to a single GGAA element could not activate transcription and even inhibited gene expression, marked by the H3K9me3 histone modification (see **Figure 2B**) [32]. This might be due to insufficient attraction and binding of p300 since the fusion protein lacks a p300 binding site while wild-type ETS transcription with p300 binding sites could attract p300 and activate transcription [31,100]. In pediatric mesenchymal stem cells, induction of EWSR1-FLI1 led to a histone pattern at the EWSR1-FLI1 bound GGAA microsatellites which was similar to the pattern in EWS cell lines. Inhibition of EWSR1-FLI1 led to a decrease in activation of histone mark H3K27ac, which supports an active role of EWSR1-FLI1 in chromatin remodeling [31,32]. The H3K27 acetylation was especially associated with EWSR1-FLI1 bound enhancers [32]. It has to be noted that the overlap of ChIP-seq detected EWSR1-ETS binding sites was low with only 21% between *EWSR1-FLI1* carrying cell lines and 17.2% between *EWSR1-FLI1* and *EWSR1-ERG* carrying cell lines [31,36]. If these are all cell culture related artifacts or are due to accessibility of the DNA is not known. Another chromatin remodeling complex bound by EWSR1-FLI1 is the NuRD complex containing HDAC2 and HDAC3 proteins. These HDACs, when together with CHD4, can be active in the NuRD complex. Consequently, binding of the NuRD complex to EWSR1-FLI1 leads to repression of gene expression [101]. EWSR1-FLI1

regulated repression of expression was reverted by HDAC inhibitors and inhibiting histone demethylase LSD1, another NuRD complex protein. The NuRD complex is involved in many processes, especially in blood vessel development and integrity [32,102–104]. The interaction of EWSR1-ETS with the epigenetic remodelers is further increased by binding of EWSR1-ETS to the promotor of enhancer of zeste homolog 2 (*EZH2*) and Sirtuin 1 (*SIRT1*), thereby upregulating this histone methyltransferase and deacetylase [105,106]. The *EZH2* mediated effect in the cell was dependent on HDAC activity, demonstrating a cross interaction between two EWSR1-ETS modulated chromatin remodelers [105]. Overall, a complex interaction between EWSR1-ETS, chromatin and chromatin remodelers is needed in Ewing sarcoma to execute its oncogenic effect. As described earlier, transient expression of EWSR1-ETS in cells from different origin resulted in different phenotypes. This might be, in part, attributed to the chromatin state near GGAA microsatellites. An open chromatin structure at the enhancer and super-enhancer sites, as identified by Tomazou *et al.* [32], may be needed for the transforming effect of a EWSR1-ETS fusion protein in the development of Ewing sarcoma and if a more closed chromatin state was present an *EWSR1-ETS* translocation would lead to different effects or cell death. [32]. Although this is an attractive and plausible hypothesis, there is no experimental evidence yet to support this notion. The microenvironment, through for example, proliferative signaling, could greatly influence the chromatin state and have an interplay between EWSR1-ETS oncogenic properties. The other way around, tumor cell induced signaling can change the differentiation status of cells allocated in the tumor and distant microenvironment.

The type of mutations identified in EWS tumors pointed towards presence of methylated CpG sites, as mentioned in the genome map chapter. DNA methylation in EWS is studied only in a limited number of studies that used various techniques. In a recent relative small retrospective study by Park *et al.* [107], it was shown that patients with a poor outcome had increased methylation of CpG islands compared to patients with a better outcome, although the total hypermethylated genes was limited with only 10% of the investigated genes [107]. Their observation showed a similar proportion of genes with methylated CpG islands to an earlier study on DNA methylation using a different methylation micro-array [108]. Although the proportions were similar, the majority of the actual detected genes identified were different, having only six genes in common (*LYN*, *EPHA3*, *ESR1*, *MAP3K1*, *NGFR* and *SOX17*) in two studies. Compared to clear cell sarcoma and rhabdoid tumor of the kidney the same low number of hypermethylation of CpG islands was observed, but the number of significant hypomethylated genes was similar [109]. Since this study contained only four Ewing sarcoma samples, a larger study with more samples using the same platform should be performed. Whole genome DNA methylation was also performed in the earlier mentioned epigenome-wide study of Tomazou *et al.* [32]. Through WGBS, they observed less DNA methylation at actively expressed genes compared to non-expressed genes, suggesting an involvement of DNA methylation in the *EWSR1-ETS* mediated gene expression effect. However knockdown of *EWSR1-ETS* did not change the DNA methylation pattern. An alternative method to investigate the DNA methylation would be by using the PACBIO RSII sequencer system (Pacific Biosciences, Menlo Park, CA, USA). This system can detect the methylated CpG sites during the sequencing process and, as it does not need any amplification or chemical modification step, it has no probe bias. An unbiased sequencing approach could help to identify DNA methylation pattern in primary tumors and see if the pattern is the same in EWS tumors compared to cell lines. Since cell lines are used as models for EWS tumors and DNA methylation at whole genome level is only studied in cell lines.

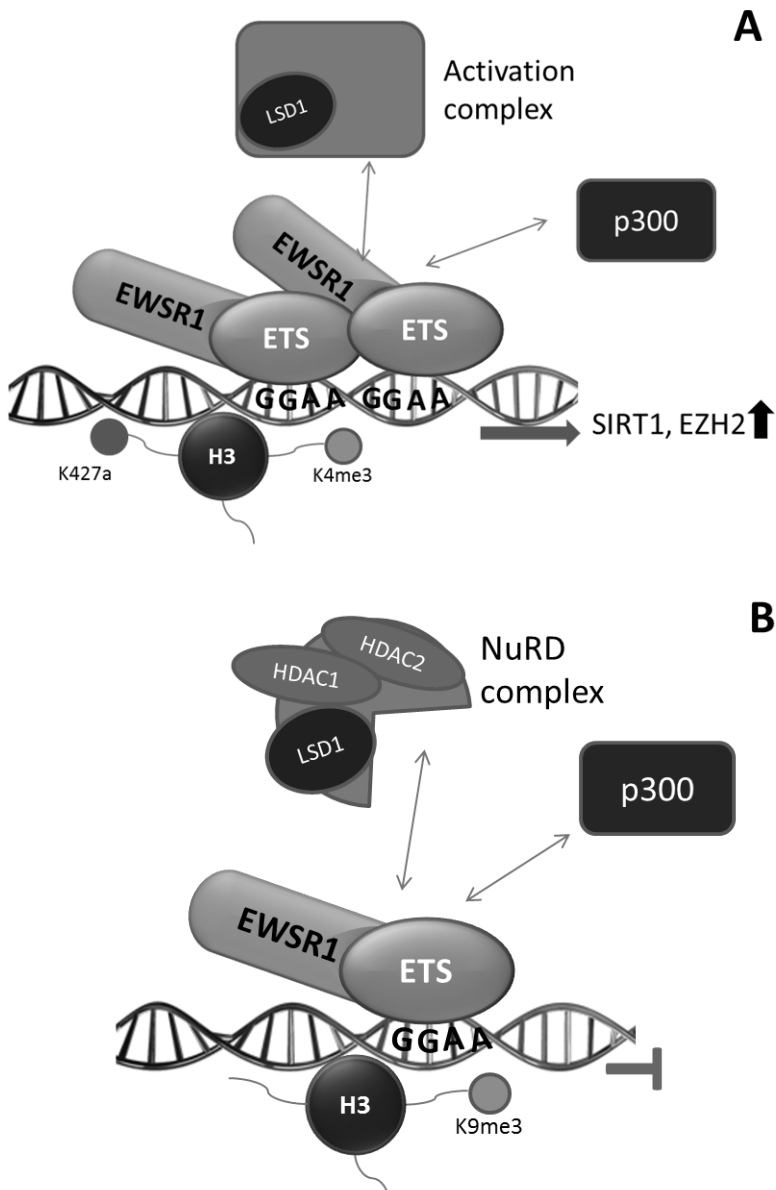


Figure 2: EWSR1-ETS mediated epigenetic activation and repression of gene expression. Possible mechanisms of how EWSR1-ETS acts as a transcription activator or repressor with different chromatin remodelers and is associated with different epigenetic histone modifications. A) EWSR1-ETS activation complex binds to GGAA microsatellites. The complex attracts LSD1 in a yet unidentified activation complex and p300, which is needed for efficient transcription. The activation complex may bind to H3K4me3 and H3K27ac histone marks which, in turn, may lead to upregulation of the epigenetic modifiers *SIRT1* and *EZH2*; B) EWSR1-ETS repression complex binds to single GGAA elements and scavenges for p300, but, as it is insufficient to create an activating complex, it may recruit NuRD repression complex which may lead to further repressed expression. In addition, these repression sites are marked with H3K9me3 histone mark.

TRANSCRIPTOME MAP

An EWSR1-ETS rearrangement affects gene expression levels, as mentioned above. In addition, it affects the expression of non-coding RNAs and splicing of RNAs by binding to the polymerase II complex protein hSRPB7 and to RNA helicase A (RHA) (**Figure 3**) [40,110,111]. The effect of EWSR1-ETS on gene expression levels has been investigated with microarrays and studied in cell and animal models [19,20,22,112]. A meta-analysis of earlier micro-array studies was performed and compared the expression levels of other sarcomas demonstrating a specific EWS signature [113]. Knockdown studies of the most common fusion protein EWSR1-FLI1 revealed that it causes both downregulation and upregulation of numerous genes involved in extracellular and intracellular processes [35,114]. Downregulated genes were involved in extracellular signaling and signaling regulation, including multiple chemokines and interleukins (such as, CXCL8, CCL2 and IL1A) [38,101]. Upregulated genes were involved in neural differentiation, transcription and cell cycle and included membrane proteins [114–117]. Examples of external validated membrane proteins upregulated by EWSR1-ETS fusion protein are *STEAP1*, *GPR64*, *CD99*, *CAV1* and *CHM1* [116,118–121]. These membrane proteins are interacting with the surrounding tumor microenvironment, thereby contributing to the high vascularization and invasive properties of EWS [116,119,122]. Validation of the EWSR1-ETS upregulated transcription factors NKX2.2, NR0B1, GLI1, BCL11B and E2F3 demonstrated an extensive attribution to the aggressive and stem-like phenotype of EWS [115,123–126]. EWSR1-ETS affects gene expression, mainly downregulation, both directly and indirectly. Directly, by binding GGAA microsatellites and indirectly, by interacting with the NuRD co-repressor complex and upregulating above mentioned transcription factors [101,115,125]. Transcription initiation is commonly not regulated by one but multiple transcription factors which interact with each other. By interacting with transcription factors, such as E2F3 and Sp1, EWSR1-ETS enhances its ability to induce gene activation [35,126,127]. Although EWSR1-ETS needs variable different cellular processes for its effect at the transcriptome level, the EWSR1-ETS map was observed to be relatively stable. When comparing the transcriptomes of cell lines with tumors in a principle component analysis, only the first principle component of pathways was significantly different. The principle component consisted of tumor-microenvironment pathways in EWS tumors and metabolic pathways in cell lines [28].

EWSR1-ETS affects not only the expression of genes but also the expression of non-coding RNAs, including both micro RNAs (miRNAs) and long non-coding RNAs (lncRNAs) [22,38,128]. miRNAs are regulating more than 60% of the human genes by mainly binding at the 3'UTR of the mRNA [129]. Around 10% of the studied miRNAs are significantly affected in EWS, both in down- and upregulation [128,130,131]. Affected pathways are diverse and include important tumorigenic pathways such as IGF signaling, chromatin remodeling, pluripotency and DNA damage repair [128,131–134]. An relatively small EWS retrospective patient survival association study on miRNAs identified a survival association with increased *miRNA34a* expression [135]. *miRNA34a* is thought not to be influenced by EWSR1-FLI1 itself but its activity is regulated by TP53 and NF- κ B and is associated with survival also in a retrospective glioblastoma study [136–138]. It regulates expression of proteins involved in growth pathway signaling, apoptosis, chromatin remodeling and genomic stress [136–138]. miRNA analysis at whole transcriptome scale might be successful to identify more miRNAs regulated by EWSR1-ETS or which are predictive for therapy.

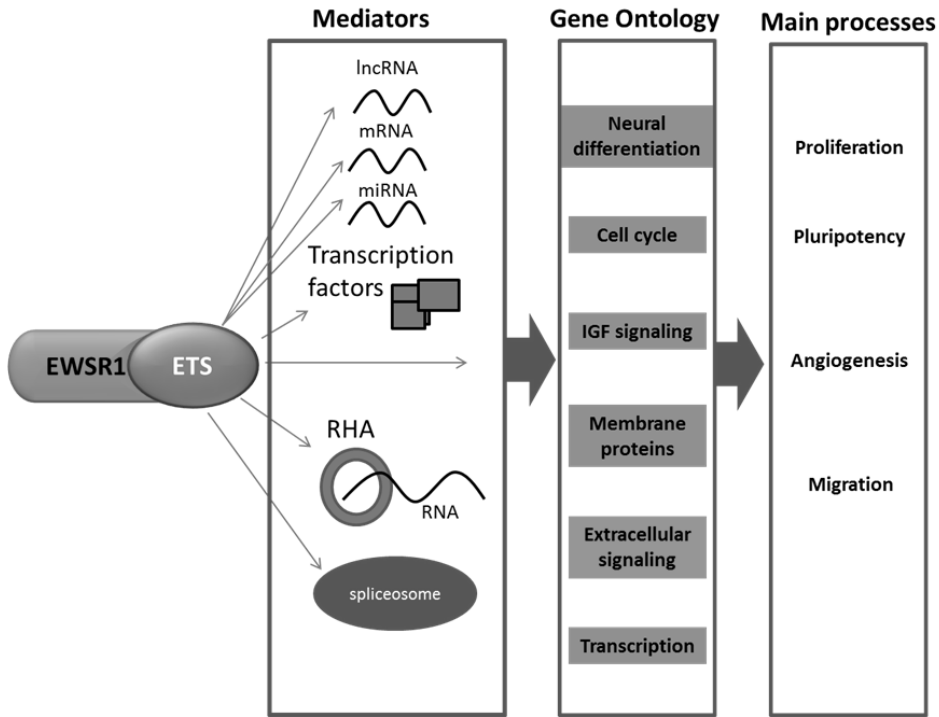


Figure 3: The influence of EWSR1-ETS fusion protein at the transcriptome level. EWSR1-ETS fusion protein acts as an aberrant transcription factor that influences the regulation of mRNA, lncRNA and miRNA expression levels. In addition, by binding to RHA additional transcripts can be bound and this might interfere with the stability of these transcripts. Alterations in epigenetic activity lead to up- and downregulation of a number of transcription factors and thereby interfere indirectly with gene expression. Furthermore, EWSR1-ETS fusion protein binds to the spliceosome and thereby altering splicing processes. By acting on these mediators, multiple cellular pathways are affected. The summarizing gene ontology clusters of the upregulated cellular pathways are cell cycle, membrane proteins, IGF signaling and transcription and the downregulated is extracellular signaling. The main processes influenced by these gene ontology clusters are an increase in proliferation, pluripotency, migration and angiogenesis.

Long non-coding RNAs are relatively recently discovered as functionally relevant and have functions both in epigenetic and post-translational regulations [139,140]. For example, *MALAT1* is a commonly expressed lncRNA, which is involved in angiogenesis and cell cycle progression [141,142]. Brunner *et al.* [143] studied expression of lncRNAs in a large tumor panel of both sarcomas and carcinomas including EWS. A large number of known and novel lncRNAs differentially expressed in EWS were identified, including *ALDH1L1-AS2*, *DICER1-AS1* and *LINC00277* [143]. In later research, *LINC00277* (*EWSAT1*) was the only lncRNA which was significantly overexpressed in *EWSR1-FLI1* transfected pediatric MSCs and downregulated in EWS cell lines when treated with *EWSR1-FLI1* shRNA [38]. *LINC00277* induction on its own affected expression levels of numerous genes which overlapped with *EWSR1-FLI1* target genes. Its effect was established partly by interacting with the RNA binding protein HNRNPK. A number of splice variants of *LINC00277* were described of which *LINC00277-2* was dominantly expressed in EWS. The modus of action of the various splice variants is unknown until now.

After transcription, RNAs are spliced and alternative splicing increases the functional diversity of proteins and noncoding RNAs. Splicing is regulated by multiple protein complexes and by interfering in this regulation many cellular processes can potentially be affected [144]. EWSR1 is involved in one of these protein complexes as scaffold protein [145,146]. EWSR1-ETS, missing the C-terminal part of EWSR1, interferes in the EWSR1 complex mediated splicing and causes the deregulated splicing of EWSR1 complex targeting RNAs [39,146–148]. One of the processes interfered with by EWSR1-ETS binding that was investigated in depth is the binding to RNA helicase A (RHA). RHA has both functions in DNA and RNA unwinding and stabilization [40,149]. Especially the RNA binding of RHA was inhibited by EWSR1-ETS binding and the new EWSR1-ETS RHA complex could bind additional targets, which were enriched for transcripts involved in extracellular signaling processes [40]. The consequences at the cellular level of the splicing interference has been illustrated by the splicing of *CCND1* (cyclin D1), a cell cycle regulator and *Vascular Endothelial Growth Factor A* (*VEGF-A*). The normal a-isoform of *CCND1* is exported from the nucleus during G1 phase to stop the cell cycle but by EWSR1-ETS interference the relative quantity of the b-isoform is increased in EWS. This isoform is not exported and increases proliferation of EWS cells [150]. *VEGF-A* splicing can result in both more and less angiogenic isoforms and, by the interference of EWSR1-ETS, the equilibrium between these isoforms is shifted to the more angiogenic isoform VEGFA-165. The effect of this shift is an increase in angiogenesis, which correlates to the highly vascularized histological features of Ewing sarcoma [151]. Despite the number of fundamental studies on the mechanism affected by EWSR1-ETS, limited studies are published on RNA targets. Whole transcriptome sequencing could be used to map the RNA targets of which splicing are affected by EWSR1-ETS but this has not yet been reported. In conclusion transcriptome mapping has shown to be of high value to characterize EWS and identify potential targets and survival markers [37,38,106,135].

UNDERSTANDING THERAPY SENSITIVITY AND IDENTIFYING TARGET CANDIDATES USING THE EWING SARCOMA SEQUENCING OVERVIEW

Before the introduction of chemotherapy, the overall survival of patients with EWS was about 10% using surgery alone. Early observation showed increased radiosensitivity of Ewing sarcoma and therefore radiotherapy as monotherapy was introduced, but the majority of patients still died of metastasis within two years when only radiotherapy was used [152,153]. The introduction of systematic chemotherapy increased the overall survival from ten percent to nowadays sixty to seventy-five percent for a localized tumor at diagnosis [2,154,155]. However, when a patient has recurrent disease, which is the case in thirty percent, or presents a metastatic disease at diagnosis, the overall survival drops to ten to forty percent [45,46]. As these patients are young, longtime curing is the treatment prospective, rather than stabilizing and short-term benefit. This translates in intense treatments but, as a pay-off, these have large consequences for long-term survival of EWS patients [156]. Prognostic markers for survival or treatment sensitivity may help to personalize the treatment [157]. New treatment protocols are needed to increase the patient survival with the least long-term effect. The uncovering of the mechanism of disease specific pathways serves as the basis for the development of targeted drugs to treat patients with the highest efficacy and the least side effects. For this, an EWSOMIC overview, using the results obtained by sequencing from various sources (**Table 1**), could help to increase this fundamental understanding and could lead to the identification of

novel therapeutic candidates for systemic, targeted and immunotherapy.

DNA Damage Response and Repair: Systemic and Targeted Therapy

Chemotherapy is an essential part in the treatment of EWS [154,158]. Over the past decades, the combination of chemotherapeutics, dosage and administration protocol has been adjusted to improve tumor response and reduce toxicity [155,159,160]. The present standard treatment protocol for EWS is based on combination of vincristine, doxorubicin, ifosfamide or cyclophosphamide and etoposide [2,159]. Most of these are DNA damaging drugs. As EWS contains a limited number of secondary mutations, it is likely that these tumors have an intact DNA damage response mechanism. Alkylating and double strand break causing agents consequently activate this mechanism leading to growth arrest and apoptosis of EWS cells. The hypothesis of an intact DNA damage response mechanism correlates with the chemotherapeutic resistance of *TP53* mutated EWS tumors, a key gene in this mechanism, since these tumors do not have an intact DNA damage response mechanism [41]. Fusion positive RMS has a limited number of mutations, similarly to EWS, but it is less sensitive to chemotherapy compared to translocation negative RMS [44]. This implies that downstream EWSR1-ETS effects may partly be responsible for the chemotherapy and radiotherapy sensitivity. In accordance, EWSR1-ETS associated DSBs have been identified and radiation induced damage turnover in EWS was reduced compared to osteosarcoma [161,162]. This makes the damage repair pathway a promising candidate to target. Compromising the DNA damage repair pathway via inhibition of poly (ADP ribose) polymerase 1 (PARP1) did indeed lead to inhibited proliferation in EWS cell lines and potentiated the response to temozolomide and irinotecan [19,161–163]. However, in EWS xenografts and patients treated with a PARP1 inhibitor, only the combination with temozolomide or irinotecan was effective [162,164]. In colon cancer xenografts this effect was observed as well [165]. The sensitivity of colon cancer to PARP1 inhibition is hypothesized to be related to a less functional homologous recombination due to cohesin complex aberrancy [75,77,166]. In glioblastoma cells, a correlation between PARP1 sensitivity and the presence or absence of the cohesin complex gene *STAG2* was demonstrated [167]. In the EWS PARP1 inhibition studies both *STAG2* wild type and mutant cell lines were sensitive to PARP1 inhibition in combination with chemotherapy [163,168]. A specific role for *STAG2* in this is therefore unlikely in EWS. Overall, it seems EWSR1-ETS interferes in the DNA damage repair pathway by a yet unexplainable way based on data obtained from genome and transcriptome sequencing studies leading to chemotherapy sensitivity. Identifying the *TP53* independent DNA damage response and repair pathway could open novel therapeutic options.

Targeting Chromatin Remodeling; EWSR1-ETS and Its Binding Partners

As mentioned, EWSR1-ETS intervenes in chromatin remodeling in multiple ways and the chromatin state around GGAA microsatellites might be related to the oncogenic capacity of EWSR1-ETS. Hence, chromatin remodeling is a good target. Understanding the action of EWSR1-ETS fusion protein in this could be used to design novel therapeutic agents that either occupies its GGAA microsatellite binding sites, targets the chromatin remodeling or blocks binding of its partners in transcription.

Chemotherapeutic drugs induce DNA damage by binding to the DNA, but the same binding can interfere with the binding of EWSR1-ETS to the DNA. Between these DNA binding chemotherapeutic agents, there is a difference in binding specificity, where Cisplatin and Doxorubicin are suggested to be less specific than Actinomycin D for removal of EWSR1-ETS

from the DNA [169]. However, due to the heavy systemic side effects Actinomycin D is no longer used to treat Ewing sarcoma patients in the U.S. [170]. Trabectedin, a toxin from the sea squirt *Ecteinascidia turbinata*, is believed to be more specific against EWSR1-ETS DNA binding sites. *In vitro* studies in EWS and myxoid liposarcoma, another fusion gene holding tumor demonstrated a high efficacy and showed interference with the activity of EWSR1-ETS and EWSR1-CHOP fusion protein, respectively [158,171]. In a clinical trial, however, trabectedin alone did not show a significant effect on overall survival in EWS [172].

Targeting chromatin remodelers, for example LSD1 and HDAC2, that attribute to the EWSR1-ETS oncogenic potential has been shown to be effective *in vitro* and in xenografts [37,106,173,174]. The effect of inhibiting LSD1 was even analyzed by whole transcriptome sequencing in cell lines with *EWSR1-FLI1* or *EWSR1-ERG* translocation to identify the overall effect on gene expression. Inhibition affected numerous genes including well-known target genes like *CAVI1*, *NKX2.2*. This inhibition study strengthened the role of the NuRD complex in the transcriptome wide effect of EWSR1-ETS [37]. HDAC2 inhibition by Vorinostat had a similar effect on the EWSR1-ETS repressed genes, replicating an earlier HDAC2 inhibition study in EWS, but did not affect genes directly activated by EWSR1-ETS [37,175]. A third potential identified target is the EWSR1-ETS upregulated histone deacetylase *SIRT1* which was identified in a *EWSR1-FLI1* knock-down screen and inhibition was effective in EWS cell lines *in vitro* and in xenografts [106]. Furthermore, *SIRT1* is regulated by miRNA34a expression, a prognostic factor in EWS, and both are associated with TP53 activity [135,137].

Riggi *et al.* [31] demonstrated that EWSR1-ETS can function as initiator in chromatin remodeling but needs to recruit other proteins for transcription initiation. Agents that inhibit the interaction between EWSR1-ETS and its binding partners by blocking the binding sites of EWSR1-ETS can be fruitful and a daunting task at the same time due to the disordered structure of EWSR1-ETS [176]. The identification of the small molecule YK-4-279 as inhibitor of the EWSR1-ETS binding to RHA confirmed that this approach is indeed promising and had a broad transcriptomic influence in EWS [40,177,178]. YK-4-279 treatment resulted in the same effect at splicing level as *EWSR1-ETS* inhibition and inhibited the binding of transcripts by the EWSR1-ETS RHA complex [39,40]. *In vivo* experiments suggest that combining this agent with other treatments could be especially effective, as shown in the combination with TP53 reactivating agent Nutlin3a in a zebrafish model [179].

Targeting EWSR1-ETS Influenced Extracellular Signaling, Transcriptome Mapping as a Lead

At the transcriptome level, EWSR1-ETS influences various pathways involved in intracellular processes and tumor microenvironmental processes that are needed for EWS development and maintenance. Both these processes are vital according to the processes collectively described as the hallmarks of cancer by Hanahan and Weinberg [180]. Major pathways by EWSR1-ETS affected are involved in extracellular signaling and membrane protein signaling. At a histo-morphological level, this is reflected by a stem-cell like tumor with high vascularization and a clinically observed high metastatic potential. Involved EWSR1-ETS key target pathways responsible for these features might be identified by transcriptome sequencing.

A well-known EWSR1-ETS targeted pathway is the IGF pathway, which is involved in tumor growth, metastasis and angiogenesis [181,182]. EWSR1-ETS increases the IGF1 pathway activity by upregulation of IGF1 expression and downregulation of insulin growth factor binding protein 3 and 5 (IGFBP3, IGFBP5) and various IGF pathway targeting miRNAs [114,117,133]. Targeting this pathway by small molecules or by monoclonal antibodies was shown to be highly effective in cell lines and it inhibited the angiogenesis in xenografts. In clinical trials, IGF1R treatment resulted in partial success due to no-response or quick resistance while a small group of patients remained stable. By studying the long-term responding patients at OMIC levels, we could identify the cause of their tumors sensitivity to anti-IGF therapy, which, in turn, would identify patients for anti-IGF therapy and understand the mechanism of the gained resistance [183–187]. In addition, combination chemotherapy with anti-IGF therapy is being investigated and may be an option. The combination of OSI-906, a dual inhibitor of IGF1R and IR, with trabectedin showed promising preclinical results [188].

The introduction of anti-angiogenic therapy with promises for all cancer types has been taking full media coverage with high initial expectations. Massive efforts to develop novel anti-angiogenic agents have led to several novel targeted therapy approaches. Although anti-angiogenic therapy alone was found to be insufficient, a combination with other treatment modalities may be effective [189]. As Ewing sarcoma is highly vascularized, targeting angiogenesis has been investigated in several *in vitro* and *in vivo* studies with success [185,190–192]. This was translated into multiple clinical trials testing anti-angiogenic drugs (NCT00516295, NCT01946529, NCT01492673 and NCT02243605). However, a pilot study in which chemotherapy with or without bevacizumab (a VEGF-A inhibitor) was used did not show a positive effect of bevacizumab [193]. Vascular mimicry has been observed in Ewing sarcoma and may be enhanced under hypoxic conditions that might reverse the anti-angiogenic effect [194–196].

As was demonstrated by micro-array studies and verified by transcriptome sequencing, EWSR1-ETS represses extracellular signaling proteins, including chemokines [28,38,113]. Chemokines are involved in all important tumor microenvironmental processes and elucidating the relation between the presence or absence of these chemokines may lead to new candidate targets or reactivating agents which would increase the chemokine expression [197]. The expression levels of the pro-inflammatory chemokines CXCL9 and 10 have been linked to the number of infiltrating T-cells and subsequently with a better overall survival in EWS patients in a relatively small retrospective study in a univariate analysis [198]. Treatment with interferon gamma (IFN- γ) enhanced the expression levels of pro-inflammatory chemokines and sensitizes resistant EWS cells *in vitro* to tumor necrosis factor apoptosis-inducing ligand (TRAIL)-induced apoptosis [198,199]. If these processes are related to each other is unknown. The only chemokine receptor which is highly expressed in EWS and not repressed by EWSR1-ETS is CXCR4 [38,200]. As a key factor in the tumor-microenvironment processes, especially metastasis, it is a very interesting receptor to study in EWS as a potential biomarker and therapeutic candidate [201,202]. Its RNA expression was, like many other tumors including osteosarcoma, correlated with lung metastasis and *in vitro* membrane CXCR4 positive cell lines migrated towards a CXCL12 gradient [200,203,204]. In contrast, no CXCR4 was detected at protein level in EWS lung metastases with immunohistochemistry but was positive in the chemotherapy-naïve tumor biopsies where it correlated with tumor volume [205]. The cause of the contradiction is unknown up to now and may be attributed to different CXCR4 isoforms or the abundant post-transcriptional modifications of CXCR4 [206–210]. The mentioned pathways are just examples of the many candidate pathways which can be targeted in

EWS. These candidate pathways connect intracellular processes with interactions in the microenvironment and can therefore be ideal for combined therapy. OMICs can contribute to identify targets at DNA and RNA level, but since these pathways are highly interconnected with each other additional post-transcriptional studies are needed for target validation and understanding the role of these signaling pathways in EWS. An example of such a post-transcriptional study is a knockdown study [211].

Targeting EWS with Immunotherapy

Immunotherapy is based on the use of two general mechanisms: (1) activating the native immune system (2) priming natural killer (NK) cells or cytotoxic T-cells for antigens specifically overexpressed in the tumor to treat. The performed OMIC studies in EWS can be of value in both cases. Expression of antigen presenting and NK cell ligands in EWS samples can be determined retrospectively and EWS specific antigens can be identified.

Determination of the tumor-associated leukocytes in pediatric tumors showed an increase in macrophages and almost lack of dendritic compare to adult tumors as a common feature the almost lack of dendritic cells [212]. The determination of the presence of intratumoral leukocytes is particularly important since high numbers of CD8+ T-cells have retrospectively been found to be associated with improved survival in an univariate analysis [198]. Indirect attraction of these CD8+ T-cells to EWS may be enhanced by the IFN- γ therapy, since it up-regulates pro-inflammatory chemokine expression levels [198]. Activation and attraction of the T-cells is presently not tested in a clinical trial but activation of endogenous or donor NK cells has been shown to be effective in EWS and phase I and II clinical trials and are currently open for enrollment (NCT01287104, NCT02100891) [213,214]. The efficacy of recognition may in fact be increased by combining this with the earlier mentioned chromatin remodeler inhibitors. *In vitro* HDAC inhibitor enhanced the NKG2D ligands expression in EWS cell lines, which are essential for NK mediated lysis [215]. For improved long-term NK activation and to overcome tumor mediated downregulation of NKG2D, prolonged *ex vivo* activation or antibody dependent cytotoxicity is needed [216]. From a preclinical perspective, allografting may be a beneficial adjuvant therapy in combination with either EWSR1-ETS blocking therapy or standard chemotherapy.

The second general method of priming cytotoxic T-cells for tumor specific membrane proteins overexpressed by EWS or unique HLA presented peptides has been investigated. Proposed targets are the tumor specific membrane proteins like PRAME, GPR64 and STEAP1 [217–219]. However, *ex vivo* priming of T-cells for antigens like PRAME and STEAP1 could not yet induce a prolonged antitumor immune response in preclinical studies. T-cells could not interact with the endogenous presented antigens at EWS cell lines or the T-cells which did recognize the presented antigens were classified as exhausted T-cells according to high PD1 expression [220,221]. The EWSR1-ETS upregulated proteins EZH2 and CHM1 were successfully used to prime allo-restricted T-cells but these are proteins expressed in many other tissues and could have serious side effects and lead to non-tumor specific targeting [221]. The ideal antigen to prime T-cells for would be EWSR1-ETS itself. The potential of this hypothesis was tested and a EWSR1-FLI1 specific antigen was identified and verified as an activating antigen for cytotoxic T-cells, but no follow-up study has been presented [222]. A possible cause for the less effective recognition demonstrated in EWS cell lines, and the potential clinical limiting factor, is the loss of major histocompatibility complex (MHC) class I and class II, which are needed for a proper immune response [223]. Genetic engineering of T-cells with chimeric antigen receptors directed to overexpressed surface markers is independent

of the MHC class system. These can be designed against proteins and even phosphoglycolipids [224]. The singular tested surface marker with this method is the neural ganglioside G_{D2} which was expressed in all 10 EWS cell lines tested and 12 of 14 analyzed patients [225]. A follow-up xenograft study was successful showing a reduction in tumor growth and number of tumors but effect on total survival was not significantly different [224]. For further research, antigens should be selected for EWS specific surface markers to prevent non-tumor cells to be targeted, like stem cells which do not express MHC class II complex but do express certain surface markers [226]. For example, the aforementioned G_{D2} is also expressed in neural crest cells and mesenchymal stem cells [227].

Overall, immunotherapy can be promising in combination with systemic or targeted therapy. Both NK-cell and T-cell related therapies have potential, especially the antibody targeted NK-cells and genetically modified T-cells. Genetically modified T-cell therapy in EWS is just starting and all membrane proteins and potential tumor specific splice variants of membrane proteins could be targets for these T-cells. In addition, the ability to target glycolipid structures opens a complete new set of possibilities, but these cannot be identified by sequencing.

CONCLUSIONS

By sequencing EWS at the genome, epigenome and transcriptome level, an atlas can be created which would help to fundamentally understand EWS and help to identify important nodes as therapeutic candidates. The *EWSR1-ETS* translocation is the characteristic pathognomonic alteration found in all tumors so far. The fusion protein act as a strong transforming oncogene and, in experimental conditions, the transfection of cells with normal cellular backgrounds rather leads to oncogene-induced apoptosis than to transformation. Recent studies, however, showed that stem cells from young individuals with the necessary permissive background did form tumors, pointing towards the importance of epigenetic controlling in cellular/tissue differentiation in providing the necessary niche for the transformation [19,22,25,38]. Therefore, mapping these genomic and functional genomic alterations can lead to identification of the cell of origin, improvements in prediction of clinical outcome, and discovery of novel therapeutic targets. These prospects have led to numerous, independent investigations using various approaches related to OMICs.

As a result, several novel findings and confirmations of earlier observations were collected. For example, some secondary structural alterations can be detected in a subset of the tumors that can identify a patient with unfavorable prognosis. Despite huge efforts to identify secondary mutations that provide a permissive background to transform cells with the pathognomonic *EWSR1-ETS* translocation, only a limited number of secondary point mutations were detected in EWS. Of these, *STAG2* and *TP53* were the most frequently mutated genes and mutations in these genes were associated with inferior prognosis. The value of these mutations as prognostic markers has to be validated in a prospective study. Transcriptome sequencing projects excluded the possibility of recurrent co-occurring fusion genes that would be responsible for the transformation to endure the fusion protein. Based on these massive sequencing efforts, it is likely that the *EWSR1-ETS* fusion can propagate transformation in cells with less differentiated features and the epigenetic landscape of these primitive cells form a permissive niche for oncogenic transformation. *EWSR1-ETS* is, both at the transcriptome and epigenome level, the most dominant actor both by activation and repression transcription and needs cooperation of binding partner proteins like chromatin remodelers. The identified key pathways in Ewing sarcoma and the *EWSR1-ETS* chromatin remodeling binding partners

include promising candidate targets. This needs to be validated with in functional studies in combination with the epigenome and transcriptome analyses.

The advantage of the genomic stability of EWS is that the endogenous pathways controlling DNA damage recognition and apoptosis are still intact and could potentially be activated when targeted specifically and especially together with agents acting on the basis of the EWSR1-ETS network of epigenomic and transcriptomic changes. For example, blocking the interaction with its binding proteins could be a very efficient combination therapy. By deciphering this network for both targeted therapy as well as immunotherapy, novel key target candidates can be identified. In the future, hopefully these therapies could, together with conventional chemotherapy, improve the outcome of these young patients.

REFERENCES

- 1 De Alava, E., Lessnick, S. L. & Sorensen, P. H. *WHO Classification of Tumours of Soft Tissue and Bone*. 4 edn, Vol. 5 306-309 (IARC, 2013).
- 2 Le Deley, M.-C. *et al.* Impact of EWS-ETS Fusion Type on Disease Progression in Ewing's Sarcoma/Peripheral Primitive Neuroectodermal Tumor: Prospective Results From the Cooperative Euro-E.W.I.N.G. 99 Trial. *J. Clin. Oncol.* **28**, 1982-8, (2010).
- 3 Pierron, G. *et al.* A new subtype of bone sarcoma defined by BCOR-CCNB3 gene fusion. *Nat. Genet.* **44**, 461-6, (2012).
- 4 Graham, C., Chilton-MacNeill, S., Zielenska, M. & Somers, G. R. The CIC-DUX4 fusion transcript is present in a subgroup of pediatric primitive round cell sarcomas. *Hum. Pathol.* **43**, 180-9, (2012).
- 5 Szuhai, K. *et al.* The NFATc2 Gene Is Involved in a Novel Cloned Translocation in a Ewing Sarcoma Variant That Couples Its Function in Immunology to Oncology. *Clin. Cancer Res.* **15**, 2259-68, (2009).
- 6 Jawad, M. U. *et al.* Ewing sarcoma demonstrates racial disparities in incidence-related and sex-related differences in outcome. *Cancer* **115**, 3526-36, (2009).
- 7 Zucman-Rossi, J., Batzer, M. A., Stoneking, M., Delattre, O. & Thomas, G. Interethnic polymorphism of EWS intron 6: genome plasticity mediated by Alu retroposition and recombination. *Hum. Genet.* **99**, 357-63, (1997).
- 8 Kolomietz, E., Meyn, M. S., Pandita, A. & Squire, J. A. The role of Alu repeat clusters as mediators of recurrent chromosomal aberrations in tumors. *Genes Chromosomes Cancer* **35**, 97-112, (2002).
- 9 Worch, J. *et al.* Racial differences in the incidence of mesenchymal tumors associated with EWSR1 translocation. *Cancer* **20**, 449-53, (2011).
- 10 Postel-Vinay, S. *et al.* Common variants near TARDBP and EGR2 are associated with susceptibility to Ewing sarcoma. *Nat. Genet.* **44**, 323-7, (2012).
- 11 Monument, M. J. *et al.* Clinical and Biochemical Function of Polymorphic *NROB1* GGAA-Microsatellites in Ewing Sarcoma: A Report from the Children's Oncology Group. *PLoS One* **9**, e104378, (2014).
- 12 Beck, R. *et al.* EWS/FLI-responsive GGAA microsatellites exhibit polymorphic differences between European and African populations. *Cancer Genet.* **205**, 304-12, (2012).
- 13 Kovar, H. Context matters: The hen or egg problem in Ewing's sarcoma. *Semin. Cancer Biol.* **15**, 189-96, (2005).
- 14 Andersson, M. K. *et al.* The multifunctional FUS, EWS and TAF15 proto-oncoproteins show cell type-specific expression patterns and involvement in cell spreading and stress response. *BMC Cell Biol.* **9**, 37-, (2008).
- 15 Kwon, I. *et al.* Phosphorylation-regulated Binding of RNA Polymerase II to Fibrous Polymers of Low Complexity Domains. *Cell* **155**, 1049-60, (2013).
- 16 Kim, K. Y. *et al.* A multifunctional protein EWS regulates the expression of Drosha and microRNAs. *Cell Death Differ.* **21**, 136-45, (2014).
- 17 Park, J. H. *et al.* A multifunctional protein EWS is essential for early brown fat lineage determination. *Dev. Cell* **26**, 393-404, (2013). 18 Riggi, N. *et al.* EWS-FLI-1 Expression Triggers a Ewing's Sarcoma Initiation Program in Primary Human Mesenchymal Stem Cells. *Cancer Res.* **68**, 2176-85, (2008).
- 19 Tanaka, M. *et al.* Ewing's sarcoma precursors are highly enriched in embryonic osteochondrogenic progenitors. *The Journal of Clinical Investigation* **124**, 3061-74, (2014).
- 20 Lessnick, S. L., Dacwag, C. S. & Golub, T. R. The Ewing's sarcoma oncoprotein EWS/FLI induces a p53-dependent growth arrest in primary human fibroblasts. *Cancer Cell* **1**, 393-401, (2002).

- 21 Miyagawa, Y. *et al.* Inducible Expression of Chimeric EWS/ETS Proteins Confers Ewing's Family Tumor-Like Phenotypes to Human Mesenchymal Progenitor Cells. *Mol. Cell. Biol.* **28**, 2125-37, (2008).
- 22 Riggi, N. *et al.* EWS-FLI-1 modulates miRNA145 and SOX2 expression to initiate mesenchymal stem cell reprogramming toward Ewing sarcoma cancer stem cells. *Genes Dev.* **24**, 916-32, (2010).
- 23 Torchia, E. C., Boyd, K., Rehg, J. E., Qu, C. & Baker, S. J. EWS/FLI-1 Induces Rapid Onset of Myeloid/Erythroid Leukemia in Mice. *Mol. Cell. Biol.* **27**, 7918-34, (2007).
- 24 Leacock, S. W. *et al.* A zebrafish transgenic model of Ewing's sarcoma reveals conserved mediators of EWS-FLI1 tumorigenesis. *Dis. Model. Mech.* **5**, 95-106, (2012).
- 25 von Levetzow, C. *et al.* Modeling Initiation of Ewing Sarcoma in Human Neural Crest Cells. *PLoS One* **6**, e19305, (2011).
- 26 Brohl, A. S. *et al.* The Genomic Landscape of the Ewing Sarcoma Family of Tumors Reveals Recurrent STAG2 Mutation. *PLoS Genet* **10**, e1004475, (2014).
- 27 Tirode, F. *et al.* Genomic Landscape of Ewing Sarcoma Defines an Aggressive Subtype with Co-Association of STAG2 and TP53 Mutations. *Cancer Discov.* **4**, 1342-53, (2014).
- 28 Crompton, B. D. *et al.* The Genomic Landscape of Pediatric Ewing Sarcoma. *Cancer Discov.* **4**, 1326-41, (2014).
- 29 Lawrence, M. S. *et al.* Mutational heterogeneity in cancer and the search for new cancer-associated genes. *Nature* **499**, 214-8, (2013).
- 30 Jiang, Y. *et al.* Novel Secondary Somatic Mutations in Ewing's Sarcoma and Desmoplastic Small Round Cell Tumors. *PLoS One* **9**, e93676, (2014).
- 31 Riggi, N. *et al.* EWS-FLI1 Utilizes Divergent Chromatin Remodeling Mechanisms to Directly Activate or Repress Enhancer Elements in Ewing Sarcoma. *Cancer Cell* **26**, 668-81, (2014).
- 32 Tomazou, E. M. *et al.* Epigenome Mapping Reveals Distinct Modes of Gene Regulation and Widespread Enhancer Reprogramming by the Oncogenic Fusion Protein EWS-FLI1. *Cell Rep.* **10**, 1082-95, (2015).
- 33 Consortium, T. E. P. The ENCODE (ENCyclopedia Of DNA Elements) Project. *Science* **306**, 636-40, (2004).
- 34 Guillon, N. *et al.* The Oncogenic EWS-FLI1 Protein Binds *In Vivo* GGAA Microsatellite Sequences with Potential Transcriptional Activation Function. *PLoS One* **4**, e4932, (2009).
- 35 Bilke, S. *et al.* Oncogenic ETS fusions deregulate E2F3 target genes in Ewing sarcoma and prostate cancer. *Genome Res.* **23**, 1797-809, (2013).
- 36 Wei, G.-H. *et al.* Genome-wide analysis of ETS-family DNA-binding in vitro and in vivo. *The EMBO Journal* **29**, 2147-60, (2010).
- 37 Sankar, S. *et al.* Reversible LSD1 inhibition interferes with global EWS/ETS transcriptional activity and impedes Ewing sarcoma tumor growth. *Clin. Cancer Res.*, (2014).
- 38 Marques Howarth, M. *et al.* Long noncoding RNA EWSAT1-mediated gene repression facilitates Ewing sarcoma oncogenesis. *The Journal of Clinical Investigation* **124**, 5275-90, (2014).
- 39 Selvanathan, S. P. *et al.* Oncogenic fusion protein EWS-FLI1 is a network hub that regulates alternative splicing. *Proceedings of the National Academy of Sciences*, (2015).
- 40 Erkizan, H. V. *et al.* RNA helicase A activity is inhibited by oncogenic transcription factor EWS-FLI1. *Nucleic Acids Res.* **43**, 1069-80, (2015).
- 41 Huang, H.-Y. *et al.* Ewing sarcomas with p53 mutation or p16/p14ARF homozygous deletion: a highly lethal subset associated with poor chemoresponse. *J. Clin. Oncol.* **23**, 548-58, (2005).
- 42 de Alava, E. *et al.* Prognostic impact of P53 status in Ewing sarcoma. *Cancer* **89**, 783-92, (2000).
- 43 Delattre, O. *et al.* Gene fusion with an ETS DNA-binding domain caused by chromosome translocation in human tumours. *Nature* **359**, 162-5, (1992).
- 44 Shern, J. F. *et al.* Comprehensive Genomic Analysis of Rhabdomyosarcoma Reveals a Landscape of Alterations Affecting a Common Genetic Axis in Fusion-Positive and Fusion-Negative Tumors. *Cancer Discov.* **4**, 216-31, (2014).
- 45 Ladenstein, R. *et al.* Primary disseminated multifocal Ewing sarcoma: results of the Euro-EWING 99 trial. *J. Clin. Oncol.* **28**, 3284-91, (2010).
- 46 Bacci, G. *et al.* Therapy and survival after recurrence of Ewing's tumors: the Rizzoli experience in 195 patients treated with adjuvant and neoadjuvant chemotherapy from 1979 to 1997. *Ann. Oncol.* **14**, 1654-9, (2003).
- 47 Hattinger, C. M. *et al.* Prognostic impact of chromosomal aberrations in Ewing tumours. *Br. J. Cancer* **86**, 1763-9, (2002).
- 48 Mackintosh, C. *et al.* 1q gain and CDT2 overexpression underlie an aggressive and highly proliferative form of Ewing sarcoma. *Oncogene* **31**, 1287-98, (2012).
- 49 Roberts, P. *et al.* Ploidy and karyotype complexity are powerful prognostic indicators in the Ewing's sarcoma family of tumors: A study by the United Kingdom Cancer Cytogenetics and the Children's Cancer

- and Leukaemia Group. *Genes Chromosomes Cancer* **47**, 207-20, (2008).
- 50 Savola, S. *et al.* Combined use of expression and CGH arrays pinpoints novel candidate genes in Ewing sarcoma family of tumors. *BMC Cancer* **9**, 17, (2009).
- 51 Yeh, A. *et al.* Chromosome arm 16q in Wilms tumors: Unbalanced chromosomal translocations, loss of heterozygosity, and assessment of the CTCF gene. *Genes Chromosomes Cancer* **35**, 156-63, (2002).
- 52 Mugneret, F., Lizard, S., Aurias, A. & Turc-Carel, C. Chromosomes in Ewing's sarcoma. II. Nonrandom additional changes, trisomy 8 and der(16)t(1;16). *Cancer Genet. Cytogenet.* **32**, 239-45, (1988).
- 53 Ozaki, T. *et al.* Genetic imbalances revealed by comparative genomic hybridization in Ewing tumors. *Genes Chromosomes Cancer* **32**, 164-71, (2001).
- 54 Gratiás, E. J. *et al.* Gain of 1q is associated with inferior event-free and overall survival in patients with favorable histology Wilms tumor: A report from the Children's Oncology Group. *Cancer* **119**, 3887-94, (2013).
- 55 Segers, H. *et al.* Gain of 1q is a marker of poor prognosis in Wilms' tumors. *Genes Chromosomes Cancer* **52**, 1065-74, (2013).
- 56 Terai, K., Shibata, E., Abbas, T. & Dutta, A. Degradation of p12 Subunit by CRL4Cdt2 E3 Ligase Inhibits Fork Progression after DNA Damage. *J. Biol. Chem.* **288**, 30509-14, (2013).
- 57 Varela, C. *et al.* Recurrent genomic instability of chromosome 1q in neural derivatives of human embryonic stem cells. *The Journal of Clinical Investigation* **122**, 569-74, (2012).
- 58 Sawyer, J. R. *et al.* Evidence for a Novel Mechanism for Gene Amplification in Multiple Myeloma: 1q12 Pericentromeric Heterochromatin Mediates Breakage-Fusion-Bridge Cycles of a 1q12-23 Amplicon. *Br. J. Haematol.* **147**, 484-94, (2009).
- 59 Sawyer, J. R., Tricot, G., Mattox, S., Jagannath, S. & Barlogie, B. Jumping Translocations of Chromosome 1q in Multiple Myeloma: Evidence for a Mechanism Involving Decondensation of Pericentromeric Heterochromatin. **91**, 1732-41, (1998).
- 60 Barki-Celli, L. *et al.* Differences in nuclear positioning of 1q12 pericentric heterochromatin in normal and tumor B lymphocytes with 1q rearrangements. *Genes Chromosomes Cancer* **43**, 339-49, (2005).
- 61 Baudis, M. & Cleary, M. L. Progenetix.net: an online repository for molecular cytogenetic aberration data. *Bioinformatics* **17**, 1228-9, (2001).
- 62 Draper, J. S. *et al.* Recurrent gain of chromosomes 17q and 12 in cultured human embryonic stem cells. *Nat. Biotechnol.* **22**, 53-4, (2004).
- 63 Yong, Z. W. E. *et al.* Genetic Alterations of Chromosome 8 Genes in Oral Cancer. *Sci. Rep.* **4**, 6073, (2014).
- 64 Inaki, K. *et al.* Systems consequences of amplicon formation in human breast cancer. *Genome Res.* **24**, 1559-71, (2014).
- 65 Tseng, Y.-Y. *et al.* PVT1 dependence in cancer with MYC copy-number increase. *Nature* **512**, 4, (2014).
- 66 Dauphinot, L. *et al.* Analysis of the expression of cell cycle regulators in Ewing cell lines: EWS-FLI-1 modulates p57KIP2 and c-Myc expression. *Oncogene* **20**, 3258-65, (2001).
- 67 Ohali, A. *et al.* High frequency of genomic instability in Ewing family of tumors. *Cancer Genet. Cytogenet.* **150**, 50-6, (2004).
- 68 Alldinger, I. *et al.* Microsatellite instability in Ewing tumor is not associated with loss of mismatch repair protein expression. *J. Cancer Res. Clin. Oncol.* **133**, 749-59, (2007).
- 69 Lynn, M. *et al.* High-resolution Genome-wide Copy-number Analyses Identify Localized Copy-number Alterations in Ewing Sarcoma. *Diagn. Mol. Pathol.* **22**, 76-84, (2013).
- 70 López-Guerrero, J. A. *et al.* Clinicopathological significance of cell cycle regulation markers in a large series of genetically confirmed Ewing's Sarcoma Family of Tumors. *Int. J. Cancer* **128**, 1139-50, (2011).
- 71 Ferreira, B. I. *et al.* Array CGH and gene-expression profiling reveals distinct genomic instability patterns associated with DNA repair and cell-cycle checkpoint pathways in Ewing's sarcoma. *Oncogene* **27**, 2084-90, (2007).
- 72 Solomon, D. A. *et al.* Frequent truncating mutations of STAG2 in bladder cancer. *Nat. Genet.* **45**, 1428-30, (2013).
- 73 Solomon, D. A. *et al.* Mutational Inactivation of STAG2 Causes Aneuploidy in Human Cancer. *Science* **333**, 1039-43, (2011).
- 74 Heidari, N. *et al.* Genome-wide map of regulatory interactions in the human genome. *Genome Res.* **24**, 1905-17, (2014).
- 75 Tittel-Elmer, M. *et al.* Cohesin association to replication sites depends on Rad50 and promotes fork restart. *Mol. Cell* **48**, 98-108, (2012).
- 76 Bauerschmidt, C. *et al.* Cohesin promotes the repair of ionizing radiation-induced DNA double-strand breaks in replicated chromatin. *Nucleic Acids Res.* **38**, 477-87, (2010).
- 77 Ström, L., Lindroos, H. B., Shirahige, K. & Sjögren, C. Postreplicative Recruitment of Cohesin to Double-Strand Breaks Is Required for DNA Repair. *Mol. Cell* **16**, 1003-15, (2004).

- 78 Thota, S. *et al.* Genetic alterations of the cohesin complex genes in myeloid malignancies. **124**, 1790-8, (2014).
- 79 Barber, T. D. *et al.* Chromatid cohesion defects may underlie chromosome instability in human colorectal cancers. *Proc. Natl. Acad. Sci. U. S. A.* **105**, 3443-8, (2008).
- 80 Kon, A. *et al.* Recurrent mutations in multiple components of the cohesin complex in myeloid neoplasms. *Nat. Genet.* **45**, 1232-7, (2013).
- 81 Taylor, C. F., Platt, F. M., Hurst, C. D., Thygesen, H. H. & Knowles, M. A. Frequent inactivating mutations of STAG2 in bladder cancer are associated with low tumour grade and stage and inversely related to chromosomal copy number changes. *Hum. Mol. Genet.* **23**, 1964-74, (2014).
- 82 Liu, J. *et al.* Genome-wide DNA methylation analysis in cohesin mutant human cell lines. *Nucleic Acids Res.* **38**, 5657-71, (2010).
- 83 Neilsen, P. M., Pishas, K. I., Callen, D. F. & Thomas, D. M. Targeting the p53 Pathway in Ewing Sarcoma. *Sarcoma* **2011**, 17, (2011).
- 84 Kovar, H. *et al.* Narrow spectrum of infrequent p53 mutations and absence of MDM2 amplification in Ewing tumours. *Oncogene* **8**, 2683-90, (1993).
- 85 Olivier, M., Hollstein, M. & Hainaut, P. TP53 Mutations in Human Cancers: Origins, Consequences, and Clinical Use. *Cold Spring Harb. Perspect. Biol.* **2**, a001008, (2010).
- 86 Singh, S. K. & Ellenrieder, V. Senescence in pancreatic carcinogenesis: from signalling to chromatin remodelling and epigenetics. *Gut* **62**, 1364-72, (2013).
- 87 Ong, C.-T. & Corces, V. G. CTCF: an architectural protein bridging genome topology and function. *Nature Reviews Genetics* **15**, 234-46, (2014).
- 88 Shukla, N. *et al.* Oncogen mutation profiling of pediatric solid tumors reveals significant subsets of embryonal rhabdomyosarcoma and neuroblastoma with mutated genes in growth signaling pathways. *Clin. Cancer Res.* **18**, 748-57, (2012).
- 89 Taiwo, O. *et al.* Methylome analysis using MeDIP-seq with low DNA concentrations. *Nat. Protoc.* **7**, 617-36, (2012).
- 90 Ziller, M. J., Hansen, K. D., Meissner, A. & Aryee, M. J. Coverage recommendations for methylation analysis by whole-genome bisulfite sequencing. *Nature Methods* **12**, 230-2, (2015).
- 91 Wang, L. *et al.* MACE: model based analysis of CHIP-exo. *Nucleic Acids Res.* **42**, e156-e, (2014).
- 92 Lazarovici, A. *et al.* Probing DNA shape and methylation state on a genomic scale with DNase I. *Proc. Natl. Acad. Sci. U. S. A.* **110**, 6376-81, (2013).
- 93 Vaish, V., Khare, T., Verma, M. & Khare, S. in *Cancer Epigenetics Vol. 1238 Methods in Molecular Biology* (ed Mukesh Verma) Ch. 40, 771-82 (Springer New York, 2015).
- 94 Ziller, M. J. *et al.* Charting a dynamic DNA methylation landscape of the human genome. *Nature* **500**, 477-81, (2013).
- 95 Hattori, T. *et al.* Recombinant antibodies to histone post-translational modifications. *Nature Methods* **10**, 992-5, (2013).
- 96 Rivera, C. M. & Ren, B. Mapping Human Epigenomes. *Cell* **155**, 39-55, (2013).
- 97 Patel, M. *et al.* Tumor-specific retargeting of an oncogenic transcription factor chimera results in dysregulation of chromatin and transcription. *Genome Res.* **22**, 259-70, (2012).
- 98 Gangwal, K. *et al.* Microsatellites as EWS/FLI response elements in Ewing's sarcoma. *Proceedings of the National Academy of Sciences* **105**, 10149-54, (2008).
- 99 Uchiumi, F., Miyazaki, S. & Tanuma, S.-I. [Biological functions of the duplicated GGAA-motifs in various human promoter regions]. *Yakugaku zasshi : Journal of the Pharmaceutical Society of Japan* **131**, 1787-800, (2011).
- 100 Hollenhorst, P. C., McIntosh, L. P. & Graves, B. J. Genomic and Biochemical Insights into the Specificity of ETS Transcription Factors. *Annu. Rev. Biochem.* **80**, 437-71, (2011).
- 101 Sankar, S. *et al.* Mechanism and relevance of EWS/FLI-mediated transcriptional repression in Ewing sarcoma. *Oncogene* **32**, 5089-100, (2013).
- 102 Ingram, K. G., Curtis, C. D., Silasi-Mansat, R., Lupu, F. & Griffin, C. T. The NuRD Chromatin-Remodeling Enzyme CHD4 Promotes Embryonic Vascular Integrity by Transcriptionally Regulating Extracellular Matrix Proteolysis. *PLoS Genet* **9**, e1004031, (2013).
- 103 Liu, J. *et al.* MTA1 regulates higher-order chromatin structure and histone H1-chromatin interaction in vivo. *Mol. Oncol.* **9**, 218-35, (2015).
- 104 Conomos, D., Reddel, R. R. & Pickett, H. A. NuRD-ZNF827 recruitment to telomeres creates a molecular scaffold for homologous recombination. *Nature Structural Molecular Biology* **21**, 760-70, (2014).
- 105 Richter, G. H. S. *et al.* EZH2 is a mediator of EWS/FLI1 driven tumor growth and metastasis blocking endothelial and neuro-ectodermal differentiation. *Proceedings of the National Academy of Sciences* **106**, 5324-9, (2009).

- 106 Ban, J. *et al.* Suppression of Deacetylase SIRT1 Mediates Tumor-Suppressive NOTCH Response and Offers a Novel Treatment Option in Metastatic Ewing Sarcoma. *Cancer Res.* **74**, 6578-88, (2014).
- 107 Park, H.-R., Jung, W.-W., Kim, H.-S. & Park, Y.-K. Microarray-based DNA methylation study of Ewing's sarcoma of the bone. *Oncol. Lett.* **8**, 1613-7, (2014).
- 108 Patel, N. *et al.* DNA Methylation and Gene Expression Profiling of Ewing Sarcoma Primary Tumors Reveal Genes That Are Potential Targets of Epigenetic Inactivation. *Sarcoma* **2012**, 11, (2012).
- 109 Ueno, H. *et al.* DNA Methylation Profile Distinguishes Clear Cell Sarcoma of the Kidney from Other Pediatric Renal Tumors. *PLoS One* **8**, e62233, (2013).
- 110 Petermann, R., Mossier, B. M. & Aryee, D. N. Oncogenic EWS-FlI1 interacts with hsRBP7, a subunit of human RNA polymerase II. *Oncogene* **17**, 603-10, (1998).
- 111 Toretsky, J. A. *et al.* Oncoprotein EWS-FLI1 Activity Is Enhanced by RNA Helicase A. *Cancer Res.* **66**, 5574-81, (2006).
- 112 Rorie, C. J. *et al.* The Ews/FlI-1 Fusion Gene Switches the Differentiation Program of Neuroblastomas to Ewing Sarcoma/Peripheral Primitive Neuroectodermal Tumors. *Cancer Res.* **64**, 1266-77, (2004).
- 113 Hancock, J. D. & Lessnick, S. L. A transcriptional profiling meta-analysis reveals a core EWS-FLI gene expression signature. *Cell Cycle* **7**, 250-6, (2008).
- 114 Prieur, A., Tirode, F., Cohen, P. & Delattre, O. EWS/FLI-1 Silencing and Gene Profiling of Ewing Cells Reveal Downstream Oncogenic Pathways and a Crucial Role for Repression of Insulin-Like Growth Factor Binding Protein 3. *Mol. Cell. Biol.* **24**, 7275-83, (2004).
- 115 Smith, R. *et al.* Expression profiling of EWS/FLI identifies NKX2.2 as a critical target gene in Ewing's sarcoma. *Cancer Cell* **9**, 405-16, (2006).
- 116 Sáinz-Jaspeado, M. *et al.* Caveolin-1 Modulates the Ability of Ewing's Sarcoma to Metastasize. *Mol. Cancer Res.* **8**, 1489-500, (2010).
- 117 Herrero-Martin, D. *et al.* Stable interference of EWS-FLI1 in an Ewing sarcoma cell line impairs IGF-1/IGF-1R signalling and reveals TOPK as a new target. *Br. J. Cancer* **101**, 80-90, (2009).
- 118 Grunewald, T. G. P. *et al.* High STEAP1 expression is associated with improved outcome of Ewing's sarcoma patients. *Ann. Oncol.* **23**, 2185-90, (2012).
- 119 Richter, G. H. S. *et al.* G-Protein coupled receptor 64 promotes invasiveness and metastasis in Ewing sarcomas through PGF and MMP1. *The Journal of Pathology* **230**, 70-81, (2013).
- 120 Rocchi, A. *et al.* CD99 inhibits neural differentiation of human Ewing sarcoma cells and thereby contributes to oncogenesis. *The Journal of Clinical Investigation* **120**, 668-80, (2010).
- 121 Staeger, M. S. *et al.* DNA Microarrays Reveal Relationship of Ewing Family Tumors to Both Endothelial and Fetal Neural Crest-Derived Cells and Define Novel Targets. *Cancer Res.* **64**, 8213-21, (2004).
- 122 Grunewald, T. G. P. *et al.* STEAP1 Is Associated with the Invasive and Oxidative Stress Phenotype of Ewing Tumors. *Mol. Cancer Res.* **10**, 52-65, (2012).
- 123 Wiles, E. T., Lui-Sargent, B., Bell, R. & Lessnick, S. L. BCL11B Is Up-Regulated by EWS/FLI and Contributes to the Transformed Phenotype in Ewing Sarcoma. *PLoS One* **8**, e59369, (2013).
- 124 Joo, J. *et al.* GLI1 Is a Central Mediator of EWS/FLI1 Signaling in Ewing Tumors. *PLoS One* **4**, e7608, (2009).
- 125 Kinsey, M., Smith, R. & Lessnick, S. L. NR0B1 Is Required for the Oncogenic Phenotype Mediated by EWS/FLI in Ewing's Sarcoma. *Mol. Cancer Res.* **4**, 851-9, (2006).
- 126 Schwentner, R. *et al.* EWS-FLI1 employs an E2F switch to drive target gene expression. *Nucleic Acids Res.* (2015).
- 127 Fuchs, B., Inwards, C. Y. & Janknecht, R. Vascular Endothelial Growth Factor Expression is Up-Regulated by EWS-ETS Oncoproteins and Sp1 and May Represent an Independent Predictor of Survival in Ewing's Sarcoma. *Clin. Cancer Res.* **10**, 1344-53, (2004).
- 128 Karnuth, B. *et al.* Differentially Expressed miRNAs in Ewing Sarcoma Compared to Mesenchymal Stem Cells: Low miR-31 Expression with Effects on Proliferation and Invasion. *PLoS One* **9**, e93067, (2014).
- 129 Friedman, R. C., Farh, K. K.-H., Burge, C. B. & Bartel, D. P. Most mammalian mRNAs are conserved targets of microRNAs. *Genome Res.* **19**, 92-105, (2009).
- 130 Ban, J. *et al.* Hsa-mir-145 is the top EWS-FLI1-repressed microRNA involved in a positive feedback loop in Ewing's sarcoma. *Oncogene* **30**, 2173-80, (2011).
- 131 De Vito, C. *et al.* Let-7a Is a Direct EWS-FLI-1 Target Implicated in Ewing's Sarcoma Development. *PLoS One* **6**, e23592, (2011).
- 132 Robin, T. P. *et al.* EWS/FLI1 Regulates EYA3 in Ewing Sarcoma via Modulation of miRNA-708, Resulting in Increased Cell Survival and Chemoresistance. *Mol. Cancer Res.* **10**, 1098-108, (2012).
- 133 McKinsey, E. L. *et al.* A novel oncogenic mechanism in Ewing sarcoma involving IGF pathway targeting by EWS/FlI1-regulated microRNAs. *Oncogene* **30**, 4910-20, (2011).
- 134 Parrish, J. K., Sechler, M., Winn, R. A. & Jedlicka, P. The histone demethylase KDM3A is a microRNA-

- 22-regulated tumor promoter in Ewing Sarcoma. *Oncogene* **34**, 257-62, (2015).
- 135 Nakatani, F. *et al.* miR-34a predicts survival of Ewing's sarcoma patients and directly influences cell
chemo-sensitivity and malignancy. *The Journal of Pathology* **226**, 796-805, (2012).
- 136 Bommer, G. T. *et al.* p53-Mediated Activation of miRNA34 Candidate Tumor-Suppressor Genes. *Curr.*
Biol. **17**, 1298-307, (2007).
- 137 Ferreira, D. M. S. *et al.* JNK1/c-Jun-Activation of the p53/miRNA-34a/Sirtuin1 Pathway Contributes to
Apoptosis Induced by Deoxycholic Acid in Rat Liver. *Mol. Cell. Biol.*, (2014).
- 138 Rathod, S. S., Rani, S. B., Khan, M., Muzumdar, D. & Shiras, A. Tumor suppressive miRNA-34a suppresses
cell proliferation and tumor growth of glioma stem cells by targeting Akt and Wnt signaling pathways.
FEBS Open Bio **4**, 485-95, (2014).
- 139 Quinodoz, S. & Guttman, M. Long noncoding RNAs: an emerging link between gene regulation and
nuclear organization. *Trends Cell Biol.* **24**, 651-63, (2014).
- 140 Hudson, W. H. & Ortlund, E. A. The structure, function and evolution of proteins that bind DNA and
RNA. *Nature Reviews Molecular Cell Biology* **15**, 749-60, (2014).
- 141 Michalik, K. M. *et al.* The Long Noncoding RNA MALAT1 Regulates Endothelial Cell Function and Ves-
sel Growth. *Circ. Res.*, (2014).
- 142 Wang, J. *et al.* Mutual inhibition between YAP and SRSF1 maintains long non-coding RNA, Malat1-
induced tumorigenesis in liver cancer. *Cell. Signal.* **26**, 1048-59, (2014).
- 143 Brunner, A. L. *et al.* Transcriptional profiling of long non-coding RNAs and novel transcribed regions
across a diverse panel of archived human cancers. *Genome Biol.* **13**, R75-R, (2012).
- 144 Fu, X.-D. & Ares Jr, M. Context-dependent control of alternative splicing by RNA-binding proteins. *Na-*
ture Reviews Genetics **15**, 689-701, (2014).
- 145 Paronetto, Maria P., Miñana, B. & Valcárcel, J. The Ewing Sarcoma Protein Regulates DNA Damage-
Induced Alternative Splicing. *Mol. Cell* **43**, 353-68, (2011).
- 146 Yang, L., Chansky, H. A. & Hickstein, D. D. EWS-Flt-1 Fusion Protein Interacts with Hyperphosphoryl-
ated RNA Polymerase II and Interferes with Serine-Arginine Protein-mediated RNA Splicing. *J. Biol.*
Chem. **275**, 37612-8, (2000).
- 147 Knoop, L. L. & Baker, S. J. The Splicing Factor U1C Represses EWS/FLI-mediated Transactivation. *J. Biol.*
Chem. **275**, 24865-71, (2000).
- 148 Knoop, L. L. & Baker, S. J. EWS/FLI Alters 5'-Splice Site Selection. *J. Biol. Chem.* **276**, 22317-22, (2001).
- 149 Jain, A. *et al.* DHX9 helicase is involved in preventing genomic instability induced by alternatively struc-
tured DNA in human cells. *Nucleic Acids Res.* **41**, 10345-57, (2013).
- 150 Sanchez, G., Delattre, O., Auboeuf, D. & Dutertre, M. Coupled alteration of transcription and splicing by
a single oncogene: Boosting the effect on cyclin D1 activity. *Cell Cycle* **7**, 2299-305, (2008).
- 151 Huang, G., Zhou, Z., Wang, H. & Kleinerman, E. S. CAPER- α alternative splicing regulates the expression
of vascular endothelial growth factor165 in Ewing sarcoma cells. *Cancer* **118**, 2106-16, (2012).
- 152 Ewing, J. Diffuse endothelioma of bone *Proc, New York Path. Soc.* **21**, 8, (1921).
- 153 Jenkin, R. D. T. Ewing's sarcoma a study of treatment methods. *Clin. Radiol.* **17**, 97-106, (1966).
- 154 Balamuth, N. J. & Womer, R. B. Ewing's sarcoma. *Lancet Oncol.* **11**, 184-92, (2010).
- 155 Womer, R. B. *et al.* Randomized Controlled Trial of Interval-Compressed Chemotherapy for the Treat-
ment of Localized Ewing Sarcoma: A Report From the Children's Oncology Group. *J. Clin. Oncol.* **30**,
4148-54, (2012).
- 156 Ginsberg, J. P. *et al.* Long-term Survivors of Childhood Ewing Sarcoma: Report From the Childhood
Cancer Survivor Study. *J. Natl. Cancer Inst.* **102**, 1272-83, (2010).
- 157 van Maldegem, A., Hogendoorn, P. & Hassan, A. The clinical use of biomarkers as prognostic factors in
Ewing sarcoma. *Clin. Sarc. Res.* **2**, 7, (2012).
- 158 Ludwig, J. A. Ewing sarcoma: historical perspectives, current state-of-the-art, and opportunities for tar-
geted therapy in the future. *Curr. Opin. Oncol.* **20**, 412-8, (2008).
- 159 Grier, H. E. *et al.* Addition of Ifosfamide and Etoposide to Standard Chemotherapy for Ewing's Sarcoma
and Primitive Neuroectodermal Tumor of Bone. *N. Engl. J. Med.* **348**, 694-701, (2003).
- 160 Granowetter, L. *et al.* Dose-Intensified Compared With Standard Chemotherapy for Nonmetastatic Ewing
Sarcoma Family of Tumors: A Children's Oncology Group Study. *J. Clin. Oncol.* **27**, 2536-41, (2009).
- 161 Brenner, J. C. *et al.* PARP-1 Inhibition as a Targeted Strategy to Treat Ewing's Sarcoma. *Cancer Res.* **72**,
1608-13, (2012).
- 162 Stewart, E. *et al.* Targeting the DNA Repair Pathway in Ewing Sarcoma. *Cell Rep.* **9**, 829-40, (2014).
- 163 Smith, M. A. *et al.* Synergistic Activity of PARP Inhibition by Talazoparib (BMN 673) with Temozolo-
mide in Pediatric Cancer Models in the Pediatric Preclinical Testing Program. *Clin. Cancer Res.* **21**, 819-
32, (2015).
- 164 Choy, E. *et al.* Phase II study of olaparib in patients with refractory Ewing sarcoma following failure of

- standard chemotherapy. *BMC Cancer* **14**, 813, (2014).
- 165 Tahara, M. *et al.* The Use of Olaparib (AZD2281) Potentiates SN-38 Cytotoxicity in Colon Cancer Cells by Indirect Inhibition of Rad51-Mediated Repair of DNA Double-Strand Breaks. *Mol. Cancer Ther.* **13**, 1170-80, (2014).
- 166 McCabe, N. *et al.* Deficiency in the Repair of DNA Damage by Homologous Recombination and Sensitivity to Poly(ADP-Ribose) Polymerase Inhibition. *Cancer Res.* **66**, 8109-15, (2006).
- 167 Bailey, M. L. *et al.* Glioblastoma Cells Containing Mutations in the Cohesin Component STAG2 Are Sensitive to PARP Inhibition. *Mol. Cancer Ther.* **13**, 724-32, (2014).
- 168 Norris, R. E., Adamson, P. C., Nguyen, V. T. & Fox, E. Preclinical evaluation of the PARP inhibitor, olaparib, in combination with cytotoxic chemotherapy in pediatric solid tumors. *Pediatr. Blood Cancer* **61**, 145-50, (2014).
- 169 Chen, C., Wonsley, D. R., Lemieux, M. E. & Kung, A. L. Differential Disruption of EWS-FLI1 Binding by DNA-Binding Agents. *PLoS One* **8**, e69714, (2013).
- 170 Smith, M. A., Ungerleider, R. S., Horowitz, M. E. & Simon, R. Influence of Doxorubicin Dose Intensity on Response and Outcome for Patients With Osteogenic Sarcoma and Ewing's Sarcoma. *J. Natl. Cancer Inst.* **83**, 1460-70, (1991).
- 171 Di Giandomenico, S. *et al.* Mode of action of trabectedin in myxoid liposarcomas. *Oncogene* **33**, 5201-10, (2014).
- 172 Baruchel, S. *et al.* A phase 2 trial of trabectedin in children with recurrent rhabdomyosarcoma, Ewing sarcoma and non-rhabdomyosarcoma soft tissue sarcomas: A report from the Children's Oncology Group. *Eur. J. Cancer* **48**, 579-85, (2012).
- 173 Bennani-Baiti, I. M., Machado, I., Llombart-Bosch, A. & Kovar, H. Lysine-specific demethylase 1 (LSD1/KDM1A/AOF2/BHC110) is expressed and is an epigenetic drug target in chondrosarcoma, Ewing's sarcoma, osteosarcoma, and rhabdomyosarcoma. *Hum. Pathol.* **43**, 1300-7, (2012).
- 174 Sakimura, R. *et al.* Antitumor effects of histone deacetylase inhibitor on Ewing's family tumors. *Int. J. Cancer* **116**, 784-92, (2005).
- 175 Owen, L. A., Kowalewski, A. A. & Lessnick, S. L. EWS/FLI Mediates Transcriptional Repression via NKX2.2 during Oncogenic Transformation in Ewing's Sarcoma. *PLoS One* **3**, e1965, (2008).
- 176 Ng, K. P. *et al.* Multiple aromatic side chains within a disordered structure are critical for transcription and transforming activity of EWS family oncoproteins. *Proc. Natl. Acad. Sci. U. S. A.* **104**, 479-84, (2007).
- 177 Erkizan, H. V. *et al.* A small molecule blocking oncogenic protein EWS-FLI1 interaction with RNA helicase A inhibits growth of Ewing's sarcoma. *Nat. Med.* **15**, 750-6, (2009).
- 178 Tosso, P. N. *et al.* Synthesis and Structure-Activity Relationship Studies of Small Molecule Disruptors of EWS-FLI1 Interactions in Ewing's Sarcoma. *J. Med. Chem.* **57**, 10290-303, (2014).
- 179 van der Ent, W. *et al.* Ewing sarcoma inhibition by disruption of EWSR1-FLI1 transcriptional activity and reactivation of p53. *J. Pathol.* **233**, 415-24, (2014).
- 180 Hanahan, D. & Weinberg, Robert A. Hallmarks of Cancer: The Next Generation. *Cell* **144**, 646-74, (2011).
- 181 Seccareccia, E. & Brodt, P. The role of the insulin-like growth factor-I receptor in malignancy: An update. *Growth Horm. IGF Res.* **22**, 193-9, (2012).
- 182 Rapraeger, A. C. Synstatin: a selective inhibitor of the syndecan-1-coupled IGF1R- α v β 3 integrin complex in tumorigenesis and angiogenesis. *The FEBS journal* **280**, 2207-15, (2013).
- 183 Mulvihill, M. J. *et al.* Discovery of OSI-906: a selective and orally efficacious dual inhibitor of the IGF-1 receptor and insulin receptor. *Future Med. Chem.* **1**, 1153-71, (2009).
- 184 Kurmasheva, R. T. *et al.* The Insulin-like Growth Factor-1 Receptor-Targeting Antibody, CP-751,871, Suppresses Tumor-Derived VEGF and Synergizes with Rapamycin in Models of Childhood Sarcoma. *Cancer Res.* **69**, 7662-71, (2009).
- 185 Ackermann, M., Morse, B., Delventhal, V., Carvajal, I. & Konerding, M. Anti-VEGFR2 and anti-IGF-1R-Adnectins inhibit Ewing's sarcoma A673-xenograft growth and normalize tumor vascular architecture. *Angiogenesis* **15**, 685-95, (2012).
- 186 Pappo, A. S. *et al.* A phase 2 trial of R1507, a monoclonal antibody to the insulin-like growth factor-1 receptor (IGF-1R), in patients with recurrent or refractory rhabdomyosarcoma, osteosarcoma, synovial sarcoma, and other soft tissue sarcomas: Results of a Sarcoma Alliance for Research Through Collaboration study. *Cancer* **120**, 2448-56, (2014).
- 187 Schöffski, P. *et al.* An open-label, phase 2 study evaluating the efficacy and safety of the anti-IGF-1R antibody cixutumumab in patients with previously treated advanced or metastatic soft-tissue sarcoma or Ewing family of tumours. *Eur. J. Cancer* **49**, 3219-28, (2013).
- 188 Amaral, A. T. *et al.* Trabectedin efficacy in Ewing sarcoma is greatly increased by combination with anti-IGF signaling agents. *Clin. Cancer Res.*, (2015).
- 189 Zhao, Y. & Adjei, A. A. Targeting Angiogenesis in Cancer Therapy: Moving Beyond Vascular Endothelial

- Growth Factor. *The Oncologist*, (2015).
- 190 Reddy, K. *et al.* Stromal cell-derived factor-1 stimulates vasculogenesis and enhances Ewing's sarcoma
tumor growth in the absence of vascular endothelial growth factor. *Int. J. Cancer* **123**, 831-7, (2008).
- 191 Zhou, Z., Yu, L. & Kleinerman, E. S. EWS-FLI-1 regulates the neuronal repressor gene REST, which con-
trols Ewing sarcoma growth and vascular morphology. *Cancer* **120**, 579-88, (2014).
- 192 DuBois, S. G., Marina, N. & Glade-Bender, J. Angiogenesis and vascular targeting in Ewing sarcoma.
Cancer **116**, 749-57, (2010).
- 193 Wagner, L. *et al.* Pilot study of vincristine, oral irinotecan, and temozolomide (VOIT regimen) combined
with bevacizumab in pediatric patients with recurrent solid tumors or brain tumors. *Pediatr. Blood Can-
cer* **60**, 1447-51, (2013).
- 194 Hillen, F. *et al.* A transgenic Tie2-GFP athymic mouse model; a tool for vascular biology in xenograft
tumors. *Biochem. Biophys. Res. Commun.* **368**, 364-7, (2008).
- 195 van der Schaft, D. W. J. *et al.* Tumor Cell Plasticity in Ewing Sarcoma, an Alternative Circulatory System
Stimulated by Hypoxia. *Cancer Res.* **65**, 11520-8, (2005).
- 196 Pardali, E. *et al.* Critical role of endoglin in tumor cell plasticity of Ewing sarcoma and melanoma. *Onco-
gene* **30**, 334-45, (2011).
- 197 Mantovani, A. *et al.* The chemokine system in cancer biology and therapy. *Cytokine Growth Factor Rev.*
21, 27-39, (2010).
- 198 Berghuis, D. *et al.* Pro-inflammatory chemokine-chemokine receptor interactions within the Ewing sar-
coma microenvironment determine CD8+ T-lymphocyte infiltration and affect tumour progression. *J.
Pathol.* **223**, 347-57, (2011).
- 199 Lissat, A. *et al.* Interferon- γ sensitizes resistant Ewing's sarcoma cells to tumor necrosis factor apoptosis-
inducing ligand-induced apoptosis by up-regulation of caspase-8 without altering chemosensitivity. *Am.
J. Pathol.* **170**, 1917-30, (2007).
- 200 Bennani-Baiti, I. M. *et al.* Intercohort Gene Expression Co-Analysis Reveals Chemokine Receptors as
Prognostic Indicators in Ewing's Sarcoma. *Clin. Cancer Res.* **16**, 3769-78, (2010).
- 201 Domanska, U. M. *et al.* A review on CXCR4/CXCL12 axis in oncology: No place to hide. *Eur. J. Cancer*
49, 219-30, (2013).
- 202 Lippitz, B. E. Cytokine patterns in patients with cancer: a systematic review. *Lancet Oncol.* **14**, e218-e28,
(2013).
- 203 Brennecke, P. *et al.* CXCR4 antibody treatment suppresses metastatic spread to the lung of intratibial hu-
man osteosarcoma xenografts in mice. *Clin. Exp. Metastasis* **31**, 339-49, (2014).
- 204 Krook, M. A. *et al.* Stress-Induced CXCR4 Promotes Migration and Invasion of Ewing Sarcoma. *Mol.
Cancer Res.* **12**, 953-64, (2014).
- 205 Berghuis, D. *et al.* The CXCR4-CXCL12 axis in Ewing sarcoma: promotion of tumor growth rather than
metastatic disease. *Clin. Sarc. Res.* **2**, 24, (2012).
- 206 Gupta, S. K. & Pillarisetti, K. Cutting Edge: CXCR4-Lo: Molecular Cloning and Functional Expression of
a Novel Human CXCR4 Splice Variant. *J. Immunol.* **163**, 2368-72, (1999).
- 207 Farzan, M. *et al.* The Role of Post-translational Modifications of the CXCR4 Amino Terminus in Stromal-
derived Factor 1 α Association and HIV-1 Entry. *J. Biol. Chem.* **277**, 29484-9, (2002).
- 208 Zhou, N. *et al.* Structural and Functional Characterization of Human CXCR4 as a Chemokine Receptor
and HIV-1 Co-receptor by Mutagenesis and Molecular Modeling Studies. *J. Biol. Chem.* **276**, 42826-33,
(2001).
- 209 Rapp, C., Snow, S., Laufer, T. & McClendon, C. L. The role of tyrosine sulfation in the dimerization of the
CXCR4:SDF-1 complex. *Protein Sci.* **22**, 1025-36, (2013).
- 210 Chabot, D. J., Chen, H., Dimitrov, D. S. & Broder, C. C. N-Linked Glycosylation of CXCR4 Masks Co-
receptor Function for CCR5-Dependent Human Immunodeficiency Virus Type 1 Isolates. *J. Virol.* **74**,
4404-13, (2000).
- 211 Stoll, G. *et al.* Systems biology of Ewing sarcoma: a network model of EWS-FLI1 effect on proliferation
and apoptosis. *Nucleic Acids Res.* **41**, 8853-71, (2013).
- 212 Vakkila, J., Jaffe, R., Michelow, M. & Lotze, M. T. Pediatric xancers are infiltrated predominantly by mac-
rophages and contain a paucity of dendritic cells: a major nosologic difference with adult tumors. *Clin.
Cancer Res.* **12**, 2049-54, (2006).
- 213 Verhoeven, D. H. J. *et al.* NK cells recognize and lyse Ewing sarcoma cells through NKG2D and DNAM-1
receptor dependent pathways. *Mol. Immunol.* **45**, 3917-25, (2008).
- 214 Cho, D. *et al.* Cytotoxicity of activated natural killer cells against pediatric solid tumors. *Clinical cancer
research : an official journal of the American Association for Cancer Research* **16**, 3901-9, (2010).
- 215 Berghuis, D. *et al.* Histone deacetylase inhibitors enhance expression of NKG2D ligands in Ewing sar-
coma and sensitize for natural killer cell-mediated cytotoxicity. *Clin. Sarc. Res.* **2**, 8, (2012).

- 216 Pahl, J. W. *et al.* Antibody-dependent cell lysis by NK cells is preserved after sarcoma-induced inhibition
of NK cell cytotoxicity. *Cancer Immunol. Immunother.* **62**, 1235-47, (2013).
- 217 Goodison, S. & Urquidi, V. The cancer testis antigen PRAME as a biomarker for solid tumor cancer man-
agement. *Biomark. Med.* **6**, 629-32, (2012).
- 218 Osterhoff, C., Ivell, R. & Kirchhoff, C. Cloning of a Human Epididymis-Specific mRNA, HE6, Encoding a
Novel Member of the Seven Transmembrane-Domain Receptor Superfamily. *DNA Cell Biol.* **16**, 379-89,
(1997).
- 219 Moreaux, J., Kassambara, A., Hose, D. & Klein, B. STEAP1 is overexpressed in cancers: A promising
therapeutic target. *Biochem. Biophys. Res. Commun.* **429**, 148-55, (2012).
- 220 Altwater, B. *et al.* Common Ewing sarcoma-associated antigens fail to induce natural T cell responses in
both patients and healthy individuals. *Cancer Immunol. Immunother.* **63**, 1047-60, (2014).
- 221 Thiel, U. *et al.* Specific recognition and inhibition of Ewing tumour growth by antigen-specific allo-re-
stricted cytotoxic T cells. *Br. J. Cancer* **104**, 948-56, (2011).
- 222 Evans, C. H. *et al.* EWS-FLI-1-targeted cytotoxic T-cell killing of multiple tumor types belonging to the
Ewing sarcoma family of tumors. *Clin. Cancer Res.* **18**, 5341-51, (2012).
- 223 Berghuis, D. *et al.* Reduced human leukocyte antigen expression in advanced-stage Ewing sarcoma: im-
plications for immune recognition. *The Journal of Pathology* **218**, 222-31, (2009).
- 224 Liebsch, L. *et al.* Ewing sarcoma dissemination and response to T-cell therapy in mice assessed by whole-
body magnetic resonance imaging. *Br. J. Cancer* **109**, 658-66, (2013).
- 225 Kailayangiri, S. *et al.* The ganglioside antigen GD2 is surface-expressed in Ewing sarcoma and allows for
MHC-independent immune targeting. *Br. J. Cancer* **106**, 1123-33, (2012).
- 226 Dominici, M. *et al.* Minimal criteria for defining multipotent mesenchymal stromal cells. The Interna-
tional Society for Cellular Therapy position statement. *Cytotherapy* **8**, 315-7, (2006).
- 227 Martinez, C., Hofmann, T. J., Marino, R., Dominici, M. & Horwitz, E. M. Human bone marrow mesen-
chymal stromal cells express the neural ganglioside GD2: a novel surface marker for the identification of
MSCs. *Blood* **109**, 4245-8, (2007).

Chapter 3

Expression of CCL21 in Ewing sarcoma shows an inverse correlation with metastases and is a candidate target for immunotherapy

L.G.L. Sand, D. Berghuis, K. Szuhai and P.C.W. Hogendoorn

Cancer Immunology and Immunotherapy, 2016, 65(8), 995-1002

ABSTRACT

Ewing sarcoma is an aggressive neoplasm predominantly occurring in adolescents and has a poor prognosis when metastasized. For patients with metastatic disease in particular, immunotherapy has been proposed as possible additive therapy with benefit. CCL21 activation-based immunotherapy was successful in preclinical studies in other tumor types, therefore we investigated CCL21 expression in EWS as potential target for immunotherapy. The *CCL21* RNA expression was determined in 21 Ewing sarcoma cell lines and 18 primary therapy-naïve Ewing sarcoma samples. In the tumor samples this was correlated to the number and CD4⁺/CD8⁺ ratio of infiltrating T-cells and clinical parameters. Higher RNA expression levels of *CCL21* significantly correlated with a lower CD4⁺/CD8⁺ T-cell ratio (P=0.009), good chemotherapeutic response (P=0.01) and improved outcome (P<0.001). In patients with metastases *CCL21* expression was significantly lower than in patients without (P<0.0005). *CCL21* expression was significantly higher in Ewing sarcoma tissue samples as compared to cell lines (P<0.01), implying the involvement of a stromal factor. Protein expression analysis of CCL21 and its receptor CCR7 in 24 therapy-naïve tumor demonstrated overall no expression in Ewing sarcoma cells. In conclusion, CCL21 is expressed in clinical Ewing sarcoma samples by non-tumor infiltrating stroma cells. The observed positive correlation with survival implies that CCL21 might be a potential prognostic marker for EWS and marks the potential of CCL21 immunotherapy in EWS.

KEYWORDS

bone tumor; soft tissue tumor; immunotherapy; tumor microenvironment; immune response

INTRODUCTION

Ewing sarcoma (EWS) is the third most common primary bone sarcoma predominantly occurring in children and adolescents [1]. It is characterized by aggressive/destructive local growth and has a high-grade malignant behavior, with (micro-) metastases at the time of presentation being common. Patients with metastases or recurrent disease have a poor outcome with 15-30% long-term survival [2,3].

To date, after the initial introduction of multimodal chemotherapy, no further improvement in survival of these patients has been accomplished and besides the classical parameters such as tumor site, resectability, response to chemotherapy and size no prognostic markers are in clinical use for decision making. EWS contains very low number of mutations compared to other tumors, which suggests that corrective apoptosis pathways are still functional, like the TNF-related apoptosis-inducing ligand (TRAIL) pathway [4-6]. The death receptor pathways and other apoptotic pathways are active in EWS and consequently the tumor is sensitive for activation of these pathways by natural killer (NK)-cells and cytotoxic T-cells [7-9]. Immunotherapy in Ewing sarcoma has been shown to have a promising potential role in vitro and is being tested in two clinical trials by administrating donor NK-cells (NCT01287104, NCT02100891) [7,8,10].

We previously investigated the immune microenvironment in EWS and demonstrated a relation between the number of infiltrating cytotoxic T-cells and patient outcome [11]. Expression levels of pro-inflammatory chemokines (particularly CXCL9, CXCL10 and CCL5) correlated positively with the number of infiltrating CD8⁺ T-cells [11]. Another potent T-cell

chemoattractant is CCL21, which acts via its receptor CCR7 as a single attractant or in combination with CXCL9 and CXCL10 [12,13]. In addition, CCL21 may increase dendritic cell-provoked T-cell responses, leading to more efficient anti-tumor immune responses [14,15]. As immunotherapy, the use of CCL21 has successfully been tested and a trial with dendritic cells expressing CCL21 showed even better results than CCL21 alone in non-small lung cancer [16]. Because of the immunogenic role of CCL21 and its immunotherapeutic potential, we studied the CCL21 expression in primary therapy-naïve Ewing sarcoma samples and EWS cell lines by analyzing the RNA expression levels of *CCL21*. The measured RNA expression levels were correlated with the number of infiltrating T-cells and the CD4⁺/CD8⁺ T-cell ratio in Ewing sarcoma samples. A reversed CD4⁺/CD8⁺ T-cell ratio has been reported as predictor of improved outcome in other tumors [17,18]. In our study the CD4⁺/CD8⁺T-cell ratio showed inverse correlation with the *CCL21* expression level and increased *CCL21* expression levels were associated with better survival. This relation suggests that testing for CCL21 levels in therapy-naïve EWS tumor samples might be used as a prognostic marker and supports a potential role for this cytokine in anti-tumor immunity.

MATERIALS AND METHODS

Clinical information on patient samples

18 cryopreserved primary therapy-naïve samples from 18 EWS patients, all containing more than 80% tumor cells as assessed by light microscopy, and a validation tissue microarray of formalin fixed paraffin embedded (FFPE) specimens of 16 tumors of 16 patients were obtained from the Department of Pathology, Leiden University Medical Center and were handled in a coded fashion, according the Dutch national ethical guidelines ('Code for Proper Secondary Use of Human Tissue'). Ewing sarcoma diagnosis was established according to WHO criteria, including immunohistochemistry (IHC) and *EWSR1* translocation detection either by real-time quantitative-reverse transcriptase PCR (RT-Q-PCR) or interphase FISH. Good chemotherapeutic response was defined by less than 10% morphologically viable tumor cells upon histopathologic evaluation of the post-chemotherapy resection specimen [20,21]. Median patient age at diagnosis of the cohort was 17.5 years (range of 5-35 years) (**Table S1**).

Ewing sarcoma cell lines

Ewing sarcoma cell lines (n=21) were obtained from multiple sources: L-1062 and L-872 were established in-house [22]; CHP100, RM-82, IARC-EW7, TC32 and 6647, CHP100, RM-82, IARC-EW-7, WE-68, IARC-EW-3, STA-ET-2.1, TTC-466, STA-ET-10, CADO-ES1, TC-71, VH-64, COH and STA-ET-1 were obtained from the EuroBoNeT consortium collection (Institute of Pathology, University Medical Center, Düsseldorf, Germany) [23] and SK-ES-1, SK-NM-C, A-673 and R-D-ES from the American Type Culture Collection (ATCC). All cell lines and primary culture L-4027 were cultured in a monolayer under equal conditions and in Iscove's Modified Dulbecco's Medium containing GlutaMAX supplement, supplemented with 1% streptomycin/penicillin and 10% heat-inactivated FCS (all from Life Technologies, Bleiswijk, The Netherlands). Authentication of cell lines using Powerplex 1.2 and CellID STR (Promega, Leiden, The Netherlands) and mycoplasma DNA Q-PCR screening were regularly performed on all cell lines.

RNA isolation

Total RNA was isolated using TRIzol Reagent (Life Technologies, Bleiswijk, The Nether-

lands) according to manufacturer's instructions. RNA concentration was measured using Nanodrop and quality of the RNA was determined using Bioanalyzer2000 RNA Nano chip (Agilent Technology, Amstelveen, The Netherlands). Samples with a RNA integrity number ≥ 5 were included for RT-Q-PCR analysis.

RT-Q-PCR analysis and Fluidigm

cDNA generation and RT-Q-PCR using Fluidigm BioMark system was performed according to the H format protocol of the manufacturer (QIAGEN, Venlo, The Netherlands). Samples were prepared for RT-Q-PCR using a 96x96 dynamic array chip and performed using BioMark HD system (Fluidigm, San Francisco, CA, USA). All primers for this array chip were obtained from QIAGEN (Venlo, The Netherlands) including nine control genes: RPL13A, BTF3, YWHAZ, UBE2D2, ATP6V1G1, IPO8, HBS1L, AHSP and TBP. Samples were measured in duplicates and analyzed using BioMark software, delivered with the HD system.

Detection of infiltrating T-lymphocytes

Number of CD4 and CD8 positive T-cells were determined according to Berghuis *et al.* [11]. In brief, FFPE tumor sections were stained for CD3 (Dako, Heverlee, Belgium), CD4 and CD8 (Novocastra, Newcastle upon Tyne, United Kingdom) and scanned with Zeiss LSM-510 confocal microscope (Carl Zeiss AG, Göttingen, Germany). In each section 10 areas were selected, digital photographed and lymphocytes were counted.

Immunohistochemistry

Tumor sections were stained with anti- CCL21 (Sigma-Aldrich, Steinheim, Germany) and CCR7 (Abcam, Cambridge, United Kingdom) antibodies. Extensive validation data for anti-CCL21 antibody (HPA051210) using IHC on various tissue microarray and western blot are accessible at the Human Protein Atlas portal [23]. Sections were dewaxed, rehydrated and were subjected to citrate pH6.0 (CCL21) or Tris-EDTA pH9 (CCR7) antigen retrieval. Sections stained for CCL21 expression were incubated with 5% ELK milk for 30 min at room temperature and incubated with anti-CCL21 (1:600) in 5% ELK overnight at 4 °C. Sections stained for CCR7 expression were incubated 1.5% BSA with anti-CCR7 (1:2000) overnight at 4 °C. Afterwards sections were incubated with Immunologic Poly-HRP-GAM/R/R IgG (Leica Biosystems, Eindhoven, The Netherlands) and Dako liquid DAB⁺ Substrate Chromogen System (Dako, Heverlee, Belgium). Scanning of the slides was performed by Philips Ultra Fast Scanner (Philips Healthcare, Eindhoven, Netherlands). Tonsil tissues, both regular and

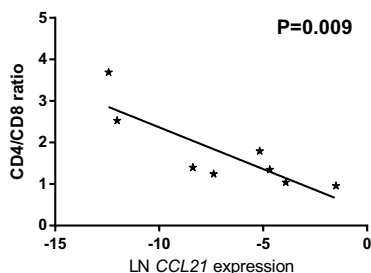


Figure 1: Increased CCL21 RNA expression correlates with reversed CD4+/CD8+ ratio of infiltrating T-cells. CCL21 RNA expression levels of samples with available high quality RNA and high quality FFPE material (n=8) were natural log transformed and correlated to the ratio between the total counted CD3⁺CD4⁺ and CD3⁺CD8⁺ infiltrating T-cells. P-value of the linear regression analysis is demonstrated.

decalcified FFPE processed, were used as a control. All slides were evaluated by at least two experienced persons of which one was a reference pathologist (PCWH).

Statistical analysis

Survival curves were calculated using the Kaplan-Meier method and P-values were calculated using the log-rank test using SPSS 20 (IBM Inc. Amsterdam, The Netherlands) and Prism Graphpad 6 (Graphpad Software Inc. La Jolla, CA, USA). Multivariate analysis of the parameters could not be performed do to the limited number of samples. Correlations were calculated with SPSS 20 using Pearson or Spearman correlation. Linear correlations were calculated with Prims Graphpad 6. High RNA expression was set as expression above the median. Student t-tests P-value was calculated using Prism Graphpad assuming non parametric distribution due to limited numbers of samples and was corrected using Manley-Welch correction.

RESULTS

RNA expression of *CCL21* was analyzed in 18 primary therapy-naïve tumor samples and the expression levels were correlated with the immunohistochemical staining of the CD4⁺ and CD8⁺ infiltrating T-cells in eight tissue samples for which sufficient FFPE material was still available (Table S2). In these samples, the *CCL21* expression was inversely correlated to CD4⁺/CD8⁺ T-cell ratio (Figure 1). However, the absolute numbers of CD8⁺ or CD4⁺ T-cells did not correlate with *CCL21* expression and varied widely between the samples (data not shown). Since a high CD8⁺ T-cells infiltration was associated in Ewing sarcoma with a better outcome, we correlated *CCL21* RNA expression levels in therapy-naïve tumor samples with development of metastases, survival and chemotherapeutic response. Kaplan-Meier survival analysis demonstrated that an increased *CCL21* expression correlated significantly both with improved EFS and OS (P=0.0001; P=0.0004) (Figure 2A-B). Moreover, natural logarithm transformed *CCL21* expression was significantly higher in patient samples who did not develop a metastasis compared to patients who did (P<0.0005) (Figure 2C). However, no correla-

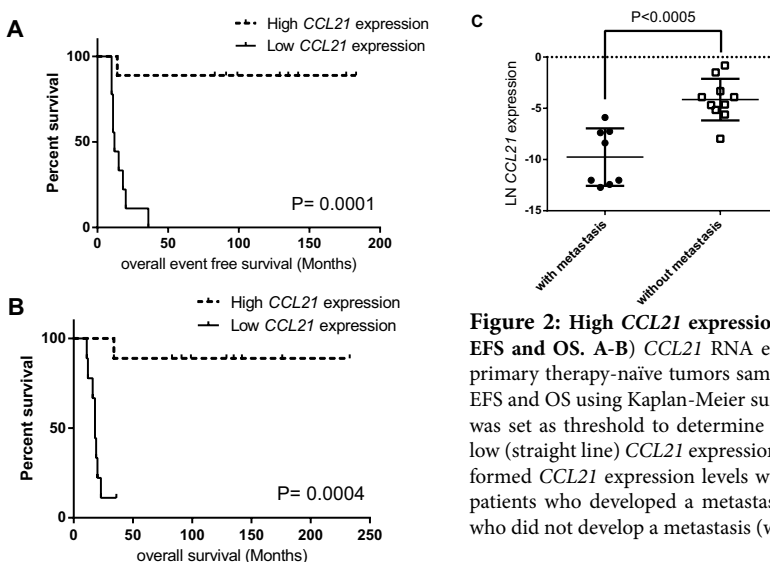


Figure 2: High *CCL21* expression correlated to better EFS and OS. A-B) *CCL21* RNA expression levels of the primary therapy-naïve tumors samples were correlated to EFS and OS using Kaplan-Meier survival analysis. Median was set as threshold to determine high (dotted line) and low (straight line) *CCL21* expression. C) Natural log transformed *CCL21* expression levels were compared between patients who developed a metastasis (with) and patients who did not develop a metastasis (without).

tion with metastasis at diagnosis was observed (data not shown). The improved survival may be linked to a better chemotherapeutic response as correlation between good response and increased *CCL21* expression was observed ($P=0.02$). It should be noted that good response to chemotherapy was correlated with improved outcome ($P=0.008$).

In addition, we investigated the *CCL21* RNA expression in 21 cell lines and 1 primary culture. The *CCL21* expression level in the cell lines was significantly lower than the in therapy-naïve tumor samples (Figure 3), with a large variation of expression levels between tumor samples as compared to cell lines.

To show that the expression difference of *CCL21* is derived from infiltrating immune cells in the tumor tissues we studied *CCL21* expression at protein level. The eight cases of which sufficient FFPE material was available were stained for *CCL21* using IHC. In addition, the tumor samples were stained for CCR7, the receptor of *CCL21*. In the tumor tissue Ewing sarcoma cells were negative for *CCL21* and CCR7 while infiltrating stromal cells did show expression of both *CCL21* and CCR7. An additional tissue micro array contacting 16 EWS cases was included for validation of the CCR7 and *CCL21* expression. Similarly to the other cases, all but one of the cases included in the TMA block were all EWS cells were negative for both CCR7 and *CCL21* (Figure 4).

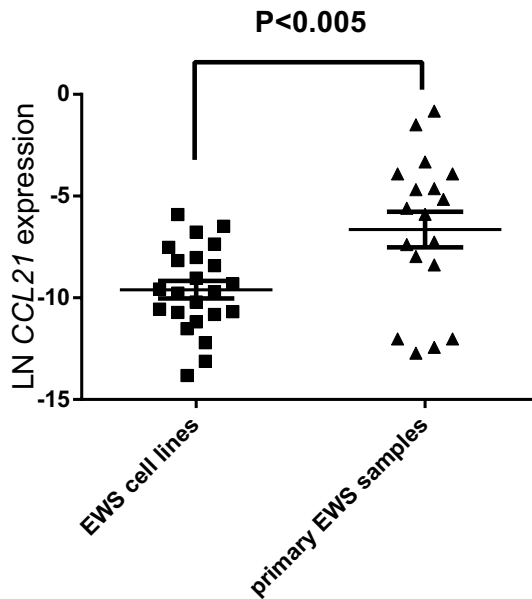


Figure 3: RNA expression levels of *CCL21* were significantly higher in tumors compared to cell lines. *CCL21* expression levels of 21 cell lines and 1 primary culture were compared to expression levels of the primary therapy-naïve tumor samples.

DISCUSSION

Previously, we demonstrated that pro-inflammatory chemokines CXCL9 and CXCL10 were associated with an increase in tumor infiltrating CD8⁺ T-cells [11]. CCL21 is, like CXCL9 and CXCL10, a CD8⁺ T-cell chemoattractant and its potency is enhanced by the interaction with CXCL9, CXCL10 and interferon gamma (IFN γ) [13]. This prompted us to further investigate the role of CCL21 in Ewing sarcoma. We observed that an increased *CCL21* RNA expression was correlated with an decreased CD4⁺/CD8⁺ ratio. It is likely that these CD3⁺CD8⁺ positive

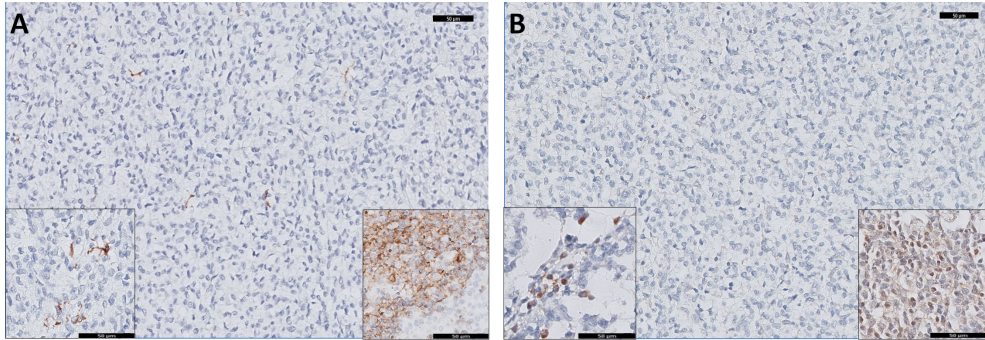


Figure 4: Neither CCR7 nor CCL21 expression observed in Ewing sarcoma cells by immune-histochemical detection. Eight tumor samples included in the RNA expression analysis and a TMA with 16 samples in duplicate were stained for CCR7 and CCL21 (20 times magnification). **A)** Tumor cells showed no expression, while infiltrating stromal cells showed expression of CCR7 (left inset, 40 times magnification), positive control is in the right inset from tonsil. **B)** Tumor cells showed no expression, while infiltrating stromal cells showed expression of CCL21 (left inset, 40 times magnification), positive control is in the right inset from tonsil. A scale bar of 50 μ m is included in the images.

lymphocytes are T-cells but the presence of CD3⁺CD8⁺ NK T-cells cannot be excluded [24]. In addition, increased *CCL21* expression correlated with both better EFS and OS and inversely correlated with the development of metastasis. These observations may point to a role of *CCL21* in the anti-tumor immune response related to the proportion and type of immune cells present in or around the tumor in EWS patients [25-27]. Even though the presence of infiltrating immune cells in pediatric sarcomas, particularly in Ewing sarcoma, was found to be limited [28], the effect of these cells with regards to therapy response is significant.

A second factor which might have had an influence on the observed correlation with patient survival is the chemotherapeutic response of the tumor, which is known to be a marker for survival [29,20,30]. Patients with a good chemotherapeutic response had a higher *CCL21* expression in the tumor sample compared to patients with a poor response. Although it is generally believed that chemotherapy has an immunosuppressive effect by decreasing the number of leukocytes, by now it has become clear that certain chemotherapeutic agents can augment the tumor immunogenicity and stimulate dendritic cell maturation [31-33]. In mice combining *CCL21* immunotherapy with the chemotherapeutic agent paclitaxel had a synergistic effect [34]. *CCL21* attracts dendritic cells and is suggested to improve the T-cell activation of mature dendritic cells [35,14]. Increased expression of *CCL21* might be associated with increased number of dendritic cells or an improved immunologic response upon tumor cell death. In patients with *CCL21* producing cells present chemotherapy could enhance the antitumor immunity and would lead to a better chemotherapeutic response. We note that our

study based on a small patient cohort, therefore a larger study would be needed to validate the observed correlations using therapy-naïve samples.

The significantly higher *CCL21* expression in primary therapy-naïve tumors compared to EWS cell lines suggests the involvement of a stromal factor in *CCL21* expression. *CCL21* expression can be enhanced by the interaction with CXCL9, CXCL10 and IFN γ [13]. However, we reported earlier the absence of *CCL21* expression in cell lines even after IFN γ stimulation indicating that this might be regulated by the EWSR1-FLI1 transcription factor [11,3]. In this study some cell lines had, although low, *CCL21* expression. The difference in *CCL21* expression between tumor samples and cell lines might be not only caused by a stromal factor but could also be due to selective *in vitro* culture conditions. Therefore, the protein expression levels and localization of *CCL21* was determined in EWS patients samples using IHC and demonstrated that *CCL21* expression was restricted to tumor infiltrating cells and not present in Ewing sarcoma cells. In addition, only in one sample CCR7 expression was detected in EWS cells. EWSR1-ETS is known to downregulate many chemokines and chemokine receptors, directly or indirectly, for example by altering regulatory miRNA expression levels and pattern[3]. Of these the let-7 miRNA family is known to regulate expression of the *CCL21*-CCR7 [36]. The tumor suppressor let-7a is, for example, known to be directly downregulated by EWSR1-ETS but this decrease of let-7a does not lead to increased CCR7 expression like in breast cancer cells [37,38]. In several studies have investigated the role of the let-7 family in EWS and demonstrated increase of some members, mainly let-7g, in tumor samples. These studies also revealed various pathways in which these let-7 family members play a role, however none of them have could establish a direct connection between *CCL21* or CCR7 and let-7 [39-41,37,38].

It is important to note that high *CCL21* expression observed in the tumor cell reported in other tumors, for example bladder cancer and breast cancer, were found to be associated with an increased proliferation, number of metastases and a suppressive immune reaction. These tumors expressed high levels of *CCL21* and/or CCR7, which might have led to paracrine or autocrine activation of a pro-tumorigenic *CCL21*/CCR7 axis [42,25,27]. However, as no *CCL21* expression was detected in the EWS cells and CCR7 expression only in one sample, an active *CCL21*/CCR7 axis in EWS cells is unlikely. In studies correlating *CCL21* and CCR7 expression not only the expression level but also the source tumor derived versus infiltrating stromal cells should be considered and recorded.

The potency of immunotherapy to treat EWS has been demonstrated by a number of studies [7,8,10,43]. *CCL21* is a chemoattractant for dendritic cells, cytotoxic T-cells and natural killer cells and can improve the immune response, therefore it has been tested as an immunotherapeutic in preclinical and clinical settings [15,34,16]. It has been tested as a single agent and combining it with chemotherapy can have a synergistic effect [34]. This might be true for EWS as well, considering the increased expression *CCL21* in patients with a good chemotherapeutic response. However, prior to administration of *CCL21* immunotherapy determination of CCR7 expression of in EWS samples may be needed, as increased expression of *CCL21* and CCR7 expression in tumor cells was found to have negative effect and, one out the 24 tested EWS samples showed high CCR7 expression. For this case *CCL21* administration might have resulted in an adverse effect, but further studies are needed to draw a firm conclusion on that. In addition, the potential of *CCL21* treatment in not *CCL21* primed tumors, meaning no *CCL21* expression was present, should be further investigated.

In conclusion, in this study we showed that patients with increased *CCL21* RNA expression have a better EFS and OS. In addition, protein expression of *CCL21* and its receptor CCR7

were overall not detected in EWS cells, indicating the absence of pro-tumorigenic paracrine and autocrine loops in most EWS samples. This tumor entity might therefore serve as a good target for an immunotherapy approach based on the use of CCL21. Furthermore, expression levels of *CCL21* might be used as a potential prognostic marker for survival.

ACKNOWLEDGEMENTS

This study was supported by National organization for Scientific Research (NWO) Grant NWO-TOP GO 854.10.012 and we thank Inge Briaire-de Bruijn (Department of Pathology) for her technical expertise and Ron Wolterbeek (Department of Medical Statistics) for his expertise on statistics.

REFERENCES

- 1 De Alava, E., Lessnick, S. L. & Sorensen, P. H. in *WHO Classification of Tumors of Soft Tissue and Bone* (eds C.D.M. Fletcher, J.A. Bridge, P. C. W. Hogendoorn, & F. Mertens) 306-9 (IARC, 2013).
- 2 Ladenstein, R. *et al.* Primary disseminated multifocal Ewing sarcoma: results of the Euro-EWING 99 trial. *J Clin Oncol* **28**, 3284-91, (2010).
- 3 Sand, L. G. L., Szuhai, K. & Hogendoorn, P. C. W. Sequencing overview of Ewing sarcoma: a journey across genomic, epigenomic and transcriptomic landscapes. *Int J Mol Sci* **16**, 16176-215, (2015).
- 4 Lawrence, M. S. *et al.* Mutational heterogeneity in cancer and the search for new cancer-associated genes. *Nature* **499**, 214-8, (2013).
- 5 Kontny, H. U. *et al.* Sensitivity of Ewing's sarcoma to TRAIL-induced apoptosis. *Cell Death Differ* **8**, 506-14, (2001).
- 6 Lissat, A. *et al.* Interferon- γ sensitizes resistant Ewing's sarcoma cells to tumor necrosis factor apoptosis-inducing ligand-induced apoptosis by up-regulation of caspase-8 without altering chemosensitivity. *Am J Pathol* **170**, 1917-30, (2007).
- 7 Verhoeven, D. H. J. *et al.* NK cells recognize and lyse Ewing sarcoma cells through NKG2D and DNAM-1 receptor dependent pathways. *Mol Immunol* **45**, 3917-25, (2008).
- 8 Pahl, J. W. *et al.* Antibody-dependent cell lysis by NK cells is preserved after sarcoma-induced inhibition of NK cell cytotoxicity. *Cancer Immunol Immunother* **62**, 1235-47, (2013).
- 9 de Hooge, A. S. K. *et al.* Expression of cellular FLICE inhibitory protein, caspase-8, and protease inhibitor-9 in Ewing sarcoma and implications for susceptibility to cytotoxic pathways. *Clin Cancer Res* **13**, 206-14, (2007).
- 10 Evans, C. H. *et al.* EWS-FLI-1-targeted cytotoxic T-cell killing of multiple tumor types belonging to the Ewing sarcoma family of tumors. *Clin Cancer Res* **18**, 5341-51, (2012).
- 11 Berghuis, D. *et al.* Pro-inflammatory chemokine-chemokine receptor interactions within the Ewing sarcoma microenvironment determine CD8+ T-lymphocyte infiltration and affect tumour progression. *J Pathol* **223**, 347-57, (2011).
- 12 Lo, J. C. *et al.* Differential regulation of CCL21 in lymphoid/nonlymphoid tissues for effectively attracting T cells to peripheral tissues. *J Clin Invest* **112**, 1495-505, (2003).
- 13 Sharma, S. *et al.* SLC/CCL21-mediated anti-tumor responses require IFN γ , MIG/CXCL9 and IP-10/CXCL10. *Mol Cancer* **2**, 22-, (2003).
- 14 Hong, C. Y., Lee, H. J., Kim, H. J. & Lee, J. J. The lymphoidchemokine CCL21 enhances the cytotoxic T lymphocyte-inducing functions of dendritic cells. *Scand J Immunol* **79**, 173-80, (2014).
- 15 Lin, Y., Sharma, S. & John, M. S. CCL21 Cancer Immunotherapy. *Cancers (Basel)* **6**, 1098-110, (2014).
- 16 Lee, J. M. *et al.* Phase I trial of trans-thoracic injection of CCL21 gene modified dendritic cells in human non-small cell lung carcinoma. *J Surg Res* **186**, 558, (2014).
- 17 Shah, W. *et al.* A reversed CD4/CD8 ratio of tumor-infiltrating lymphocytes and a high percentage of CD4(+)/FOXP3(+) regulatory T cells are significantly associated with clinical outcome in squamous cell carcinoma of the cervix. *Cell Mol Immunol* **8**, 59-66, (2011).
- 18 García-Martínez, E. *et al.* Tumor-infiltrating immune cell profiles and their change after neoadjuvant chemotherapy predict response and prognosis of breast cancer. *Breast Cancer Res* **16**, 488, (2014).
- 19 van der Woude, H. J. *et al.* Monitoring the effect of chemotherapy in Ewing's sarcoma of bone with MR imaging. *Skeletal Radiol* **23**, 493-500, (1994).

- 20 Picci, P. *et al.* Prognostic significance of histopathologic response to chemotherapy in nonmetastatic Ewing's sarcoma of the extremities. *J Clin Oncol* **11**, 1763-9, (1993).
- 21 Szuhai, K., Ijszenga, M., Tanke, H. J., Rosenberg, C. & Hogendoorn, P. C. W. Molecular cytogenetic characterization of four previously established and two newly established Ewing sarcoma cell lines. *Cancer Genet Cytogenet* **166**, 173-9, (2006).
- 22 Ottaviano, L. *et al.* Molecular characterization of commonly used cell lines for bone tumor research: A trans-European EuroBoNet effort. *Genes Chromosomes Cancer* **49**, 40-51, (2010).
- 23 Pontén, F., Jirstrom, K. & Uhlen, M. The Human Protein Atlas—a tool for pathology. *J Pathol* **216**, 387-93, (2008).
- 24 Kronenberg, M. TOWARD AN UNDERSTANDING OF NKT CELL BIOLOGY: Progress and Paradoxes. *Annu Rev Immunol* **23**, 877-900, (2005).
- 25 Tutunea-Fatan, E., Majumder, M., Xin, X. & Lala, P. K. The role of CCL21/CCR7 chemokine axis in breast cancer-induced lymphangiogenesis. *Mol Cancer* **14**, 35, (2015).
- 26 Shields, J. D. *et al.* Chemokine-mediated migration of melanoma cells towards lymphatics - a mechanism contributing to metastasis. *Oncogene* **26**, 2997-3005, (2007).
- 27 Shields, J. D., Kourtis, I. C., Tomei, A. A., Roberts, J. M. & Swartz, M. A. Induction of lymphoidlike stroma and immune escape by tumors that express the chemokine CCL21. *Science* **328**, 749-52, (2010).
- 28 Vakkila, J., Jaffe, R., Michelow, M. & Lotze, M. T. Pediatric cancers are infiltrated predominantly by macrophages and contain a paucity of dendritic cells: a major nosologic difference with adult tumors. *Clin Cancer Res* **12**, 2049-54, (2006).
- 29 Picci, P. *et al.* Chemotherapy-induced tumor necrosis as a prognostic factor in localized Ewing's sarcoma of the extremities. *J Clin Oncol* **15**, 1553-9, (1997).
- 30 Huang, H.-Y. *et al.* Ewing sarcomas with p53 mutation or p16/p14ARF homozygous deletion: a highly lethal subset associated with poor chemoresponse. *J Clin Oncol* **23**, 548-58, (2005).
- 31 Zitvogel, L., Apetoh, L., Ghiringhelli, F. & Kroemer, G. Immunological aspects of cancer chemotherapy. *Nat Rev Immunol* **8**, 59-73, (2008).
- 32 Ma, Y. *et al.* Anticancer Chemotherapy-Induced Intratumoral Recruitment and Differentiation of Antigen-Presenting Cells. *Immunity* **38**, 729-41, (2013).
- 33 Emens, L. A. & Middleton, G. The Interplay of Immunotherapy and Chemotherapy: Harnessing Potential Synergies. *Cancer Immunol. Res.* **3**, 436-43, (2015).
- 34 Chen, P. *et al.* Low-dose paclitaxel improves the therapeutic efficacy of recombinant adenovirus encoding CCL21 chemokine against murine cancer. *Cancer Sci* **105**, 1393-401, (2014).
- 35 Murphy, P. M. Double Duty for CCL21 in Dendritic Cell Trafficking. *Immunity* **32**, 590-2, (2010).
- 36 Kim, S.-J. *et al.* MicroRNA let-7a suppresses breast cancer cell migration and invasion through downregulation of C-C chemokine receptor type 7. *Breast Cancer Res* **14**, R14, (2012).
- 37 De Vito, C. *et al.* Let-7a Is a Direct EWS-FLI-1 Target Implicated in Ewing's sarcoma Development. *PLoS One* **6**, e23592, (2011).
- 38 Zhang, Z. *et al.* Let-7a Functions as a Tumor Suppressor in Ewing's Sarcoma Cell Lines Partly by Targeting Cyclin-Dependent Kinase 6. *DNA Cell Biol* **33**, 136-47, (2014).
- 39 Karnuth, B. *et al.* Differentially Expressed miRNAs in Ewing sarcoma Compared to Mesenchymal Stem Cells: Low miR-31 Expression with Effects on Proliferation and Invasion. *PLoS One* **9**, e93067, (2014).
- 40 Hameiri-Grossman, M. *et al.* The association between let-7, RAS and HIF-1 α in Ewing Sarcoma tumor growth. *Oncotarget; Vol 6, No 32*, (2015).
- 41 Sohn, E. J., Park, J., Kang, S.-i. & Wu, Y.-P. Accumulation of pre-let-7g and downregulation of mature let-7g with the depletion of EWS. *Biochem Biophys Res Commun* **426**, 89-93, (2012).
- 42 Mo, M. *et al.* CCL21/CCR7 enhances the proliferation, migration, and invasion of human bladder cancer T24 cells. *PLoS One* **10**, e0119506, (2015).
- 43 Berghuis, D. *et al.* Histone deacetylase inhibitors enhance expression of NKG2D ligands in Ewing sarcoma and sensitize for natural killer cell-mediated cytotoxicity. *Clin Sarc Res* **2**, 8, (2012).

SUPPLEMENTARY DATA

Table S1: Clinical details of the primary therapy-naïve tumor samples.

| Patient number | Age (yrs) | Sex | Primary tumor site | Metastasis at diagnosis ^a | Starting treatment protocol | Response to chemotherapy ^b | Translocation | Metastasis later ^c | Re-lapse ^d | EFS Time (month) | EFS ^e OS Time (month) | OS ^f | |
|----------------|-----------|--------|--------------------|--------------------------------------|-----------------------------|---------------------------------------|--------------------------|-------------------------------|-----------------------|------------------|----------------------------------|-----------------|---|
| L318 | 35 | male | proximal radius | 0 | CESS86 | 1 | EWS-FLI1 | 0 | 0 | 183 | 0 | 233 | 0 |
| L463 | 24 | male | thorax wall | 0 | CESS86 | ND | EWS-FLI1 | 1 | 1 | 12 | 1 | 20 | 1 |
| L469 | 19 | female | distal fibula | 0 | EICES | 0 | EWS-FLI1 | 1 | 1 | 20 | 1 | 23 | 1 |
| L513 | 11 | male | pelvis | 1 | EICES | ND | EWS-FLI1 | 0 | ND | 18 | 1 | 18 | 1 |
| L629 | 5 | male | tibia + fibula | 1 | EuroEwing99 | 1 | Clinical Ewing sarcoma * | 0 | 0 | 135 | 0 | 135 | 0 |
| L683 | 17 | male | tibia | 0 | EICES | 0 | EWS-FLI1 | 1 | 0 | 10 | 1 | 16 | 1 |
| L848 | 15 | female | humerus | 1 | EuroEwing99 | 1 | EWS-FLI1 | 0 | 0 | 142 | 0 | 142 | 0 |
| L1034 | 18 | male | pelvis | 1 | EuroEwing99 | 0 | EWS-FLI1 | 1 | 0 | 11 | 1 | 18 | 1 |
| L1098 | 10 | male | femur | 0 | EuroEwing99 | 1 | EWS-FLI1 | 0 | 0 | 129 | 0 | 129 | 0 |
| L1220 | 19 | male | os pubis | 1 | EuroEwing99 | ND | EWS-FLI1 | 1 | 0 | 10 | 1 | 11 | 1 |
| L1232 | 14 | male | humerus | 0 | EuroEwing99 | ND | EWS-FLI1 | 0 | ND | 14 | 1 | 34 | 1 |
| L1379 | 13 | male | fibula | 1 | EuroEwing99 | 0 | EWS-FLI1 | 0 | 0 | 99 | 0 | 99 | 0 |
| L1489 | 25 | male | pelvis | 0 | EuroEwing99 | 1 | EWS break by FISH | 0 | 0 | 91 | 0 | 91 | 0 |
| L1570 | 12 | male | humerus | 0 | EuroEwing99 | 1 | EWS-FLI1 | 0 | 0 | 83 | 0 | 83 | 0 |
| L1722 | 18 | male | humerus | 0 | EuroEwing99 | 1 | EWS-FLI1 | 1 | 1 | 36 | 1 | 36 | 0 |
| L2154 | 11 | female | femur | 1 | EuroEwing99 | 1 | EWS-FLI1 | 0 | 0 | 176 | 0 | 176 | 0 |
| L2161 | 19 | male | pelvis | 0 | EuroEwing99 | 0 | EWS-FLI1 | 1 | 0 | 11 | 1 | 12 | 1 |
| L2162 | 19 | male | pelvis | 1 | EuroEwing99 | ND | EWS-FLI1 | 1 | 0 | 15 | 1 | 19 | 1 |

ND: Not determined; EFS: Event free survival; OS: Overall survival ^{a-c,d,e} 1: Event reported or 0: No event reported; ^b 1: < 10% tumor vitality or 0 > 10% tumor vitality
^f 1: Dead or 0: Alive.

*: a case with RT-Q-PCR negativity for *EWSR1-FLI1*, *EWSR1-ERG* in diagnostic settings, negativity for *BCOR-CCNB3* RT-Q-PCR and the lack of *EWSR1*, *FUS* and *CIC* split apart signals from FFPE sections. Clinical as well as morphological and immunohistochemically consistent with Ewing Sarcoma.

ND: Not determined

EFS: Event free survival

OS: Overall survival

^{a,c,d,e} 1: Event reported or 0: No event reported

^b 1: < 10% tumor vitality or 0 > 10% tumor vitality

^f 1: Dead or 0: Alive.

*: a case with RT-Q-PCR negativity for *EWSR1-FLI1*, *EWSR1-ERG* in diagnostic settings, negativity for *BCOR-CCNB3* RT-Q-PCR and the lack of *EWSR1*, *FUS* and *CIC* split apart signals from FFPE sections. Clinical as well as morphological and immunohistochemically consistent with Ewing Sarcoma.

Table S2: Counts of T-cells and CCL21 RNA expression levels

| Patient | Normalized CCL21 RNA expression | Tumor infiltrating T-cells (cells/mm ²) | | |
|---------|------------------------------------|---|----------|-----------------|
| | | CD3+CD4+ | CD3+CD8+ | CD4+/CD8+ ratio |
| L2162 | 0.000004 | 118 | 32 | 3.68 |
| L1722 | 0.000006 | 96 | 38 | 2.53 |
| L1220 | 0.00023 | 49 | 35 | 1.40 |
| L1034 | 0.00063 | 61 | 49 | 1.24 |
| L1570 | 0.0058 | 138 | 77 | 1.79 |
| L2154 | 0.0093 | 155 | 115 | 1.35 |
| L1098 | 0.020 | 26 | 25 | 1.04 |
| L1489 | 0.22 | 91 | 95 | 0.96 |

Chapter 4

***CXCL14, CXCR7* expression and *CXCR4* splice variant ratio associate with survival and metastases in Ewing sarcoma patients**

L.G.L. Sand, K. Scotlandi, D. Berghuis, B.E. Snaar-Jagalska, P. Picci, T. Schmidt, K. Szuhai and P.C.W. Hogendoorn

European Journal of Cancer, 2015, 51(17), 2624-2633

ABSTRACT

Ewing sarcoma (EWS) is the second most common sarcoma of bone in children and young adults. Patients with disseminated disease at diagnosis or early relapse have a poor prognosis. Our goal was to identify novel predictive biomarkers for these patients, focusing on chemokines, specifically genes involved in the CXCR4-pathway because of their established role in metastasis and tumor growth.

Total RNA isolated from therapy-naïve tumor samples (n = 18; panel I) and cell lines (n = 21) was used to study expression of CXCR4-pathway related genes and CXCR4 splice variants (*CXCR4-2* and *CXCR4-1*) by RT-Q-PCR. *CXCL12*, *CXCR4*, *CXCR7* and *CXCL14*, and both splice variants were expressed in cell lines and tumor samples. *CXCR4-1/CXCR4-2* ratio was significantly higher in tumor samples compared to cell lines and showed a positive correlation with overall survival (OS) and event free survival (EFS). In addition, high *CXCR7* and *CXCL14* expression levels were correlated with improved EFS and OS and negatively correlated with metastasis development. The results from the test panel were validated in an independent sample panel. This identified set of genes which are involved in CXCR4 signaling might be used as a marker to predict survival and metastasis development in Ewing sarcoma.

KEYWORDS

Splice variant; Tumor microenvironment; Biomarker; Molecular targeted therapy

INTRODUCTION

Ewing sarcoma (EWS) is the second most common bone neoplasm in children and young adolescents while soft tissue and organ related involvement is more often observed in adults [1]. Genetically, EWS is characterized by a recurrent translocation of the *EWSR1* gene to a member of the family of ETS transcription factors [1-2]. Rarely, tumors with Ewing sarcoma-like features exist where *EWSR1* is fused to a non-ETS family member or between *BCOR-CCNB3* or *CIC-DUX4* genes [1, 3-5].

The introduction of multi-agent chemotherapy in combination with advancements in surgery and radiotherapy has improved the 5-year overall survival (OS) of EWS patients with localized disease from less than 10–70% nowadays, irrespective of the type of classical Ewing sarcoma specific translocation [6-7]. However, the OS drops to less than 30% when metastases are present at the time of diagnosis which is the case in 15–30% of new presentations- or with tumor relapse [8-9]. For these high risk patients many markers have been suggested, but at present only classical markers, such as tumor location, are used in clinic [10]. EWS is recognized from the onset of its original description by James Ewing as a highly vascularized tumor and amongst many other pathways, chemokine and the TGF- β pathway might play a role for this excessive vascularization pattern [11-13]. Besides angiogenesis, these pathways are involved in migration that might be reflected by the high metastatic propensity of EWS [1, 13, 14]. In several tumor types a positive correlation between increased expression of CXCR4 and metastatic propensity was reported, but contradictory results were reported in EWS [15], [16] and [17].

CXCR4 is a chemokine receptor from the G-protein coupled receptor family binding the CXC chemokines. CXCR4 ligands are chemokine CXCL12, also known as stromal cell-de-

rived factor 1 (SDF1) and CXCL14, also known as BRAK [18-19].

For *CXCR4* two common splice variants have been described in humans by Gupta et al. containing either two exons *CXCR4-2* or one exon by utilizing another transcription initiation code inside intron one *CXCR4-1* [20]. At the protein level, the first five amino acids at the N-terminus of *CXCR4-2* are replaced with nine amino acids in the *CXCR4-1* variant. Hence, the N-terminal part of *CXCR4* is crucial in CXCL12 binding therefore this change may interfere with *CXCR4* activation [20-21]. The expression levels of these two splice variants have neither been studied in tumor samples nor associated with survival.

To study the role of different chemokines and their receptors in combination with the detection of different *CXCR4* isoforms we performed whole transcriptome RNA sequencing and a real-time quantitative-reverse transcriptase PCR (RT-Q-PCR) on EWS cell lines and two panels of therapy-naïve tumor samples (test and a validation set: panel I and panel II). Results of the RT-Q-PCR were correlated to clinical parameters. Survival analysis of panel I showed that high *CXCR4-1* over *CXCR4-2* ratio and high expression of *CXCL14* and *CXCR7* positively correlated with EFS and OS. These findings were overall confirmed by a validation set (panel II). Thus, *CXCL14*, *CXCR7* and the ratio between *CXCR4-2* and *CXCR4-1* could predict EFS and OS in Ewing sarcoma patients, which is probably related to their role in *CXCR4* signaling pathway.

MATERIAL AND METHODS

Clinical information patient samples

Ewing sarcoma diagnosis was established according to World Health Organization (WHO) criteria, including immunohistochemistry and *EWSR1* translocation detection either by RT-Q-PCR or interphase FISH. 18 cryopreserved therapy-naïve samples from 18 patients containing at least 80% tumor were collected at the Department of Pathology, Leiden University Medical Center (**Table 1A; panel I**). Median patient age at diagnosis was 17.5 years (range of 5–35 years). All patient samples were handled in a coded fashion, according to the Dutch national ethical guidelines ('Code for Proper Secondary Use of Human Tissue', Dutch Federation of Medical Scientific Societies). For validation a panel of 25 cryopreserved therapy-naïve samples from 25 patients were obtained from the Rizzoli Orthopedics Institute with a median age at diagnosis of 16 years (range 3–45 years) (**Table 1B; panel II**).

Ewing sarcoma cell lines

21 Ewing sarcoma cell lines were obtained from multiple sources: L-1062 and L-872 were established in-house; SK-ES-1, SK-NM-C, A-673 and R-D-ES from the American Type Culture Collection and CHP100, RM-82, IARC-EW-7, WE-68, IARC-EW-3, STA-ET-2.1, TTC-466, TC-32, STA-ET-10, CADO-ES1, STA-ET-1, TC-71, COH and VH-64 were obtained from the EuroBoNET consortium collection located at the Institute of Pathology, University Medical Center, Düsseldorf, Germany; 6647 was kindly provided by Dr. Timothy Triche (CHLA, Los Angeles, CA, USA). All cell lines and primary culture L-4027 were cultured in Iscove's Modified Dulbecco's Medium containing GlutaMAX supplement, supplemented with 1% streptomycin/penicillin and 10% heat-inactivated FCS (all from Life Technologies, Bleiswijk, The Netherlands). Regular Mycoplasma DNA Q-PCR screening [22] and authentication of cell lines using Powerplex 1.2 and CellID STR (Promega, Leiden, The Netherlands) were performed on all cell lines.

Table 1: Clinical details of the two study panels**Table1a: Clinical details of patients in study panel I**

| Patient number | Age (years) | Sex | Primary tumor site | Ex-tremity ^a | Pelvic ^b | Starting treatment protocol | Tumor volume ^c | Neoadjuvant chemotherapy ^d | Neoadjuvant Radiotherapy ^e |
|----------------|-------------|--------|--------------------|-------------------------|---------------------|-----------------------------|---------------------------|---------------------------------------|---------------------------------------|
| L318 | 35 | male | prox radius | 1 | 0 | CESS86 | ND | 1 | 0 |
| L463 | 24 | male | thorax wall | 0 | 0 | CESS86 | ND | 0 | 0 |
| L469 | 19 | female | distal fibula | 1 | 0 | EICESS | 1 | 1 | 0 |
| L513 | 11 | male | pelvis | 0 | 1 | EICESS | 1 | ND | 1 |
| L629 | 5 | male | tibia + fibula | 1 | 0 | EuroEwing99 | 1 | 1 | 0 |
| L683 | 17 | male | tibia | 1 | 0 | EICESS | ND | 1 | 0 |
| L848 | 15 | female | humerus | 1 | 0 | EuroEwing99 | 0 | 1 | 0 |
| L1034 | 18 | male | pelvis | 0 | 1 | EuroEwing99 | 1 | 1 | 0 |
| L1098 | 10 | male | femur | 1 | 0 | EuroEwing99 | 0 | 1 | 0 |
| L1220 | 19 | male | os pubis | 0 | 1 | EuroEwing99 | 1 | 1 | - |
| L1232 | 14 | male | humerus | 1 | 0 | EuroEwing99 | ND | ND | 0 |
| L1379 | 13 | male | fibula | 1 | 0 | EuroEwing99 | ND | 1 | 0 |
| L1489 | 25 | male | pelvis | 0 | 1 | EuroEwing99 | 1 | 1 | 1 |
| L1570 | 12 | male | humerus | 1 | 0 | EuroEwing99 | ND | 1 | 0 |
| L1722 | 18 | male | humerus | 1 | 0 | EuroEwing99 | 1 | 1 | 0 |
| L2154 | 11 | female | femur | 1 | 0 | EuroEwing99 | 0 | 1 | - |
| L2161 | 19 | male | pelvis | 0 | 1 | EuroEwing99 | 1 | 1 | 0 |
| L2162 | 19 | male | pelvis | 0 | 1 | EuroEwing99 | 1 | 1 | 0 |

ND: Not determined

EFS: Event free survival

OS: overall survival

^{a,b,d,e,f,g,l,k,j} **1**: event reported or **0**: no event reported

^c **1** tumor volume > 200 ml or **0**: < 200 ml

^h **1**: < 10% tumor vitality or **0**: > 10% tumor vitality

^b **1**: Dead or **0**: alive.

| Surgery ^f | Resectable with free margins ^g | Response to chemotherapy ^h | Metastasis at diagnosis ⁱ | Metastasis later ^j | Local recurrence/Relapse ^k | EFS Time (month) | EFS ^l | OS Time (month) | OS ^m |
|----------------------|---|---------------------------------------|--------------------------------------|-------------------------------|---------------------------------------|------------------|------------------|-----------------|-----------------|
| 1 | 1 | 1 | 0 | 0 | 0 | 183 | 0 | 233 | 0 |
| 1 | 1 | ND | 0 | 1 | 1 | 12 | 1 | 20 | 1 |
| 1 | 0 | 0 | 0 | 1 | 1 | 20 | 1 | 23 | 1 |
| 0 | - | ND | 1 | 0 | ND | 18 | 1 | 18 | 1 |
| 1 | 1 | 1 | 1 | 0 | 0 | 135 | 0 | 135 | 0 |
| 1 | 0 | 0 | 0 | 1 | 0 | 10 | 1 | 16 | 1 |
| 1 | 1 | 1 | 1 | 0 | 0 | 142 | 0 | 142 | 0 |
| 1 | 0 | 0 | 1 | 1 | 0 | 11 | 1 | 18 | 1 |
| 1 | 0 | 1 | 0 | 0 | 0 | 129 | 0 | 129 | 0 |
| 0 | | ND | 1 | 1 | 0 | 10 | 1 | 11 | 1 |
| 1 | 1 | ND | 0 | 0 | ND | 14 | 1 | 34 | 1 |
| 1 | 1 | 0 | 1 | 0 | 0 | 99 | 0 | 99 | 0 |
| 1 | 1 | 1 | 0 | 0 | 0 | 91 | 0 | 91 | 0 |
| 1 | 1 | 1 | 0 | 0 | 0 | 83 | 0 | 83 | 0 |
| 1 | 1 | 1 | 0 | 1 | 1 | 36 | 1 | 36 | 0 |
| 1 | 1 | 1 | 1 | 0 | 0 | 176 | 0 | 176 | 0 |
| 0 | - | 0 | 0 | 1 | 0 | 11 | 1 | 12 | 1 |
| 0 | - | ND | 1 | 1 | 0 | 15 | 1 | 19 | 1 |

Table 1b: Clinical details of patients in validation panel II

| Patient number | Age (years) | Sex | Primary tumor site | Ex-tremity ^a | Pelvic ^b | Starting treatment protocol | Tumor volume ^c | Neoadjuvant chemotherapy ^d | Neoadjuvant Radiotherapy ^e |
|----------------|-------------|--------|--------------------|-------------------------|---------------------|-----------------------------|---------------------------|---------------------------------------|---------------------------------------|
| R040 | 24 | male | femur | 1 | 0 | IOR NEO3 | 1 | 1 | 0 |
| R042 | 18 | male | femur | 1 | 0 | IOR NEO3 | 0 | 1 | 0 |
| R046 | 7 | female | radius | 1 | 0 | IOR NEO3 | 0 | 1 | 0 |
| R060 | 12 | male | pelvis | 0 | 1 | IOR NEO3 | 0 | 1 | 1 |
| R063 | 13 | male | pelvis | 0 | 1 | ISG-SSG3 | 0 | 1 | 1 |
| R078 | 11 | female | pelvis | 0 | 1 | ISG-SSG4 | 1 | 1 | 1 |
| R080 | 8 | female | femur | 1 | 0 | ISG-SSG3 | 0 | 1 | 0 |
| R517 | 3 | male | humerus | 1 | 0 | ISG-SSG PILOT | 0 | 1 | 0 |
| R650 | 26 | female | femur | 1 | 0 | ISG-SSG3 | 0 | 1 | 0 |
| R653 | 9 | male | tibia | 1 | 0 | ISG-SSG4 | 0 | 1 | 0 |
| R658 | 17 | female | tibia | 1 | 0 | IOR NEO2 | 0 | 1 | 1 |
| R673 | 15 | female | humerus | 1 | 0 | ISG-SSG3 | 0 | 1 | 0 |
| R680 | 17 | male | fibula | 1 | 0 | ISG-SSG3 | 0 | 1 | 0 |
| R681 | 12 | female | femur | 1 | 0 | ISG-SSG3 | 0 | 1 | 0 |
| R822 | 31 | male | tibia | 1 | 0 | ISG-SSG3 | 0 | 1 | 0 |
| R833 | 17 | female | femur | 1 | 0 | ISG-SSG3 | 0 | 1 | 0 |
| R835 | 26 | male | scapula | 1 | 0 | ISG-SSG3 | 0 | 1 | 0 |
| R863 | 18 | male | tibia | 1 | 0 | ISG-SSG3 | 0 | 1 | 0 |
| R880 | 10 | male | radius | 1 | 0 | ISG-AIEOP | 0 | 1 | 0 |
| R891 | 21 | male | femur | 1 | 0 | ISG-SSG3 | 0 | 1 | 0 |
| R892 | 37 | female | femur | 1 | 0 | ISG-AIEOP | 1 | 1 | 0 |
| R906 | 10 | male | humerus | 1 | 0 | ISG-AIEOP | 1 | 1 | 0 |
| R910 | 45 | male | scapula | 1 | 0 | ISG-AIEOP | 1 | 1 | 0 |
| R914 | 10 | male | femur | 1 | 0 | EUROEW-ING99 | 0 | 1 | 0 |
| R917 | 14 | male | metatarsus | 1 | 0 | ISG-AIEOP | 1 | 1 | 0 |

ND: Not determined

EFS: Event free survival

OS: overall survival

^{a,b,d,e,f,g,i,k,j} **1**: event reported or **0**: no event reported

^c **1** tumor volume > 200 ml or **0**: < 200 ml

^h **1**: < 10% tumor vitality or **0**: > 10% tumor vitality

^b **1**: Dead or **0**: alive

| Surgery ^f | Resectable with free margins ^g | Response to chemotherapy ^h | Metastasis at diagnosis ⁱ | Metastasis later ^j | Local recurrence/Relapse ^k | EFS Time (month) | EFS ^l | OS Time (month) | OS ^m |
|----------------------|---|---------------------------------------|--------------------------------------|-------------------------------|---------------------------------------|------------------|------------------|-----------------|-----------------|
| 1 | 1 | 0 | 0 | 1 | 0 | 17 | 1 | 135 | 0 |
| 1 | 1 | 0 | 0 | 0 | 0 | 262 | 0 | 262 | 0 |
| 1 | 1 | 0 | 0 | 1 | 0 | 21 | 1 | 63 | 1 |
| 0 | ND | ND | 0 | 0 | 0 | 226 | 0 | 226 | 0 |
| 0 | ND | ND | 0 | 0 | 0 | 109 | 0 | 109 | 0 |
| 0 | ND | ND | 1 | 0 | 0 | 183 | 0 | 183 | 0 |
| 1 | 0 | 0 | 0 | 1 | 0 | 57 | 1 | 72 | 1 |
| 1 | 0 | 0 | 0 | 0 | 0 | 161 | 0 | 161 | 0 |
| 1 | 0 | 0 | 0 | 1 | 0 | 28 | 1 | 141 | 0 |
| 1 | 1 | 1 | 1 | 1 | 0 | 30 | 1 | 52 | 1 |
| 0 | ND | ND | 0 | 1 | 1 | 24 | 1 | 35 | 1 |
| 1 | 1 | 1 | 0 | 0 | 0 | 122 | 0 | 122 | 0 |
| 1 | 1 | 1 | 0 | 0 | 0 | 122 | 0 | 122 | 0 |
| 1 | 1 | 1 | 0 | 0 | 0 | 151 | 0 | 151 | 0 |
| 1 | 1 | 0 | 0 | 1 | 0 | 11 | 1 | 21 | 1 |
| 1 | 1 | 0 | 0 | 1 | 0 | 43 | 1 | 63 | 1 |
| 1 | 1 | 0 | 0 | 0 | 0 | 128 | 0 | 128 | 0 |
| 1 | 1 | 0 | 0 | 0 | 0 | 106 | 0 | 106 | 0 |
| 1 | 1 | 1 | 0 | 0 | 0 | 84 | 0 | 84 | 0 |
| 1 | 1 | 0 | 0 | 0 | 0 | 89 | 0 | 89 | 0 |
| 1 | 1 | 0 | 0 | 0 | 0 | 84 | 0 | 84 | 0 |
| 1 | 0 | 0 | 0 | 1 | 0 | 12 | 1 | 25 | 1 |
| 1 | 1 | 0 | 0 | 1 | 0 | 19 | 1 | 33 | 1 |
| 1 | 1 | 0 | 0 | 1 | 0 | 52 | 1 | 64 | 1 |
| 1 | 1 | 1 | 1 | 0 | 0 | 59 | 0 | 59 | 0 |

RNA isolation

Total RNA was isolated using TRIzol Reagent (Life Technologies, Bleiswijk, The Netherlands) according to manufacturer's instruction. RNA concentration was measured using Nanodrop and quality of the RNA was determined using Bioanalyzer2000 RNA Nano chip (Agilent Technology, Amstelveen, The Netherlands). For whole transcriptome RNA sequencing analysis a RNA Integrity Number (RIN) of 8 was set as threshold. For the RT-Q-PCR analysis the inclusion criteria were at least a RIN of 5 and measurable expression levels.

CXCR4 splice variant specific primer design and detection

CXCR4 splice variant specific primers sets were designed for RT-Q-PCR based expression analysis. CXCR4-2 primers CXCR4-2F 5'AGGTAGCAAAGTGACGCCGA 3' and CXCR4-2R 5' TAGTCCCCTGAGCCCATTTCC 3' were intron spanning by priming exon 1 and exon 2. CXCR4-1 primers were CXCR4-1F 5' GACTTTGAAACCCTCAGCGTC 3' and CXCR4-1R 5' TCCTACAACCTCTCTCCCCAT 3'. Products were detected by using 10ul RT-Q-PCR mixture using iQ SYBR Green supermix (Biorad, Hercules, CA, USA).

RT-Q-PCR analysis and Fluidigm

cDNA generation and RT-Q-PCR using Fluidigm biomark system was performed according to the H format instructions of the manufacturer (QIAGEN, Venlo, The Netherlands). Samples were prepared for RT-Q-PCR using a 96 × 96 dynamic array chip and performed using BioMark HD system (Fluidigm, San, CA, USA). All primers for this array chip were obtained from QIAGEN (Venlo, The Netherlands) including nine control genes: RPL13A, BTF3, YWHAZ, UBE2D2, ATP6V1G1, IPO8, HBS1L, AHSP and TBP. Samples were measured in duplicates and analyzed using BioMark software, delivered with the HD system.

Whole transcriptome RNA sequencing

RNA sequencing was performed at BGI genomics (Hong Kong, People's Republic of China) following standard protocol established by BGI genomics. In short, total isolated RNA was enriched for mRNA using Oligo(dT) beads and generated fragments were size selected for amplification. Amplified fragments were quality controlled and sequenced using Illumina HiSeq 2000. Reads were aligned to a reference sequence using SOAPaligner/SOAP2. Gene expression was calculated using Reads Per Kilobase per Million mapped reads (RPKM) method [23].

Statistical analysis

Survival curves were calculated using the Kaplan–Meier method and P-values were calculated using the log-rank and Gehan Breslow Wilcoxon test using SPSS 20 (IBM Inc. Amsterdam, The Netherlands) and Prism Graphpad 6 (Graphpad Software Inc. La Jolla, CA, USA). Correlations were calculated with SPSS 20 using Spearman or Pearson correlation. High RNA expression was set as expression above the median. Student *t*-tests *P*-value was calculated using Prism Graphpad assuming non-parametric distribution due to limited numbers of samples and were corrected using Manley–Welch correction.

RESULTS

EWS expresses all CXCR4–CXCR7 axis genes and tumor samples have an increased CXCR4-1/CXCR4-2 ratio

RNA expression levels of chemokines and their receptors in cell lines were analyzed using both Fluidigm RT-Q-PCR and whole transcriptome analysis. Both methods showed comparable expression levels and that all genes involved in the CXCR4–CXCR7 axis were expressed (**Figure 1**). We performed an expression analysis of a CXCR4–CXCR7 axis chemokine and their receptor gene set, from which expression differences were observed for CXCR7 and CXCL12 between cell lines and tumor samples, using a panel of 18 therapy naïve tumor samples, 21 cell lines and 1 primary culture (**Tables 1A and 2**). The cell line RT-Q-PCR expression levels of the CXCR4–CXCR7 axis genes were compared with expression levels in tumor samples and showed an increased expression of CXCL12 and CXCR7 in tumor samples. Furthermore, within the cell lines and among individual tumor samples a large variation was observed (**Figure 2A**).

Both splice variants of CXCR4 were expressed in all tumor samples and cell lines except the A673 cell line and no significant difference was observed between the groups (**Figure 2B**). The ratio between splice variants has been shown to be functionally relevant, therefore we further analyzed the ratio between expression levels of CXCR4-1 and CXCR4-2 in our samples [24]. The CXCR4-1/CXCR4-2 ratio was uniformly distributed in the cell line panel with two outliers; A673 cell line without CXCR4-1 expression and COH cell line with a high CXCR4-1/CXCR4-2 ratio (**Table S1**). Tumor samples of panel I demonstrated a wide distribution (range 0.06–0.003, SD = 0.015) and an overall significantly higher CXCR4-1/CXCR4-2 ratio when it was compared to cell lines (median of 0.030 versus 0.012, $P < 0.001$) (**Figure 2C**).

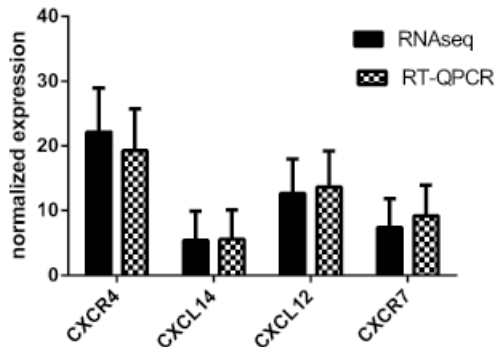


Figure 1: RT-Q-PCR and transcriptome analysis resulted in comparable expression levels of CXCR4–CXCR7 genes using all studied samples. Housekeeping gene normalised RT-Q-PCR expression levels were measured in duplicates (mean \pm SEM)

CXCR4-1 over CXCR4-2 ratio, CXCR7 and CXCL14 expression associate with development of metastases and survival

The large observed variation in CXCR4–CXCR7 axis genes and in the CXCR4-1/CXCR4-2 between individual tumor samples prompted us to perform a comparison between patient samples. A survival analysis was performed using the CXCR4–CXCR7 axis gene expressions

Table 2. Ewing sarcoma cell lines and their origin

| Cell line | Sex | Age (years) | Tumor source | Translocation ^a | TP53 literature | TP53 status [#] | TP53 expression (RPKM) | CDKN2A expression (RPKM) |
|------------------------|--------|-------------|----------------------------|----------------------------|----------------------|--------------------------------------|------------------------|--------------------------|
| RM-82 ^a | male | 8 | femur | EWS-ERG | p.Arg273His | rs28934576 [†] | 79.78 | 54.99 |
| CADO-ES-1 ^a | female | 19 | malignant pleural effusion | EWS-ERG | wt | wt | 26.79 | - |
| TTC-466 ^a | female | 5 | lung metastasis | EWS-ERG | NA | rs28934578 [*] | 63.06 | 81.28 |
| IARC-EW-3 ^a | male | 14 | malignant pleural effusion | EWS-ERG | c-852_858del | c-852_858del [†] | 18.72 | 24.72 |
| L-4027 ^c | male | - | NA | EWS-ERG | NA | wt | 65.4 | - |
| STA-ET-10 | NA | NA | NA | EWS-FEV | wt | wt | 57.29 | 5.33 |
| L-872 ^b | male | 20 | Rib | EWS-FLI1 type I | c 641 A>G, p.H214R | chr17:7578208 A > G [†] | 47.37 | 19.35 |
| L-1062 ^b | male | 17 | femur | EWS-FLI1 type I | c 404 G > T, p.C135F | chr17:7578526 G > T [†] | 90.27 | 31.69 |
| IARC-EW-7 ^a | female | 20 | NA | EWS-FLI1 type I | NA | wt | 48.35 | 1.04 |
| TC-32 ^a | female | 17 | pelvis bone marrow | EWS-FLI1 type I | NA | wt | 99.81 | - |
| TC-71 ^a | male | 23 | humerus | EWS-FLI1 type I | p.Arg213X | missing exon 5,6,7 | 1.97 | - |
| STA-ET-1 ^a | female | 13 | humerus | EWS-FLI1 type I | wt | rs28934576 [*] heterozygous | 30.09 | - |
| WE-68a | female | 19 | fibula | EWS-FLI1 type I | wt | wt | 62.14 | - |
| SK-NM-C ^a | female | 14 | supraorbital metastasis | EWS-FLI1 type I | c.17-_572del | c.17-_572del [†] | 64.22 | 100.3 |
| A-673 ^a | male | 15 | NA | EWS-FLI1 type II | 552insCA | NA | 3.65 | - |
| RD-ES ^a | male | 19 | humerus | EWS-FLI1 type II | p.Arg273Cys | rs121913343 [†] | 62.06 | 24.29 |
| SK-ES-1 ^a | male | 18 | NA | EWS-FLI1 type II | p.Cys176Phe | chr17:7578403 G>T [†] | 72.18 | 41.81 |
| CHP-100 ^a | female | 12 | mediastinum | EWS-FLI1 type II | wt | wt | 3.25 | 45.13 |
| 6647 ^a | NA | NA | NA | EWS-FLI1 type II | NA | rs28934573 [*] | 66.97 | 21.69 |
| VH-64 ^a | male | 24 | malignant pleural effusion | EWS-FLI1 type II | wt | wt | 48.28 | - |
| COH | NA | NA | femur | EWS-FLI1 type III | wt | wt | 61.90 | 12.03 |

Translocation, TP53 status and CDKN2A expression were analysed using transcriptome profiling from this study.

wt: wild type TP53; NA: Not available; RPKM: Reads Per Kilobase per Million mapped reads; -: lacking expression.

^aDescribed by van Valen [43]. ^b Characterized by K. Suzhai et al. [44]. ^cPrimary culture. [†]Corresponding with in literature described TP53 mutation.

^{*}Known pathogenic mutation in TP53. [#] Detected by whole transcriptome analysis

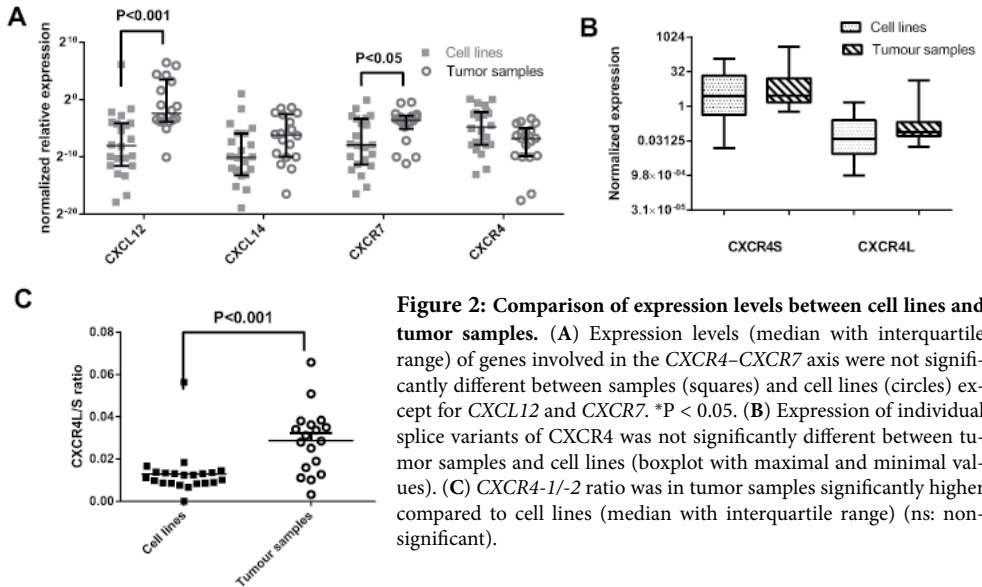


Figure 2: Comparison of expression levels between cell lines and tumor samples. (A) Expression levels (median with interquartile range) of genes involved in the *CXCR4*–*CXCR7* axis were not significantly different between samples (squares) and cell lines (circles) except for *CXCL12* and *CXCR7*. * $P < 0.05$. (B) Expression of individual splice variants of *CXCR4* was not significantly different between tumor samples and cell lines (boxplot with maximal and minimal values). (C) *CXCR4-1/-2* ratio was in tumor samples significantly higher compared to cell lines (median with interquartile range) (ns: non-significant).

and the *CXCR4-1/CXCR4-2* ratio of the primary therapy-naïve tumor samples. We observed that a high *CXCR4-1/CXCR4-2* ratio and high expression of *CXCL14* and *CXCR7* correlated with an improved event free survival (EFS) ($P < 0.03, P < 0.01, P < 0.02$) and OS ($P < 0.03, P < 0.02, P < 0.01$), respectively (**Figure 3A–C, G–I**). Consistent with the correlations with improved survival were increased *CXCL14* ($P < 0.02$) and *CXCR7* ($P < 0.02$) expression negatively correlated with the development of metastasis. The results were validated with an independent second panel of 25 therapy-naïve tumor samples using the same methods (Table 1B; panel II). The same pattern of survival associations with improved EFS was observed for increased *CXCR4-1/CXCR4-2* ratio ($P < 0.05$) and expression of *CXCL14* ($P < 0.04$) (**Figure 3D,I**), while the expression of *CXCL14* ($P < 0.02$) and *CXCR7* ($P < 0.03$) showed a negative correlation with the development of metastasis. Expression of *CXCR7* was associated with improved EFS but did not reach a significant level (**Figure 3F**). No association to overall survival was observed in panel II (**Figure 3J–K**). Expression levels of *CXCR4* or *CXCL12* did not show significant correlation with survival in either panel. (**Figure S1A–H**). As control experiment a survival analysis was performed using the classical prognostic parameters tumor volume, metastasis at diagnosis, location and metastasis after diagnosis of both panels [25]. The development of metastasis after diagnosis was strongly associated with poor survival ($P < 0.01$) consistent with panel I. A pelvic located tumor correlated with a significant poor EFS and OS in panel I, while these were not significant in panel II. Intriguingly, metastasis at diagnosis did not correlate significantly with survival in both panels (**Figure S2**).

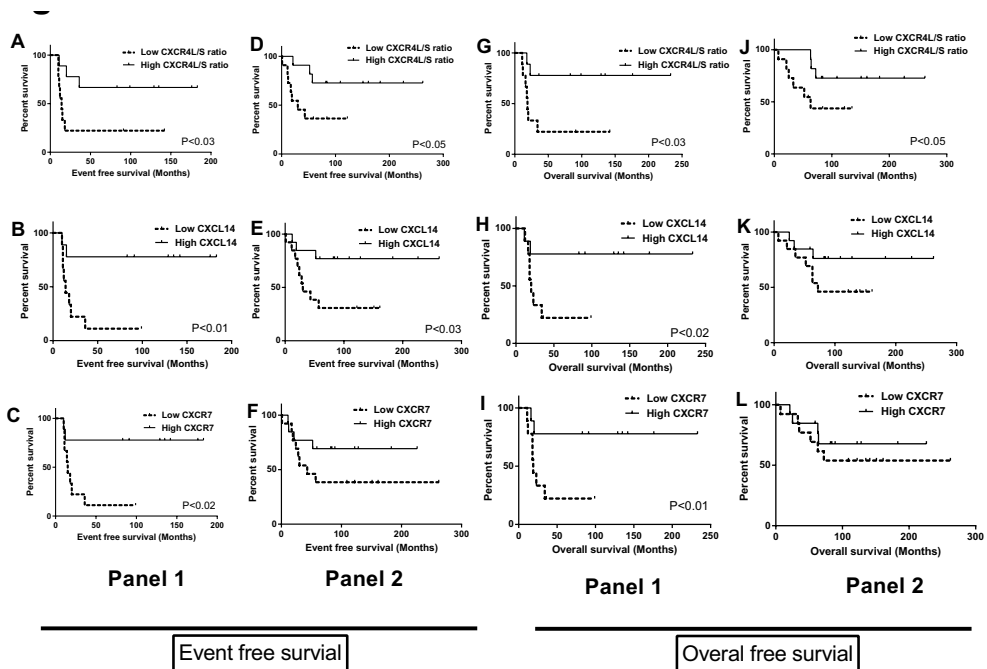


Figure 3: Overview of CXCR4–CXCR7 axis genes and event free survival (EFS), overall survival (OS) in panel 1 and panel 2. *CXCR4-1/-2* ratio and *CXCL14* expression were associated with a significant better EFS in both panels, *CXCR7* in panel I with OS in panel I. RNA expressions of the *CXCR4–CXCR7* axis genes of the therapy-naïve tumor samples of panel I ($n = 18$) (A–C, G–I) and panel II ($n = 25$) (D–F, J–L) were correlated using Kaplan–Meier survival analysis. Median was set as threshold between high (straight line, panel I $n = 9$, panel II $n = 13$) and low expression (dotted line, panel I $n = 9$, panel II $n = 12$). A significant association between high *CXCR4-1/CXCR4-2* ratio and improved EFS or OS was observed in both panels.

DISCUSSION

In earlier studies a crucial role of the *CXCR4/CXCR7* axis in solid tumor development and prognosis has been reported [17, 19, 26]. Recent discoveries regarding the receptor–receptor and novel ligand–receptor interaction between *CXCR4*, *CXCR7*, *CXCL12* and *CXCL14* have been reported. Contradictory results in Ewing sarcoma prompted us to study the role of these chemokines in therapy-naïve patient material and cell lines [15, 16, 18]. In addition, we studied expression levels of the earlier reported *CXCR4* isoforms in tumor samples as the expression of these isoforms in particular might partly be responsible for the contradictory results [15, 16, 20]. All chemokines and receptors of the *CXCR4–CXCR7* axis were expressed in EWS but a large variation was observed between individual samples, consistent with previous observations [16, 27]. The observed increased expression of *CXCR7* and *CXCL12* in tumor samples compared to cell lines could be stromal derived since both endothelial and perivascular cells express *CXCR7* and *CXCL12* and EWS is highly vascularized [28, 29]. In our results, increased expressions of *CXCL14*, *CXCR7* and *CXCR4-1/CXCR4-2* ratios were associated with better EFS and OS in panel I. In panel II increased *CXCL14* expression and *CXCR4-1/CXCR4-2* ratio were associated with better EFS. However, *CXCL12* and *CXCR4* mRNA expression levels did not correlate significantly with EFS or OS. In both panels there was an inverse correlation of increased expression of *CXCL14* and *CXCR7* and development of me-

tastases. This can be related to immune cell infiltration [30, 31]. Classical clinical parameters were included to compare with the newly identified parameters. In panel II none of the classical parameters were significant predictors of survival. This cohort has been extensively treated by different rescue protocols after failure of the initial treatment.

Contrary to our results, increased expression of CXCR4 or CXCR7 has been reported to be associated with poor survival in EWS and other tumors [16-17]. This might be attributed to different methodologies and patient groups used in different studies or might be related to biological effects between different tumor types. For example, the effect of CXCR4 and CXCR7 is dependent on their spatial-temporal distribution. When they are expressed in the same cell, heterodimers can be formed leading to an enhanced CXCR4 downstream signaling [26]. When CXCR7 is expressed alone it can act as scavenging receptor for CXCL12 and subsequently reduces CXCR4 activation by CXCL12 [32]. By flow cytometry and immunohistochemistry a heterogeneous CXCR4 expression has been shown in EWS and this may hold for CXCR7 as well [27]. The local tumor microenvironment can be an influencing factor here as well. CXCR7, CXCR4 and CXCL12 are expressed by tumor-associated vessels and immune cells, where CXCR7 is detected largely intracellular in immune cells [31]. Furthermore, infiltrating macrophages, for example, have been reported to predict a worse survival in classical Hodgkin's lymphoma and were associated with reduced metastasis and improved survival in high-grade osteosarcoma [33-34].

Based on our data the following model can be proposed (**Figure 4**): The paracrine and autocrine CXCR4 signaling present in EWS might be altered by CXCR4-1/-2 ratio, CXCL14 and CXCR7 expressions. High expression of CXCL14 antagonizes CXCL12 binding to CXCR4 and increased CXCR7 sequesters CXCL12 co-operatively leading to a reduced CXCR4 signaling [18, 32]. The investigated CXCR4 isoforms might be present in dimers or oligomers. The presence of CXCR4-1 in these complexes could lead to down regulation of CXCR4 signaling as it has been shown in rat basal leukemia 2H3 cells [20]. Moreover, the CXCR4-1 isoform may have a higher affinity for CXCL14 than CXCR4-2, consequently further increasing the antagonizing effect of CXCL14 [18].

Hence, CXCR4 signaling is a potential targetable pathway and inhibition of CXCR4 signaling in EWS *in vitro* and in xenografts has already been shown to reduce tumor migration growth and angiogenesis [15, 27, 35]. Potential drugs to treat EWS are; CXCL12 neutralizing ligands, like chalcone 4, CXCR4 antagonists, like AMD3100 and CXCL14 analogues (**Figure 4**) [19, 36-37].

Here we document that the increased expression of genes involved in the down regulation of CXCR4 signaling and the CXCR4 splice variant balance predict the prognosis of therapy-naïve Ewing sarcoma patients. In addition the *CXCR4-1/-2 ratio*, the level of *CXCL14* and level of *CXCR7* may be used as markers for therapeutic inhibition of the CXCR4 pathway. Based on our results, additional studies to further characterize the role of altered CXCL14, CXCR7 and CXCR4-1/-2 ratio in CXCR4 signaling, could be performed in model systems, such as well-established zebrafish models [38].

ACKNOWLEDGEMENTS

This study was supported by National Organisation for Scientific Research (NWO) Grant-NWO-TOP GO 854.10.012. Authors thank Pauline Wijers-Koster and Cristina Baricordi for their technical expertise and Ron Wolterbeek for his expertise on statistics.

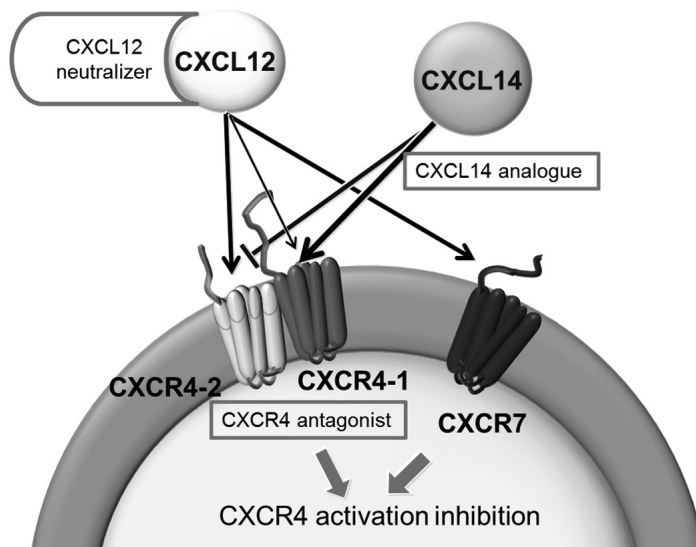


Figure 4: Model for CXCR4 signaling in Ewing sarcoma: CXCL12 binds and activates CXCR4-2, which is inhibited by CXCL14 and CXCR7 by inhibiting receptor binding and scavenging of CXCL12. Dimerization of CXCR4-1 and CXCR4-2 results in CXCR4 activation inhibition due to either change in CXCR4-2 signalling or by higher CXCR4-1 affinity for CXCL14. As available therapeutic options (boxed) are CXCL14 analogues, CXCL12 neutralizers and CXCR4 inhibitors (see [19, 36-37]).

REFERENCES

- 1 De Alava, E., Lessnick, S. L. & Sorensen, P. H. in *WHO Classification of Tumors of Soft Tissue and Bone* (eds C.D.M. Fletcher, J.A. Bridge, P. C. W. Hogendoorn, & F. Mertens) 306-9 (IARC, 2013).
- 2 Sand, L. G. L., Szuhai, K. & Hogendoorn, P. C. W. Sequencing overview of Ewing sarcoma: a journey across genomic, epigenomic and transcriptomic landscapes. *Int J Mol Sci* **16**, 16176-215, (2015).
- 3 Pierron, G. *et al.* A new subtype of bone sarcoma defined by BCOR-CCNB3 gene fusion. *Nat Genet* **44**, 461-6, (2012).
- 4 Szuhai, K. *et al.* The NFATc2 Gene Is Involved in a Novel Cloned Translocation in a Ewing sarcoma Variant That Couples Its Function in Immunology to Oncology. *Clin Cancer Res* **15**, 2259-68, (2009).
- 5 Graham, C., Chilton-MacNeill, S., Zielenska, M. & Somers, G. R. The CIC-DUX4 fusion transcript is present in a subgroup of pediatric primitive round cell sarcomas. *Hum Pathol* **43**, 180-9, (2012).
- 6 Balamuth, N. J. & Womer, R. B. Ewing's sarcoma. *Lancet Oncol* **11**, 184-92, (2010).
- 7 Le Deley, M.-C. *et al.* Impact of EWS-ETS Fusion Type on Disease Progression in Ewing's sarcoma/peripheral primitive neuroectodermal tumor: Prospective Results From the Cooperative Euro-EWING 99 Trial. *J Clin Oncol* **28**, 1982-8, (2010).
- 8 Bacci, G. *et al.* Therapy and survival after recurrence of Ewing's tumors: the Rizzoli experience in 195 patients treated with adjuvant and neoadjuvant chemotherapy from 1979 to 1997. *Ann Oncol* **14**, 1654-9, (2003).
- 9 Ladenstein, R. *et al.* Primary disseminated multifocal Ewing sarcoma: results of the Euro-EWING 99 trial. *J Clin Oncol* **28**, 3284-91, (2010).
- 10 van Maldegem, A., Hogendoorn, P. & Hassan, A. The clinical use of biomarkers as prognostic factors in Ewing sarcoma. *Clin Sarc Res* **2**, 7, (2012).
- 11 Ewing, J. Diffuse endothelioma of bone *Proc New York Path Soc* **21**, 17-24, (1921).
- 12 DuBois, S. G., Marina, N. & Glade-Bender, J. Angiogenesis and vascular targeting in Ewing sarcoma. *Cancer* **116**, 749-57, (2010).
- 13 Pardali, E. *et al.* Critical role of endoglin in tumor cell plasticity of Ewing sarcoma and melanoma. *Oncogene* **30**, 334-45, (2011).
- 14 Bührenmann, C. *et al.* Quantification of the Heterogeneity of Prognostic Cellular Biomarkers in Ewing sarcoma Using Automated Image and Random Survival Forest Analysis. *PLoS One* **9**, e107105, (2014).

- 15 Berghuis, D. *et al.* The CXCR4-CXCL12 axis in Ewing sarcoma: promotion of tumor growth rather than metastatic disease. *Clin Sarc Res* **2**, 24, (2012).
- 16 Bennani-Baiti, I. M. *et al.* Intercohort Gene Expression Co-Analysis Reveals Chemokine Receptors as Prognostic Indicators in Ewing's sarcoma. *Clin Cancer Res* **16**, 3769-78, (2010).
- 17 Lippitz, B. E. Cytokine patterns in patients with cancer: a systematic review. *Lancet Oncol* **14**, e218-e28, (2013).
- 18 Tanegashima, K. *et al.* CXCL14 is a natural inhibitor of the CXCL12-CXCR4 signaling axis. *FEBS Lett* **587**, 1731-5, (2013).
- 19 Domanska, U. M. *et al.* A review on CXCR4/CXCL12 axis in oncology: No place to hide. *Eur J Cancer* **49**, 219-30, (2013).
- 20 Gupta, S. K. & Pillarisetti, K. Cutting Edge: CXCR4-Lo: Molecular Cloning and Functional Expression of a Novel Human CXCR4 Splice Variant. *J Immunol* **163**, 2368-72, (1999).
- 21 Tamamis, P. & Floudas, C. A. Elucidating a Key Component of Cancer Metastasis: CXCL12 (SDF-1 α) Binding to CXCR4. *J Chem Inf Model* **54**, 1174-88, (2014).
- 22 van Kuppeveld, F. J. *et al.* Genus- and species-specific identification of mycoplasmas by 16S rRNA amplification. *Appl Environ Microbiol* **58**, 2606-15, (1992).
- 23 Mortazavi, A., Williams, B. A., McCue, K., Schaeffer, L. & Wold, B. Mapping and quantifying mammalian transcriptomes by RNA-Seq. *Nat Meth* **5**, 621-8, (2008).
- 24 Bates, D. O. *et al.* Association between VEGF Splice Isoforms and Progression-Free Survival in Metastatic Colorectal Cancer Patients Treated with Bevacizumab. *Clin Cancer Res* **18**, 6384-91, (2012).
- 25 Hogendoorn, P. C. W. *et al.* Bone sarcomas: ESMO Clinical Practice Guidelines for diagnosis, treatment and follow-up. *Ann Oncol* **21**, v204-v13, (2010).
- 26 Décaillot, F. M. *et al.* CXCR7/CXCR4 Heterodimer Constitutively Recruits β -Arrestin to Enhance Cell Migration. *J Biol Chem* **286**, 32188-97, (2011).
- 27 Krook, M. A. *et al.* Stress-induced CXCR4 Promotes Migration and Invasion of Ewing Sarcoma. *Molecular Cancer Research*, (2014).
- 28 Ding, L. & Morrison, S. J. Haematopoietic stem cells and early lymphoid progenitors occupy distinct bone marrow niches. *Nature* **495**, 231-5, (2013).
- 29 Berahovich, R. D. *et al.* Endothelial expression of CXCR7 and the regulation of systemic CXCL12 levels. *Immunology* **141**, 111-22, (2014).
- 30 Rivera, Lee B. *et al.* Intratumoral Myeloid Cells Regulate Responsiveness and Resistance to Antiangiogenic Therapy. *Cell Rep* **11**, 577-91, (2015).
- 31 Sánchez-Martín, L., Sánchez-Mateos, P. & Cabañas, C. CXCR7 impact on CXCL12 biology and disease. *Trends Mol Med* **19**, 12-22, (2013).
- 32 Hoffmann, F. *et al.* Rapid Uptake and Degradation of CXCL12 Depend on CXCR7 Carboxyl-terminal Serine/Threonine Residues. *J Biol Chem* **287**, 28362-77, (2012).
- 33 Steidl, C. *et al.* Tumor-Associated Macrophages and Survival in Classic Hodgkin's Lymphoma. *N Engl J Med* **362**, 875-85, (2010).
- 34 Buddingh, E. P. *et al.* Tumor-Infiltrating Macrophages Are Associated with Metastasis Suppression in High-Grade Osteosarcoma: A Rationale for Treatment with Macrophage Activating Agents. *Clin Cancer Res* **17**, 2110-9, (2011).
- 35 Hamdan, R., Zhou, Z. & Kleinerman, E. S. Blocking SDF-1 α /CXCR4 Downregulates PDGF-B and Inhibits Bone Marrow-Derived Pericyte Differentiation and Tumor Vascular Expansion in Ewing Tumors. *Molecular Cancer Therapeutics*, (2013).
- 36 Daubeuf, F. *et al.* An Antedrug of the CXCL12 Neutraligand Blocks Experimental Allergic Asthma without Systemic Effect in Mice. *J Biol Chem* **288**, 11865-76, (2013).
- 37 Tanegashima, K. *et al.* Dimeric peptides of the C-terminal region of CXCL14 function as CXCL12 inhibitors. *FEBS Lett* **587**, 3770-5, (2013).
- 38 van der Ent, W. *et al.* Ewing sarcoma inhibition by disruption of EWSR1-FLI1 transcriptional activity and reactivation of p53. *J Pathol* **233**, 415-24, (2014).

SUPPLEMENTARY DATA

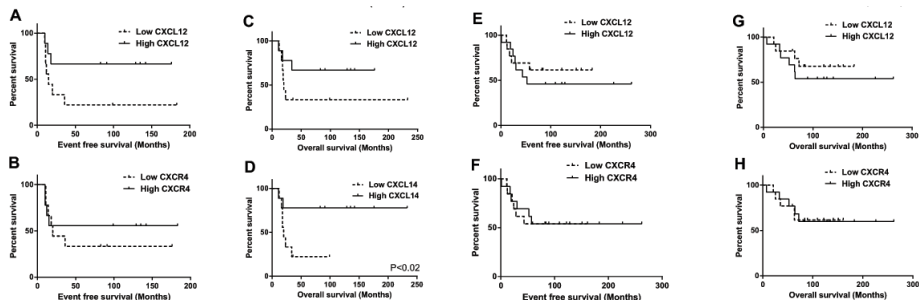


Figure S1: EFS and OS analysis of CXCR4 and CXCL12 of panel I and panel II. Kaplan-Meier survival analysis of panel I (A-D) and panel II (E-H) for OS and EFS association with CXCL12 and CXCR4 expression levels. None of them were significantly associated with OS or EFS. A straight line corresponds to a high ratio or expression and a dotted line is low ratio or expression.

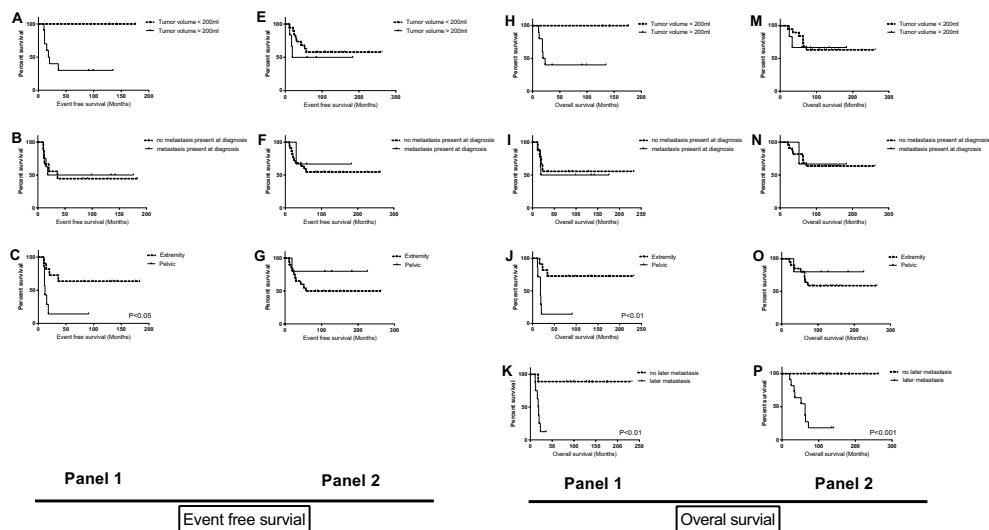


Figure S2: EFS and OS analysis of classical parameters of panel I and panel II. Kaplan-Meier survival analysis of panel I (A-C,H-K) and panel II (D-F,L-P) for OS and EFS association with classical parameters; tumor volume, metastasis at diagnosis, tumor location at diagnosis and only OS association with development of later metastasis. Pelvic location of primary tumor at diagnosis was only in panel I significant. Development of later metastasis was highly significant in both panel I and panel II.

Table S1: Normalized expression of CXCR4-2 and CXCR4-1 and ratio between CXCR4-1 and CXCR4-2

| Cell lines | Expression | | |
|------------|------------|---------|------------|
| | CXCR4-2 | CXCR4-1 | CXCR4-1/-2 |
| L-1062 | 3.877 | 0.052 | 0.013 |
| 6647 | 33.314 | 0.284 | 0.009 |
| CHP-100 | 48.492 | 0.406 | 0.008 |
| RM-82 | 0.426 | 0.004 | 0.008 |
| A-673 | 0.015 | 0.000 | 0.000 |
| IARC-EW-7 | 1.074 | 0.007 | 0.007 |
| SK-ES-1 | 0.180 | 0.002 | 0.011 |
| L-4027 | 3.009 | 0.039 | 0.013 |
| WE-68 | 17.255 | 0.213 | 0.012 |
| L-872 | 1.057 | 0.010 | 0.010 |
| IARC-EW-3 | 120.196 | 1.493 | 0.012 |
| STA-ET-2.1 | 0.421 | 0.006 | 0.014 |
| TTC-466 | 1.858 | 0.024 | 0.013 |
| TC-32 | 56.346 | 0.937 | 0.017 |
| STA-ET-10 | 6.658 | 0.059 | 0.009 |
| SK-NM-C | 1.077 | 0.015 | 0.014 |
| CADO-ES1 | 52.325 | 0.962 | 0.018 |
| STA-ET-1 | 10.085 | 0.101 | 0.010 |
| TC-71 | 0.130 | 0.001 | 0.008 |
| RD-ES | 5.449 | 0.079 | 0.014 |
| COH | 0.219 | 0.012 | 0.056 |
| VH-64 | 2.536 | 0.022 | 0.009 |

Chapter 5

Novel splice variants of *CXCR4* identified by transcriptome sequencing

L.G.L Sand, A.G. Jochemsen, E. Beletkaia, T. Schmidt, P.C.W. Hogendoorn and K. Szuhai

Biochemical, Biophysical Research Communication, 2015, 466(1), 89-94

ABSTRACT

Chemokine receptor CXCR4 is involved in tumor growth, angiogenesis and metastasis. Its function is regulated in many ways and one of them is alternative splicing. We identified two novel coding splice variants (*CXCR4-3* and *CXCR4-4*) of *CXCR4* in Ewing sarcoma (EWS) cell lines by whole transcriptome sequencing and validated these with reverse transcriptase-PCR and Sanger sequencing. The novel splice variants were expressed at RNA level in Ewing sarcoma samples and in other tumor cell lines and placenta, but not in lung. Due to inclusion of an additional exon the new isoforms have a 70 and 33 amino acid elongation of the N-terminal end of CXCR4. For validation at protein and functional level, the identified isoforms and normal CXCR4 were cloned into an EYFP tagged vector and ectopically expressed in HEK293T cell line and EWS cell line A673. Of the novel isoforms CXCR4-3 showed cell membrane localization and a functional response after addition of CXCR4 ligand CXCL12a. CXCR4-4 showed strong cytoplasmic accumulation and no response to ligand treatment. The role of the newly discovered isoforms in CXCR4 signaling is likely to be limited. Our data stresses the importance of functional validation of newly identified isoforms.

KEYWORDS

CXCR4; Splicing; Next generation sequencing; Ewing sarcoma; Bone tumors; Soft tissue tumor

INTRODUCTION

Chemokines are low molecular weight signaling proteins and characterized by a cysteine motif. The primary function of chemokines is related to inflammatory response and immune-surveillance. In addition, chemokines play a key role in tumor development and progression. The tumor microenvironment has a key role in growth, angiogenesis and metastasis [1-3]. Hence, chemokines show enhanced tumorigenic functions as they are involved in angiogenesis, tumor growth, immune suppression and metastasis[2]. The presence and activation of the chemokine receptor CXCR4 has been shown to be associated with metastasis and consequently decreased survival [4-6]. The function of CXCR4 is regulated at multiple levels both with regard to inter- and intracellular interactions through transcriptional processing via alternative splicing, posttranslational modifications and receptor dimerizations [7-10].

Ewing sarcoma (EWS), a highly malignant bone and soft tissue tumor, is characterized by a pathognomonic translocation between the *EWSR1* gene and a member of the ETS family of transcription factor genes [11-12]. The fusion protein influences, transcription, alternative splicing and protein-protein interactions [12]. The fusion protein is partly responsible for the aggressive growth, high vascularization and metastatic properties in EWS and in all these processes CXCR4 is involved. As the prognosis for EWS patients with established metastases at diagnosis or relapse remains dismal, investigation of the CXCR4 involvement in tumor progression and metastasis could be of clinical relevance [13-14]. RNA and protein studies have associated CXCR4 expression with various properties, like metastasis, tumor growth and survival [5,15]. Recently, we found that increased expression levels of CXCR7 and CXCL14, factors inhibiting CXCR4 signaling were associated with improved survival and, *vice versa*, the absence of these factors correlated with metastasis development [16]. Fur-

thermore, an improved survival was associated with the ratio between the known splice variants of CXCR4, CXCR4-1 and CXCR4-2. These variants consist of either two exons dubbed as CXCR4-2 or one exon by utilizing an alternative start codon inside intron one dubbed as CXCR4-1 [22]. At the protein level, in the CXCR4-1 variant, compared to the CXCR4-2 variant, the first five amino acids at the N-terminus are replaced with nine other amino acids (Figure 1). As the N-terminus of CXCR4 is crucial in CXCL12 binding, the differences between the two splice variants may lead to an altered CXCR4 activation efficacy [10]. We performed transcriptome analysis using a next generation sequencing approach to identify new splice variants in Ewing sarcoma cell lines and tumor samples. Next to the earlier described splice variants of CXCR4, we identified two novel splice variants CXCR4-3 and CXCR4-4, which resulted in a 70 and 33 amino acid extension of the receptor at the N-terminus domain, respectively. Although the novel isoforms were expressed, it is likely that function of these splice variants is limited. In addition, our work demonstrates that functional validation of novel isoforms identified by transcriptome analysis is necessary.

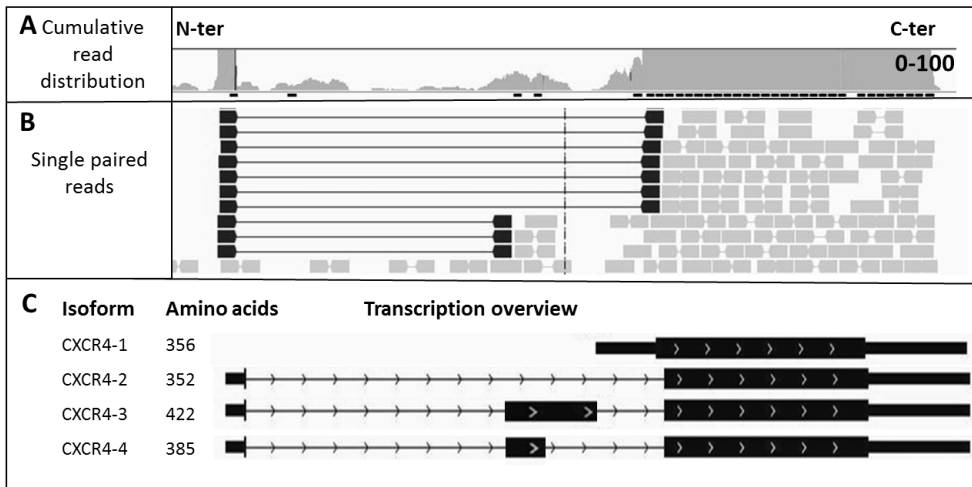


Figure 1: Identification of new CXCR4 isoforms. IGV plot of transcriptome sequencing data showing the potential alternative spliced exon in intron 1 of CXCR4. **A)** Read coverage of IGV plot at 0–100 read range and **B)** single alignments of whole transcriptome sequences of CXCR4 from EWS cell line EW3 (black connected blocks are paired end reads over a large distance of the genome, marking exons). **C)** Overview of all CXCR4 isoforms with the genomic position of the exons and number of amino acids when translated.

MATERIAL & METHODS

Ewing sarcoma cell lines

Twenty-three EWS cell lines and one primary culture were cultured as described by Sand *et al.* [16]. Human embryonic kidney cell line HEK293T was cultured in DMEM with 10% FCS without antibiotics; human T cell leukemia cell line Jurkat, colon carcinoma cell lines SW480, HT29 and HCT116; cervical carcinoma cell lines Hela, Siha and Caski; breast carcinoma cell lines MDA-MB-231 and MCF7 were obtained from ATCC² and cultured in RPMI with 10% heat inactivated FCS without antibiotics. All cell lines were regularly tested on mycoplasma and authentication with DNA Q-PCR screening and CellID STR, respectively (Promega, Leiden, The Netherlands).

Patient samples

Twenty-five frozen tumor samples from twenty EWS patients and two samples of lung and placenta were obtained from the Department of Pathology, Leiden University Medical Center. Eighteen tumor samples were therapy-naïve samples and seven were obtained post-chemotherapy samples, including three lung metastases and four local relapses. All tumor samples contained at least 80% tumor cells estimated by histological examination. All patient samples were handled in a coded fashion, according to the Dutch national ethical guidelines ('Code for Proper Secondary Use of Human Tissue').

RNA isolation

Total RNA was isolated from cell lines and tumor samples using TRIzol Reagent (Life Technologies). The RNA concentration and quality was established by using Nanodrop and Bioanalyzer2000 RNA Nano chip (Agilent Technology, Amstelveen, The Netherlands).

Whole transcriptome sequencing

RNA with a quality RIN value of eight of EWS cell lines EW3, CADO-ES1 and 6647 was sequenced by BGI genomics (Hong Kong, People's Republic of China) following their standard protocol as mentioned by Sand et al. [16]. Mapped reads were sorted and result files were visualized with Integrative Genomics Viewer (IGV) using UCSC Human genome built 19 as a reference [17-18].

Reverse transcriptase PCR, sequencing and reverse transcriptase-quantitative-PCR

For validation of transcriptome sequencing data, a sequencing primer pair was designed (Table 1). Amplified products generated with High Fidelity FAST-TAQ polymerase were analyzed by agarose gel (Life Technologies) and cloned into *pCR2.1* TOPO cloning vectors. Isolated plasmids were Sanger sequenced by Macrogen (Macrogen, Amsterdam, Netherlands) using *M13* tailed primers and sequences were aligned by blasting (NCBI). RNA expression of *CXCR4-3* and *CXCR4-4* together were obtained using in-house designed RT-Q-PCR primers (Table 1) and performed as described by Sand et al. [16].

Table 1: Primer sequences used for cloning and RT-Q-PCR

| Name | Sequence |
|-------------|-------------------------------------|
| CXCR4seqF | 5' GATCGGTACCATGGAGGGGATCAGTAAAAATG |
| CXCR4seqR | 5' AAGCCAGGATGAGGACACT |
| CXCR4rtpcrF | 5' AGGTAGCAAAGTGACGCCGA |
| CXCR4rtpcrR | 5' ATTTTCTGACACTCCCGCCC |

CXCR4-3 and CXCR4-4 cloning, transfection and imaging

pCR2.1 TOPO cloning vectors containing *CXCR4-3* and *CXCR4-4* were cloned into *ap-EYFP-N1* plasmid containing *CXCR4-2*. The resulting plasmids were quality controlled by BstEII-EcoRI digestion and sequencing using CMV-Fw and CXCR4-R primers. *pEYFP-N1* *CXCR4-2*, *CXCR4-3* and *CXCR4-4* were transiently transfected into HEK239T and A673 cells using FuGENE HD (Promega, Leiden, The Netherlands). Imaging was performed next day in serum-free medium while kept at culture conditions using the INUBG2E-ZILCS (TokaiHit, Japan).

Calcium mobilization assay

Intracellular calcium level was determined using cell permeant Fluo4-AM (Life Technologies, The Netherlands). Cells were pre-incubated with 1 μ M Fluo4-AM for 30 min. The Fluo4-AM fluorescence was detected using time-lapse confocal microscopy with a 488 nm excitation laser beam. After 30 s 100 nM of CXCL12a was added. Intensity change calculations were done using in-house developed scripts in MatLab (Mathworks Inc., Massachusetts, USA).

Western blot

Transfected HEK293T and A673 cells were lysed 48 h after transfection and were treated 6 h before lysis with 10 μ M MG132 proteasome inhibitor (Sigma-Aldrich). Cell lysates were prepared using Giordano buffer (50 mM Tris-HCl, pH 7.4, 0.1% Triton X-100, 250 mM NaCl, 5 mM EDTA) containing phosphatase and protease inhibitors (Sigma-Aldrich). After blotting and blocking with 10% low fat skimmed milk, membranes were stained with anti-GFP (Rabbit, 1:1000, GeneTex, Alton, US).

In silico prediction software

Splice sites were predicted by ASSP software using as input complete sequence of CXCR4 gene according to UCSC hg19 genome reference, using the standard settings [19]. With this software tool, predicted splice sites considered to be positive above threshold value of four and above seven the false positive discovery rate considered to be minimal.

RESULTS

Identification of splice variant of CXCR4

mRNA from EW3, CADO-ES and 6647 EWS cell lines were analyzed by transcriptome sequencing using deep sequencing approach with paired-end reads. Sequence read files were mapped to coding regions of the genome and visualized with IGV application (**Figure 1A,B**). A tiling coverage of paired-end reads in intron 1 were observed. These read pairs were connected to exon 1 and to exon 2 of CXCR4, indicating the presence of additional transcribed splice variants (**Figure 1B**).

Putative splice sites were *in silico* searched in the entire CXCR4 DNA sequence. At the 5' end of the newly identified exon one splice donor site and multiple acceptor splice sites were predicted (**Table 2**). The probability scores varied between 5 and 9, out of the maximal score of 16 indicating a strong likelihood of true splice sites. For experimental verification a sequencing primer pair covering the complete new exon, including an exon 1 and new exon overlapping forward primer were designed (**Table 1**). Amplification of the putative exon resulted in a PCR product with two different lengths after gel electrophoresis size separation. The amplified products were cloned and sequenced using Sanger sequencing. With the sequencing we identified two novel splice variants as a result of splicing of a novel exon in the CXCR4 gene. Splicing-in at the predicted splice acceptor site and the splice donor sites #3 and #2 resulted in two in-frame splice variants CXCR4-3 with an addition of 210 bp of the new exon and CXCR4-4 with an addition 99 bp of the new exon (**Figure 1C**). Translation of these new isoforms resulted in elongation of N-terminus of CXCR4 with 70 (CXCR4-3) or 33 (CXCR4-4) amino acids compared to CXCR4-2.

Table 2: Predicted splice sites in the CXCR4 intron

| Position | Sequence | Score ^a |
|-----------------------------|----------------------|--------------------|
| Splice site donor | | |
| potential Start new exon | ctccaccagGAAAATGCCC | 8.9 |
| Splice site acceptor | | |
| potential End new Exon#1 | AACGCGCCAAgtgataaaca | 4.9 |
| potential End new Exon#2 | GGGGGAGGAGgtgccctttg | 6.3 |
| potential End new Exon#3 | GCCCAGAATGgtttgtattt | 7.6 |

^a Composed score reflecting strength of splice site by using ASSP tool, a threshold of 4 was used to limit false positive [19]. Capital letter represent coding sequence

Analysis of new CXCR4 isoform expression in clinical samples

RNA expression of the separate new splice variants could not be obtained since exon overlapping RT-Q-PCR primers could not be designed, while primers for obtaining expression of both splice variants could be established (Table 1). RNA expression was analyzed in Ewing sarcoma cell lines and tumor samples, in a panel of cancer cell lines and HEK293T cell line together with normal lung and placenta tissues. In fourteen of the twenty five EWS samples expression was detected, consisting of eleven primary therapy-naïve tumors and three metastatic or recurrent tumor samples. Sixteen of the twenty-three EWS cell lines showed expression of the new splice variants (Table 3). Of the analyzed normal tissues samples only placenta, but not lung tissue showed expression (Figure 2A). When the expression of CXCR4-2 was used as a reference, the measured expression was found to be much higher than the novel variant (Figure 2B).

Table 3: Expression of CXCR4-3 and CXCR4-4 together in Ewing sarcoma tumor samples and cell lines (% of total)

| | EWS tumor samples | | EWS cell lines/primary cultures |
|----------------|-------------------|--------------------|---------------------------------|
| | Primary | Metastasis/relapse | |
| RNA expression | 11/18 (61%) | 3/7 (43%) | 16/23 (70%) |

Protein analysis and cellular distribution of novel CXCR4 isoforms

The expression and cellular distribution of the novel CXCR4 protein isoforms, CXCR4-3 and CXCR4-4, were studied using pEYFP-N1 tagged plasmid vectors in the HEK293T cell line and A673 EWS cell lines. As control the CXCR4-2-pEYFP-N1 plasmid transfection was used. The ectopically expressed CXCR4-2 protein was localized at the cell membrane, while

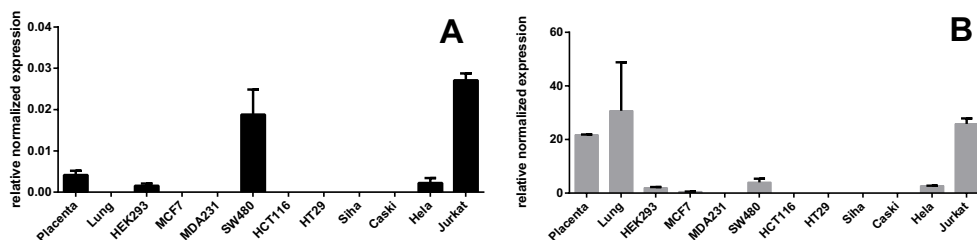
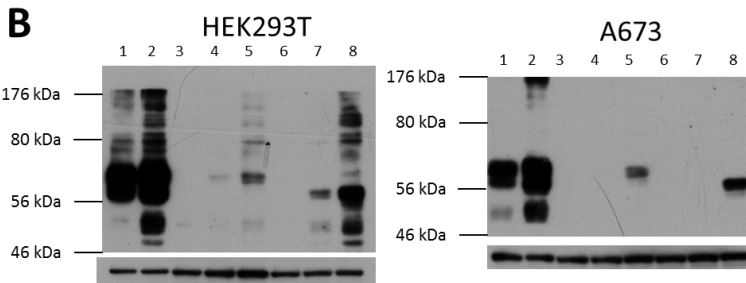
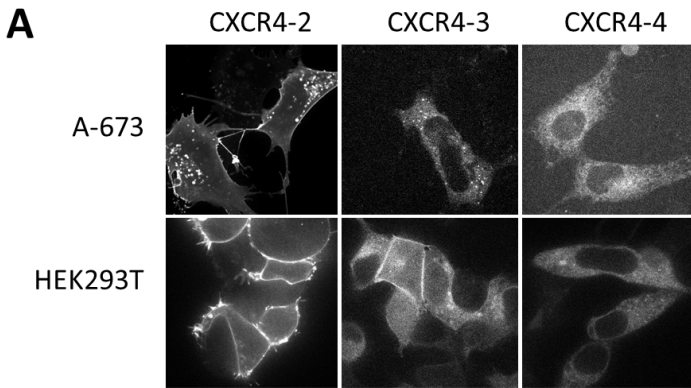


Figure 2: Expression of the novel splice variants in cell line and tissue panel. Housekeeping gene normalized expression of (A) new CXCR4 exon and of (B) CXCR4-2 in tissue and cell lines (mean \pm SEM, n = 3). The highest expression of the novel splice variants was detected in Jurkat and SW480 cell lines.

CXCR4-4 showed a sole cytoplasmic distribution. For CXCR4-3 differences were observed between A673 and HEK293T, with only a cytoplasmic localization detected in A673 and both a membrane and cytoplasmic localization detected in HEK293T (**Figure 3A**). To further compare the expression levels and molecular weight of the different isoforms all three isoforms were analyzed by western blot using anti-GFP antibody (**Figure 3B**). Despite using an identical vector construct in HEK293T cell line, the expression levels of CXCR4-3 and CXCR4-4 were remarkably lower compared to the expression level of CXCR4-2. Intriguingly, the expression of CXCR4-3 and CXCR4-4 protein isoforms was below the detection limit in A673 cell line. Transfected cell lines were then treated with MG132 proteasome inhibitor that resulted in an increased expression of the CXCR4-3 and CXCR4-4 in both cell lines indicating that the isoforms were unstable and the majority of expressed protein was degraded. The calculated molecular weights without any possible post-translational modification for CXCR4-2, CXCR4-3 and CXCR4-4, including the YFP tag, are 66.6, 70.3 and 74.6 kDa, respectively. Western blot analysis showed multiple bands with two dominant ones at ~65 and 70 kDa of the CXCR4-2 protein (**Figure 3B**). When comparing the lanes from CXCR4-3 and CXCR4-4 we observed that CXCR4-3 has an increased molecular weight, corresponding to the calculated molecular weight. However, for CXCR4-4 transfected samples, bands lower than the calculated molecular weight with size comparable to CXCR4-2 were observed indicating the possibility of protein cleavage for this splice variant. As even after proteasome inhibitor treat-



- 1 CXCR4-2
- 2 CXCR4-2, 6 hour treated with 10 μ M MG132
- 3 empty pEGFP-n1 plasmid
- 4 CXCR4-3
- 5 CXCR4-3, 6 hour treated with 10 μ M MG132
- 6 mock
- 7 CXCR4-4
- 8 CXCR4-4, 6 hour treated with 10 μ M MG132

with CXCR4 isoforms CXCR4-3 (lane 4,5), CXCR4-4 (lane 7,8). As controls CXCR4-2 (lane 1,2), empty pEYFP-N1 plasmid and mock-transfected samples were used. Isoform transfected cells were incubated for 6 h with or without proteasome inhibitor MG13 prior to lysis.

Figure 3: CXCR4 isoforms subcellular localization and protein expression. A) Representative images from transient transfection experiment with the three different CXCR4 isoforms expressed in A673 and HEK293T cell line. Life cells were imaged with a spinning-disc confocal microscope. CXCR4-2 was dominantly localized at the cell membrane in both cell lines. CXCR4-3 showed cytoplasmic localization in A673 cells and partial membrane localization in HEK293T cells. CXCR4-4 exhibited only cytoplasmic localization in both cell lines. B) Western blots of transiently transfected HEK293T and A673 cells

ment the expression levels of CXCR-3 and CXCR-4 were relatively low the RNA expression levels of the *CXCR4-EYFP* isoforms were analyzed. For this we designed primers annealing on *CXCR4* and *EYFP* parts, to amplify transfected CXCR4 variant only and a primer pair that *neo* selection gene expression that was present in the transfection vector to analyze relative transfection efficiency (**Figure 4A,B**). Transfection efficiency was estimated by comparing *CXCR4-3* and *CXCR4-4* expression levels to *CXCR4-2* and were found to be 3 and 10 fold lower, respectively (**Figure 4C**).

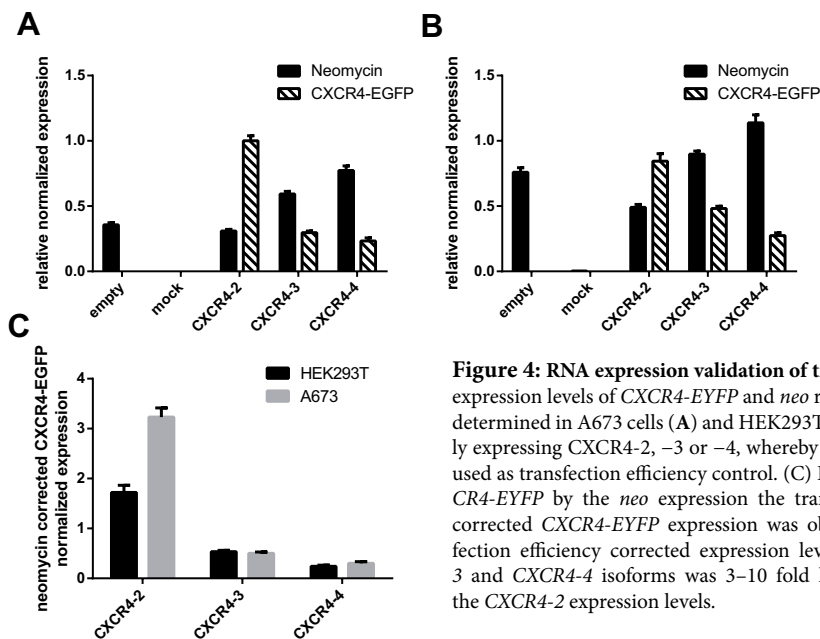


Figure 4: RNA expression validation of transfections. RNA expression levels of *CXCR4-EYFP* and *neo* resistance gene were determined in A673 cells (A) and HEK293T cells (B) ectopically expressing CXCR4-2, -3 or -4, whereby *neo* expression was used as transfection efficiency control. (C) By dividing the *CXCR4-EYFP* by the *neo* expression the transfection efficiency corrected *CXCR4-EYFP* expression was obtained. The transfection efficiency corrected expression levels of the *CXCR4-3* and *CXCR4-4* isoforms was 3–10 fold lower compared to the *CXCR4-2* expression levels.

Calcium mobilization assay

The activity of the receptor isoforms after CXCL12 stimulation was determined by a Ca^{2+} mobilization assay [20]. Upon binding of CXCL12 to CXCR4 receptor a downstream signaling gets activated that include calcium ions influx response. In A673 and HEK293T cells transfected with *CXCR4-2*, *CXCR4-3* or *CXCR4-4* plasmid the Ca^{2+} influx was measured over time before and after CXCL12a administration (**Figure 5**). For A673, only the *CXCR4-2* transfected cells demonstrated a clear effect. All HEK293T cells, including non-transfected cells, demonstrated an effect, indicating activation of some of the endogenous CXCR4 receptors. However, HEK293T cells transfected with *CXCR4-2* or *CXCR4-3* exhibited an elevated Ca^{2+} influx compared to non-transfected cells, suggesting that these receptors were activated by CXCL12a.

DISCUSSION

Two splice variants of CXCR4 have been identified earlier, *CXCR4-1* consisting of one exon only and the most dominantly expressed *CXCR4-2* existing of two exons. Using whole transcriptome analysis in EWS cell lines we discovered two novel CXCR4 splice variants *CXCR4-3* and *CXCR4-4*. The new splice variants were expressed in EWS tumor and cell line samples

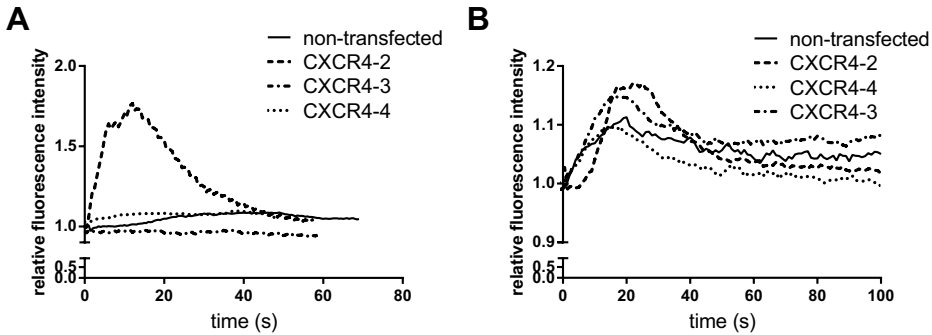


Figure 4: CXCR4 isoform activity indirectly measured by calcium influx. Cell lines A673 (A) and HEK293T (B) transfected with CXCR4-2, CXCR4-3 or CXCR4-4 constructs were pre-incubated with Fluo4-AM for 30 min. Time-lapse live cell confocal imaging prior to and after administration of 100 nM CXCL12a was performed. A representative graph of the relative fluorescence intensity change of Fluo4-AM over time is shown (n = 3).

and other tumor cell lines and in placenta indicating that its expression is not a Ewing sarcoma specific event. The expression of both splice variants together was more than ten-fold lower than expression of the canonical CXCR4-2 isoform. Notably, none of the samples showed expression of the splice variants without the expression of CXCR4-2. This implies that the expression of the new isoforms is depended on the upstream promoter used for CXCR4-2. With the use transcriptome sequencing the number of novel splice variants detected has increased largely. A substantial part of these variants are coding. However, the function of these novel isoforms mostly is unknown. The identified novel CXCR4 isoforms were mainly localized in the cytoplasm and largely degraded by the proteasome. Similarly, a difference in protein stability in cells has been observed for two protein isoforms encoded by the *HDMX* gene. The HDMX-S isoform was reported to be more potent p53 inhibitor than HDMX and its mRNA was detected to be expressed in various tumors. However, functional test showed that this protein was unstable [21-23]. These results stress the importance to examine novel identified RNA splice variants for functionality at the protein level.

CXCL12 is the main ligand to activate CXCR4. The importance of the CXCR4 N-terminus in CXCL12 binding has been demonstrated by various models [24-28]. Changes in the N-terminus, like the CXCR4-1 isoform led to reduced CXCL12 affinity [10]. Interestingly, all reported CXCR4 isoforms, including the novel isoforms reported here, vary only at the N-terminus, suggesting that splicing might be a method to regulate CXCR4 ligand binding [10]. Our functional activity test of the novel CXCR4 isoforms revealed a minor increase in Ca^{2+} influx in CXCR4-3 transfected HEK293T cells upon CXCL12a stimulation, implying functionality of CXCR4-3 (Figure 5).

Western blot analysis of CXCR4 protein with various antibodies regularly results in multiple bands as reported in the literature, for which post-translational protein modifications are thought to be the main reason [9, 29-30]. In HEK293T lysates multiple bands were observed for the ectopically expressed CXCR4 isoforms (Figure 3B). In A673 less bands were observed, implying variations in post-translational modifications of CXCR4, which has been reported in other cell lines [9]. Directed mutagenesis of post-translation modification sites in CXCR4-2 influenced the cellular localization of CXCR4-2 [30]. Lack of these modifications might explain the lack of additional bands in observed in CXCR4-3 transfected A673 cells and might be connected to the lack of membrane localization (Figure 3A). For CXCR4-4, the detected band in both cell lines exhibited lower molecular weight (~65 kDa) than expected

(≥ 70.3 kDa) (**Figure 3B**). This could be the result of a splice site introduced during cloning or cleavage of the protein. We tested the first possibility by PCR but no splice site was introduced. The presence of a C-terminal protein cleavage is unlikely as the detection was done by using an EYFP antibody and EYFP is localized at C-terminal end. We could not prove the N-terminal cleavage of CXCR4-4. However, N-terminal cleavage has been reported for ectopically expressed CXCR4-2 variant that led to reduced membranous expression [29-30]. Thus, N-terminal cleavage might also explain the cytoplasmic localization observed for CXCR4-4 in HEK293T and A673 cells.

In conclusion, we have identified and validated novel CXCR4 isoforms CXCR4-3 and CXCR4-4, which contained a novel spliced-in exon, leading to a N-terminal protein elongation of 70 and 33 amino acids, respectively. These novel isoforms are low expressed compared to the dominantly expressed canonical CXCR4-2 isoform in all cells tested and are expressed in cell lines, tumor samples and placenta. Ectopically expressed CXCR4-3 and CXCR4-4 proteins appear to be unstable, possibly caused by the unfolded-protein response. Localization slightly varied between the tested cell lines. Cell membrane and cytoplasmic localization of the CXCR4-3 protein was observed only in HEK293T cells. Functionality of the ectopically expressed receptors was tested upon CXCL12a stimulation and we observed in both CXCR4-2 transfected cell lines receptor activation. Out of the two novel isoforms only CXCR4-3 was functional. Taken together the data, we show that CXCR4-3 isoform, despite the observed instability and partial cell membrane localization, is functional upon CXCL12a stimulation, while any activity of CXCR4-4 is absent. In addition, our data shows the importance of functional validation of novel identified isoforms.

ACKNOWLEDGMENTS

This study was supported by National organization for Scientific Research (NWO) Grant-NWO-TOP GO 854.10.012 and we thank Inge Briaire-de Bruijn for technical support and Stefano Marullo for supplying the CXCR4-2 pEYFP-N1 plasmid.

REFERENCES

- 1 Whiteside, T. L. The tumor microenvironment and its role in promoting tumor growth. *Oncogene* **27**, 5904-12, (2008).
- 2 Roussos, E. T., Condeelis, J. S. & Patsialou, A. Chemotaxis in cancer. *Nat Rev Cancer* **11**, 573-87, (2011).
- 3 Quail, D. F. & Joyce, J. A. Microenvironmental regulation of tumor progression and metastasis. *Nat Med* **19**, 1423-37, (2013).
- 4 Lippitz, B. E. Cytokine patterns in patients with cancer: a systematic review. *Lancet Oncol* **14**, e218-e28, (2013).
- 5 Berghuis, D. *et al.* The CXCR4-CXCL12 axis in Ewing sarcoma: promotion of tumor growth rather than metastatic disease. *Clin Sarc Res* **2**, 24, (2012).
- 6 Kim, J. *et al.* Chemokine Receptor CXCR4 Expression in Colorectal Cancer Patients Increases the Risk for Recurrence and for Poor Survival. *J Clin Oncol* **23**, 2744-53, (2005).
- 7 Ziarek, J. J. *et al.* Sulfopeptide Probes of the CXCR4/CXCL12 Interface Reveal Oligomer-Specific Contacts and Chemokine Allostery. *ACS Chem Biol* **8**, 1955-63, (2013).
- 8 Zhu, L., Zhao, Q. & Wu, B. Structure-based studies of chemokine receptors. *Curr Opin Struct Biol* **23**, 539-46, (2013).
- 9 Sloane, A. J. *et al.* Marked structural and functional heterogeneity in CXCR4: Separation of HIV-1 and SDF-1[alpha] responses. *Immunol Cell Biol* **83**, 129-43, (2005).
- 10 Gupta, S. K. & Pillarisetti, K. Cutting Edge: CXCR4-Lo: Molecular Cloning and Functional Expression of a Novel Human CXCR4 Splice Variant. *J Immunol* **163**, 2368-72, (1999).
- 11 De Alava, E., Lessnick, S. L. & Sorensen, P. H. in *WHO Classification of Tumors of Soft Tissue and Bone*

- (eds C.D.M. Fletcher, J.A. Bridge, P. C. W. Hogendoorn, & F. Mertens) 306-9 (IARC, 2013).
- 12 Sand, L. G. L., Szuhai, K. & Hogendoorn, P. C. W. Sequencing overview of Ewing sarcoma: a journey across genomic, epigenomic and transcriptomic landscapes. *Int J Mol Sci* **16**, 16176-215, (2015).
- 13 Balamuth, N. J. & Womer, R. B. Ewing's sarcoma. *Lancet Oncol* **11**, 184-92, (2010).
- 14 Ladenstein, R. *et al.* Primary disseminated multifocal Ewing sarcoma: results of the Euro-EWING 99 trial. *J Clin Oncol* **28**, 3284-91, (2010).
- 15 Bennani-Baiti, I. M. *et al.* Intercohort Gene Expression Co-Analysis Reveals Chemokine Receptors as Prognostic Indicators in Ewing's sarcoma. *Clin Cancer Res* **16**, 3769-78, (2010).
- 16 Sand, L. G. L. *et al.* CXCL14, CXCR7 expression and CXCR4 splice variant ratio associate with survival and metastases in Ewing sarcoma patients *Eur J Cancer*, (2015).
- 17 Thorvaldsdóttir, H., Robinson, J. T. & Mesirov, J. P. Integrative Genomics Viewer (IGV): high-performance genomics data visualization and exploration. *Briefings in Bioinformatics* **14**, 178-92, (2013).
- 18 Robinson, J. T. *et al.* Integrative genomics viewer. *Nat Biotech* **29**, 24-6, (2011).
- 19 Wang, M. & Marín, A. Characterization and prediction of alternative splice sites. *Gene* **366**, 219-27, (2006).
- 20 Princen, K., Hatse, S., Vermeire, K., De Clercq, E. & Schols, D. Evaluation of SDF-1/CXCR4-induced Ca²⁺ signaling by fluorometric imaging plate reader (FLIPR) and flow cytometry. *Cytometry Part A* **51A**, 35-45, (2003).
- 21 Rallapalli, R., Strachan, G., Cho, B., Mercer, W. E. & Hall, D. J. A Novel MDMX Transcript Expressed in a Variety of Transformed Cell Lines Encodes a Truncated Protein with Potent p53 Repressive Activity. *J Biol Chem* **274**, 8299-308, (1999).
- 22 Lenos, K. *et al.* Alternate Splicing of the p53 Inhibitor HDMX Offers a Superior Prognostic Biomarker than p53 Mutation in Human Cancer. *Cancer Res* **72**, 4074-84, (2012).
- 23 de Lange, J. *et al.* High levels of Hdmx promote cell growth in a subset of uveal melanomas. *Am J Cancer Res* **2**, 492-507, (2012).
- 24 BreLOT, A., Heveker, N., Montes, M. & Alizon, M. Identification of Residues of CXCR4 Critical for Human Immunodeficiency Virus Coreceptor and Chemokine Receptor Activities. *J Biol Chem* **275**, 23736-44, (2000).
- 25 Zhou, N. *et al.* Structural and Functional Characterization of Human CXCR4 as a Chemokine Receptor and HIV-1 Co-receptor by Mutagenesis and Molecular Modeling Studies. *J Biol Chem* **276**, 42826-33, (2001).
- 26 Xu, L., Li, Y., Sun, H., Li, D. & Hou, T. Structural basis of the interactions between CXCR4 and CXCL12/SDF-1 revealed by theoretical approaches. *Mol Biosyst* **9**, 2107-17, (2013).
- 27 Tamamis, P. & Floudas, C. A. Elucidating a Key Component of Cancer Metastasis: CXCL12 (SDF-1 α) Binding to CXCR4. *J Chem Inf Model* **54**, 1174-88, (2014).
- 28 Qin, L. *et al.* Crystal structure of the chemokine receptor CXCR4 in complex with a viral chemokine. *Science* **347**, 1117-22, (2015).
- 29 Chabot, D. J., Chen, H., Dimitrov, D. S. & Broder, C. C. N-Linked Glycosylation of CXCR4 Masks Coreceptor Function for CCR5-Dependent Human Immunodeficiency Virus Type 1 Isolates. *J Virol* **74**, 4404-13, (2000).
- 30 Wang, J. *et al.* N-linked glycosylation in the CXCR4 N-terminus inhibits binding to HIV-1 envelope glycoproteins. *Virology* **324**, 140-50, (2004).

Chapter 6

Fluorescently labeled CXCR4 targeting peptide as alternative to antibody staining in Ewing sarcoma

L.G.L. Sand, T. Buckle, F.W.B van Leeuwen, W.E. Corver, A.B. Kruisselbrink, P.C.W. Hogendoorn and K. Szuhai

In submission

ABSTRACT

Ewing sarcoma is an aggressive, highly metastatic primary bone and soft tissue tumor most frequently occurring in the bone of young adolescents. Patients, especially those diagnosed with a metastatic disease, have a poor overall survival. Chemokine receptor CXCR4 has a key pro-tumorigenic role in the tumor microenvironment of Ewing sarcoma and has been suggested to be involved in the increased metastatic propensity. Earlier studies on CXCR4 protein expression in Ewing sarcoma yielded contradictory results when compared to *CXCR4* RNA expression studies. Previously, we demonstrated that CXCR4 expression could be detected *in vivo* using the fluorescently tagged CXCR4-specific peptide MSAP-Ac-TZ14011. Therefore, we studied the membranous CXCR4 expression in Ewing sarcoma cell lines using MSAP-Ac-TZ14011. This enabled us to study both CXCR4 cell membrane expression levels and its dynamics using live cell imaging and flow cytometry. CXCR4 cell membrane expression levels detected by the fluorescent peptide, in contrast to the levels by detected the ab2074 -anti-CXCR4- antibody demonstrated a linear correlation with the *CXCR4* RNA expression levels in Ewing sarcoma cell lines. Hence the fluorescently labeled CXCR4 targeting peptide-based method provides a reliable alternative to antibody staining to study the CXCR4 membrane expression in life cells by flow cytometry and microscopy. Furthermore, this method might enable the ability to detect the *in vivo* expression of CXCR4 in Ewing sarcoma which would help to stratify cases for anti-CXCR4 therapy.

KEYWORDS

chemokines, bone tumor, sarcoma, molecular imaging, flow cytometry, peptides, live cell imaging

INTRODUCTION

The tumor microenvironment has a key role in metastasis, angiogenesis and tumor growth [1-3]. Chemokines are important signaling molecules in the tumor microenvironment [4]. The chemokine signaling axis that is involved in all main processes of the tumor microenvironment is CXCL12, also known as stromal derived factor 1, -CXCR4 axis [5,6]. CXCR4 expression has been associated with metastasis and tumor progression in various tumor types, including Ewing sarcoma (EWS) [7-10]. EWS is an aggressive primary malignant neoplasm occurring dominantly in bone in children and young adolescents [11]. Primary extraskelatal soft tissue presentation is more frequent in adults [12]. The five year overall survival in patients with a localized disease at diagnosis is 70% but drops to 10-30% when patients have a metastatic disease at diagnosis or a recurrence [13,14]. The fact that approximately 25% of the patients present metastases at the time of diagnosis potentially implies an important role for CXCR4, which is the highest expressed chemokine receptor in EWS [8]. Expression studies at RNA and protein level revealed that high CXCR4 expression levels were associated with a decreased survival in EWS patients [8,9]. However, when the expression of CXCR4 in metastases was analyzed controversial results were obtained with “high” RNA expression levels and “low” or absent protein expression. A plausible explanation for this discrepancy could be related to the used anti-CXCR4 antibody used in this study which recognizes an N-terminal epitope. Furthermore, immunohistochemistry staining patterns of CXCR4, which is a membrane receptor, were also reported in other studies in the nucleus and cytoplasm [15-17].

Reliable detection of CXCR4 could help to clarify the role of CXCR4 in tumors. CXCR4 has been the target for the development of a variety of imaging agents [18]. Of these agents, for fluorescence imaging, in particular derivatives of the antagonistic peptide (T140) –binding at the fourth transmembrane domain of CXCR4- proved to be of value [19-23]. Moreover, in a more recent study such a T140-analogue has been successfully applied to longitudinally monitor the CXCR4 expression in a ductal carcinoma *in situ* breast cancer model [24]. Therefore, we reasoned that the same peptide analogue could also help clarify the CXCR4 expression levels at the cell membrane in EWS. To investigate this, we used the T140 analogue MSAP-Ac-TZ14011 to discriminate between CXCR4 “high” and CXCR4 “low” EWS cell lines using live cell imaging and flow cytometry. In addition, we evaluated the effect of variation in the flow cytometry preparation protocol on the detected fluorescence. The flow cytometry measurements were compared to the CXCR4 RNA expression levels of the used cell lines.

METHODS

Cell culture

EWS cell lines were obtained from multiple sources: L1062 was established in-house [25]; A673 was obtained from the American Type Culture Collection; 6647 was kindly provided by Dr. Timothy Triche (CHLA, Los Angeles, CA, USA) and TC32 and IARC-EW7 were obtained from the EuroBoNET consortium collection (Institute of Pathology, University Medical Center, Düsseldorf, Germany) [26]. All EWS cell lines were cultured in Iscove’s Modified Dulbecco’s Medium (IMDM) with GlutaMAX supplement, supplemented with 10% heat-inactivated fetal calf serum (FCS) (all from Life Technologies). The B-lineage acute lymphoblastic leukemia (B-ALL) cell line “Leiden-ALL-HP” was kindly provided by the Department of Hematology, Leiden University Medical Center, Leiden, Netherlands and was cultured as described earlier [27]. MDA-MB-231 X4, a human breast cancer cell line which stably over-expresses a GFP-tagged version of the human CXCR4 receptor [28], was kindly provided by Gary Luker (University of Michigan Medical School, MI, USA) and cultured in DMEM supplemented with 10% heat-inactivated FCS (all Life Technologies, Bleiswijk, The Netherlands). This cell line was used a control during the whole study. Regular Mycoplasma DNA Q-PCR screening [29] and Cell-ID STR typing using PowerPlex 1.2 (Promega, Leiden, The Netherlands) were conducted as quality control.

Fluorescent peptide

This study made use of the previously reported hybrid peptide MSAP-Ac-TZ14011, consists of the CXCR4 targeting peptide Ac-TZ14011, a DTPA chelate capable to bind a radioactive Indium and a Cy5.5 fluorophore [30]. This enables detection by single-photon emission computed tomography (SPECT) and fluorescence imaging. Kd and specificity of the peptide are described in this previous report.

Confocal imaging

Cells were plated on a glass bottom culture dish (MatTek Corporation, Ashland, Ma, USA) 24 hours before imaging. Imaging of cells was performed upon incubation with MSAP-Ac-TZ14011 (0.27 μ M) at standard culture conditions. Binding and internalization was assessed in real-time in MDA-MB-231 X4; images were collected every 2 minutes for 3 hours. EWS cell lines TC32 and IARC-EW7 were imaged prior to, directly after addition of MSAP-Ac-TZ14011 to the culture medium (T=0) and 3 hours after incubation with MSAP-Ac-TZ14011

(T=3). Prior to imaging at T=3 cells were washed, lysosomes were stained using lysotracker DND-26 (0.5 μ M) and the nucleus was stained with Hoechst (1:2500 1mg/ml) (both Life Technologies) to discriminate between cytoplasm and nucleus. Imaging was performed on a SP5 microscope with a HCX PL APO 63.0x1.40 OIL lens (Leica, Eindhoven, The Netherlands) at the microscope facility of the Department of Molecular Cell Biology, Leiden University Medical Center. Used excitation lasers and emission detection ranges are in **Table 1**. Images were collected and evaluated using the LASAF software (Leica).

Table 1: Live cell imaging excitation and emission settings

| Signal | Laser | Excitation filter | Detection emission |
|--------------------|-------|-------------------|--------------------|
| DND-26 lysotracker | Argon | 496 | 510-530 |
| Cy5.5 | Argon | 633 | 650-700 |
| Hoechst | Diode | 405 | 415-505 |
| GFP | Argon | 488 | 500-550 |

Table 2: Flow cytometry laser and filters

| Signal | Laser | Filter |
|----------|-------|--------|
| Cy5.5 | Red | 710-40 |
| Alexa647 | Red | 660-20 |
| PI | Blue | 695-40 |
| GFP | Blue | 530-30 |

Flow cytometry

Cells were dissociated with trypsin (Life Technologies) and resuspended in 10% fetal calf serum (FCS), IMDM media. Subsequently, cells were washed and incubated in a blocking buffer PBS 5% BSA (PBA) for 30 minutes at 4°C. Afterwards cells were incubated with MSAP-Ac-TZ14011 (0.27 μ M) for 1h in PBA at 4°C and washed 3 times with PBA at 4°C. Propidium iodide (1 μ M, Sigma-Aldrich GmbH, Steinheim am Albuch, Germany) was added 30 minutes prior to flow cytometry measurement to separate dead cells from vital cells. For the comparison with ab2074 (1:50, Abcam, Cambridge, United Kingdom), the antibody used in the EWS study [9], live cells were prepared for flow cytometry analysis as described by Pelekanos *et al.* [31] using the secondary antibody Goat anti Rabbit Alexa 647 (1:200, ThermoFisher Scientific, Breda, Netherlands). This specific protocol was used since it did not fix the cells and would therefore be comparable to the other used protocols. The used filters and lasers to measure the fluorescent signals are listed in **Table 2**.

To investigate the effect of cell dissociation procedure on the intactness of the receptor and binding of the ligand, cells were handled using three methods: either Trypsin (0.025% without EDTA) or TripLE (all from Life Technologies) or 10 mM EDTA (Sigma-Aldrich GmbH) dissolved in PBS, pH 7.4.

To investigate the effect of fixation on the flow cytometric measurements, methanol fixation was performed. The MSAP-Ac-TZ14011 staining was followed by washing with PBS at 4°C and fixation with 100% methanol (-20°C) by adding the fixative drop-wise. Cells were then stored in 95% methanol for 20 minutes at -20°C, followed by washing with ice cold PBS. All measurements were performed on a LSRII flow cytometer (BD Biosciences, San Jose, CA, USA). Data files containing information from at least 10.000 live (propidium iodide (PI) negative) single cell events were analyzed using WinList 8.0 based (Verity software House, Topsham, ME, USA). The geometric means of the measured central flow cytometry fluorescence units (CFU) were baseline corrected. Cells stained with PI and the secondary antibody Alexa647 were used as baseline.

RNA isolation, RT-Q-PCR analysis and Fluidigm

RNA expression of *CXCR4* was determined as previously described [10]. In brief, total RNA

was isolated using TRIzol Reagent for cDNA generation. RT-Q-PCR was performed using the Fluidigm BioMark HD system (Fluidigm, San Francisco, CA, USA). Samples were measured in duplicates and analyzed using BioMark software, delivered with the HD system.

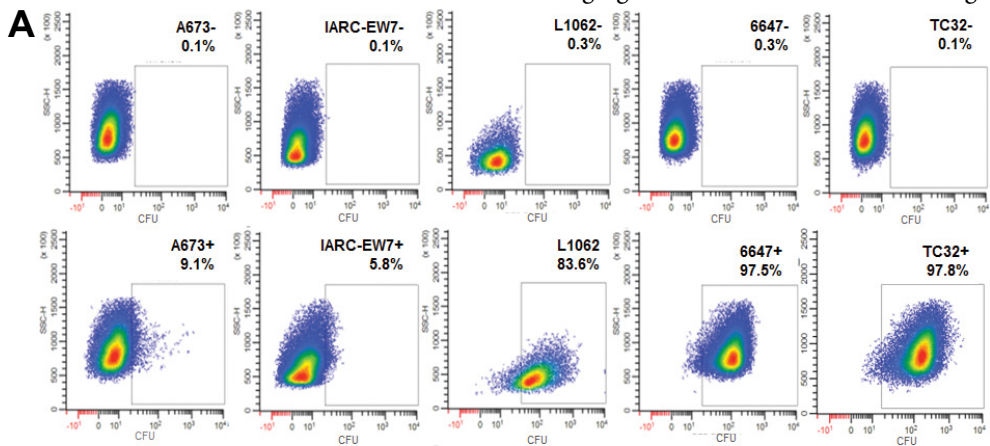
Statistical analysis

Linear regression analysis was performed by using Graphpad Prism 6 (Graphpad Software Inc. La Jolla, CA, USA).

RESULTS

Flow cytometry using MSAP-Ac-TZ14011 on live EWS cells

CXCR4 cell membrane expression levels detected by MSAP-Ac-TZ14011 of five EWS cell lines with varying CXCR4 RNA expression levels (IARC-EW7, A673, L1062, 6647 and TC32) [10] were quantified by flow cytometry. Within the previously tested panel of 20 EWS cell lines, A673 and IARC-EW7 demonstrated very low CXCR4 RNA expression levels, L1062 demonstrated a moderate CXCR4 RNA expression level, and 6647 and TC32 demonstrated high CXCR4 RNA expression levels. In IARC-EW7 and A673 almost no CXCR4 cell membrane expression was detected (>10%). In TC32 and 6647 CXCR4 cell membrane expression was observed in almost all cells (>90%) (Figure 1A). Within the population, varying detection levels were observed with standard deviations ranging from 160.4-873.36 CFU, although



B Figure 1B

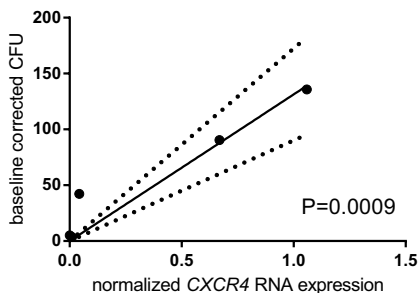


Figure 1: Semi-quantitative detection of MSAP-Ac-TZ14011 in EWS cell lines correlated significantly with previous measured CXCR4 RNA expression levels. A) Cells of the EWS cell lines A673, IARC-EW7, L1062, 6647 and TC32 were harvested without (upper graphs) or with (lower graphs) MSAP-Ac-TZ14011. Fluorescence was afterwards detected at 710-40 nm. The calculated percentage of positive cells is indicated in each panel. B) The baseline corrected geometric mean cytometry fluorescence units (CFU) detected after MSAP-Ac-TZ14011 staining of the in A described EWS cell lines were correlated to the previous determined CXCR4 RNA expression levels (x-axis). Linear regression analysis demonstrated a significant

correlation between the by MSAP-Ac-TZ14011 detected CXCR4 levels and RNA expression levels (P-value and 95% certainty borders are displaced). Both figures are representatives (n=3).

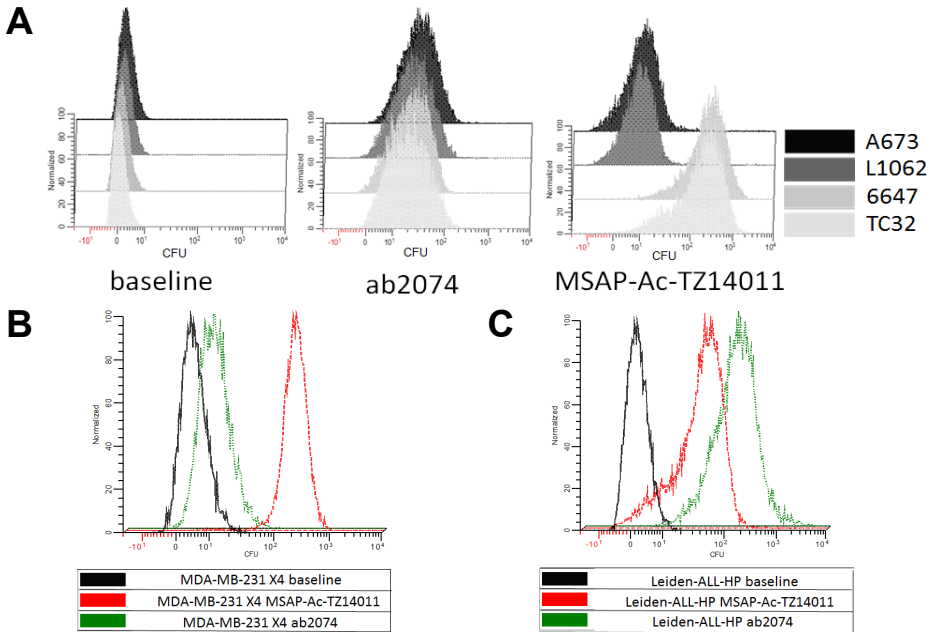


Figure 2: Fluorescence comparison between ab2074 and MSAP-Ac-TZ14011 staining. A) EWS cell lines TC32 (white), 6647 (light gray) (high *CXCR4* RNA expression), L1062 (dark gray) and A673 (black) (low *CXCR4* RNA expression) were similar prepared for the ab2074 and MSAP-Ac-TZ14011 staining following the protocol described by Pelekanos *et al.* [31]. The ab2074 did not demonstrate a difference in *CXCR4* detection between high and low *CXCR4* RNA expressing cell lines where MSAP-Ac-TZ14011 did. Representative figures (n=3) are demonstrated. B) MDA-MB-231 X4 and C) “Leiden-ALL-HP” cells were prepared and stained similar to the EWS cell lines. In MDA-MB-231 X4 the same difference between ab2074 (green) and MSAP-Ac-TZ14011 (red) staining was demonstrated but in “Leiden-ALL-HP” a higher expression was detected by ab2074 than MSAP-Ac-TZ14011 (both n=1). The normalized number of counts is demonstrated.

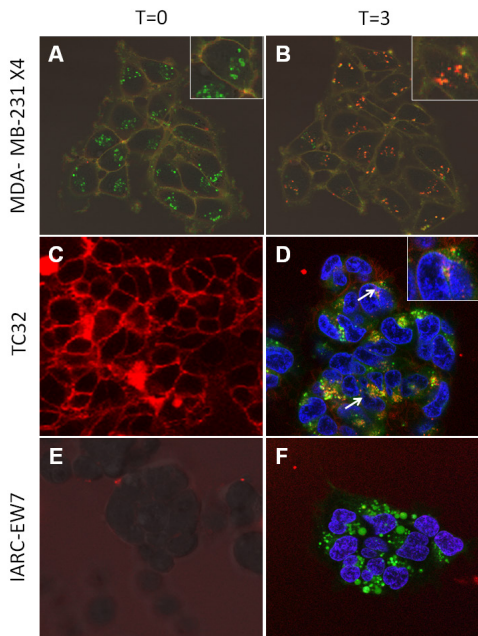


Figure 3: Live cell validation of MSAP-Ac-TZ14011 staining in EWS cells. A,B) MDA-MB-231 X4 containing transfected *CXCR4*-GFP (green) and EWS cell lines (C,D) TC32 and (E,F) IARC-EW7 were imaged by live cell confocal microscopy directly after incubation with MSAP-Ac-TZ14011 (red) (T=0) and after 3 hour incubation (T=3). At T=0 MDA-MB-231 X4 and TC32 demonstrated a membrane staining where no staining was observed in IARC-EW7. IARC-EW7 and TC32 were half an hour prior to imaging incubated with lysotracker DND-26 (green). Hoechst staining (blue) was used to stain the nucleus. All images were taken using a 63x objective. At T=3 intracellular MSAP-Ac-TZ14011 was observed and overlapped with *CXCR4*-GFP. In addition, the DND-26 signal and MSAP-Ac-TZ14011 signal overlapped in TC32 (arrow). In the top corner, if present, is a part of the image enlarged.

no clear separate populations were identified (**Figure 1A**). The variation in fluorescence within the cell lines were consistent to earlier observations [32]. The baseline corrected geometric means of the measured MSAP-Ac-TZ14011 levels were correlated to the earlier obtained CXCR4 RNA expression levels [10]. A significant linear correlation ($P=0.0009$) was obtained between these two conditions in various cell lines (**Figure 1B**).

Flow cytometric comparison of MSAP-Ac-TZ14011 with ab2074 and validation of the cell-preparation effects on these staining

The MSAP-Ac-TZ14011 fluorescence levels were compared to the levels obtained with the anti-CXCR4 antibody ab2074. In contrast to the findings with MSAP-Ac-TZ14011 peptide, ab2074 antibody staining did not demonstrate any difference between the studied EWS cell lines (**Figure 2A**). In addition, in the MDA-MB-231 X4 cells a lower signal was detected when using ab2074 compared to MSAP-Ac-TZ14011 (**Figure 2B**). As a positive control cell line of different origin growing in suspension the “Leiden-ALL-HP” cell line was used. In this cell line the detected ab2074 antibody signals were higher than the MSAP-Ac-TZ14011 levels (**Figure 2C**).

As “Leiden-ALL-HP” demonstrated a higher signal intensity level with ab2074 antibody and is growing in suspension, the influence of cell dissociation was studied on the ab2074 and MSAP-Ac-TZ14011 detected levels. Different cell dissociations methods were compared using regular trypsin (enzyme digestion) TrpLE (recombinant enzyme used in stem cell research to treat trypsin sensitive cells) and EDTA alone (non-enzymatic treatment). None of the harvesting methods (EDTA, Trypsin and TrpLE) influenced any of the staining methods (**Figure S1**). In addition, we observed that fixation with methanol after MSAP-Ac-TZ14011 incubation increased the detected fluorescence, both in high and low CXCR4 expressing cell lines (**Figure S2**).

Live cell imaging of CXCR4 by MSAP-Ac-TZ14011 in EWS cells

EWS cell lines TC32 and IARC-EW7 were further investigated by live cell imaging. TC32 and IARC-EW7 had, respectively, “high” and “low” CXCR4 RNA expression levels [10] and “high” and “low” CXCR4 levels detected by MSAP-Ac-TZ14011. As control for estimation of the MSAP-Ac-TZ14011 incubation period MDA-MB-231 X4, in which overexpressed CXCR4-GFP is located at the membrane and cytoplasm, was imaged over time (**Figure 3A-B**). Directly after addition of MSAP-Ac-TZ14011 ($T=0$) all membrane expressed CXCR4-GFP overlapped with MSAP-Ac-TZ14011 as shown in **Figure 3A** in orange. The intracellularly located CXCR4-GFP signal is not overlapping with MSAP-Ac-TZ14011 signal. Over time MSAP-Ac-TZ14011 was internalized with CXCR4-GFP and after 3 hours almost all CXCR4-GFP present was bound by MSAP-Ac-TZ14011 ($T=3$) (**Figure 3B**). This includes the CXCR4-GFP located intracellularly. TC32, a high CXCR4 mRNA expressing EWS cell line, demonstrated at $T=0$ a membranous MSAP-Ac-TZ14011 staining similar to that demonstrated by MDA-MB-231 X4 (**Figure 3C**). After 3 hours incubation internalized MSAP-Ac-TZ14011, like in MDA-MB-231 X4, was observed in TC32 (**Figure 3D**). The signal partly overlapped with the lysotracker DND-26 signal, indicating that a part CXCR4-MSAP-Ac-TZ14011 complex was directed towards the lysosomes. The low CXCR4 expressing EWS cell line IARC-EW7 cells showed neither cell membrane staining at $T=0$ nor cytoplasmic staining at $T=3$ of MSAP-Ac-TZ14011, suggesting no binding and internalization of CXCR4 was observed (**Figure 2E-F**).

DISCUSSION

In this study we have illustrated that a CXCR4 targeting fluorescent T140 analogue, MSAP-Ac-TZ14011 tracer peptide, can be used as alternative for antibodies to determine the CXCR4 cell membrane expression levels in EWS cell lines and that the binding of MSAP-Ac-TZ14011 is not significantly influenced by the used cell dissociation method. The measured levels of cell bound MSAP-Ac-TZ14011, and thereby indirectly the measured CXCR4 levels, were correlated to *CXCR4* mRNA expression and to CXCR4 cell membrane levels detected by antibody staining. As the CXCR4 signaling pathway have a stimulating role in the main processes of the tumor microenvironment in many tumor types, CXCR4 could be a candidate biomarker and a potential therapeutic target. [5,7]. Moreover, treatment with CXCR4 antagonist T140 and analogues like Ac-TZ14011 inhibited tumor growth [33]. In EWS, however, although RNA expression has been reported, protein expression in metastases was absent in paraffin embedded material using immunohistochemistry [8,9]. CXCR4 consists of multiple isoforms with varying N-terminal ends of which one, CXCR4-2, is dominantly expressed [34]. Both the N- and C-terminal ends of CXCR4 contain many potential post-translational modification sites and changes at these sites may influence antibody recognition potentially explaining the various staining patterns observed in earlier studies [35-37]. As the T140 binding site does not contain any reported post-translational modifications and *in situ* modeling suggests MSAP-Ac-TZ14011 binds at the same site this detection could be a better alternative to detect all forms of the receptor [18,23,35,38]. The detected MSAP-Ac-TZ14011 signals correlated linearly with the earlier obtained RNA expression levels in EWS cell lines and co-localize with CXCR4-GFP expressed in MDA-MB-231 X4 (**Figure 1B and 2A-B**). In addition, the detected MSAP-Ac-TZ14011 levels using flow cytometry corresponded to the observations during live cell imaging of the cells (**Figure 1A and 2C,E**). Limitations of this method are that cells should be stained alive with MSAP-Ac-TZ14011 and not fixed with methanol prior to staining.

The observed internalization of the MSAP-Ac-TZ14011 in TC32 and MDA-MB-231 X4 confirms previously reported internalization of Ac-TZ14011-FITC [22]. The CXCR4-GFP overlap with MSAP-Ac-TZ14011 during CXCR4 internalization in MDA-MB-231 X4 and the overlap of MSAP-Ac-TZ14011 with the lysotracker DND-26 in TC32 support the suggestion that upon CXCR4 binding the peptide-CXCR4 complex is internalized. This peptide therefore can be used to detect intracellular located CXCR4 in cells when incubated over a longer period at standard culture conditions. Moreover, as *in vivo* detection of CXCR4 membrane expression was demonstrated in a mouse ductal carcinoma *in situ* model [24], it might possible to detect CXCR4 expression *in vivo* in EWS patients using MSAP-Ac-TZ14011, especially since it contains both a SPECT/CT and fluorescence imaging agent.

CXCR4 is involved in metastasis and increased *CXCR4* RNA expression levels were measured in both metastasis derived cell lines compared to non-metastasis derived cell lines and metastases compared to localized tumors [8]. In addition, factors inhibiting CXCR4 activation can be used to identify high risk patients [10]. The detected MSAP-Ac-TZ14011 levels in EWS cell lines positively correlated with the *CXCR4* RNA expression levels and the MSAP-Ac-TZ14011 signal overlapped with the CXCR4-GFP membrane signal. When assuming the MSAP-Ac-TZ14011 fluorescence level is correlated to the CXCR4 cell membrane level, metastasis might have a higher CXCR4 cell membrane expression than localized tumors. Such

a positive correlation between the migration/invasiveness of a cell line and the CXCR4 cell membrane expression has been observed both in EWS and breast cancer cell lines [24,32]. However, clinical data on the cell membrane expression of CXCR4 and its relation with tumor invasiveness is still lacking. Using this method might enable determination of CXCR4 cell membrane expression in patients. This would help to stratify patients for alternative therapies, like anti-CXCR4 therapy and might serve as prognostic marker for EWS patients [9]. In conclusion, staining with MSAP-Ac-TZ14011, by using live cell imaging and flow cytometry, resulted in fluorescence levels that corresponded to the CXCR4 RNA expression levels of the used EWS cell lines. This peptide-based method was appropriate for studying qualitatively and semi-quantitatively CXCR4 cell membrane expression in live cells in EWS and other cell types and might be well suited for future *in vitro* and *in vivo* CXCR4 studies.

ACKNOWLEDGEMENTS

This study was supported by National organization for Scientific Research (NWO) Grant NWO-TOP GO 854.10.012 by a Koningin Wilhelmina Fonds (KWF) translational research award (Grant No. PGF 2009-4344), a Netherlands Organization for Scientific Research VIDI grant (Grant No. STW BGT11272), and the 2015-2016 Post-Doctoral Molecular Imaging Scholar Program Grant granted by the Society of Nuclear Medicine and Molecular imaging (SNMMI) and the Education and Research Foundation for Nuclear Medicine and Molecular Imaging.

REFERENCES

- 1 Quail, D. F. & Joyce, J. A. Microenvironmental regulation of tumor progression and metastasis. *Nat Med* **19**, 1423-37, (2013).
- 2 Bruno, A. *et al.* in *Advances in Nutrition and Cancer* Vol. 159 *Cancer Treatment and Research* (eds Vincenzo Zappia *et al.*) Ch. 23, 401-26 (Springer Berlin Heidelberg, 2014).
- 3 Whiteside, T. L. The tumor microenvironment and its role in promoting tumor growth. *Oncogene* **27**, 5904-12, (2008).
- 4 Mantovani, A. *et al.* The chemokine system in cancer biology and therapy. *Cytokine Growth Factor Rev* **21**, 27-39, (2010).
- 5 Guo, F. *et al.* CXCL12/CXCR4: a symbiotic bridge linking cancer cells and their stromal neighbors in oncogenic communication networks. *Oncogene*, (2015).
- 6 Domanska, U. M. *et al.* A review on CXCR4/CXCL12 axis in oncology: No place to hide. *Eur J Cancer* **49**, 219-30, (2013).
- 7 Lippitz, B. E. Cytokine patterns in patients with cancer: a systematic review. *Lancet Oncol* **14**, e218-e28, (2013).
- 8 Bennani-Baiti, I. M. *et al.* Intercohort Gene Expression Co-Analysis Reveals Chemokine Receptors as Prognostic Indicators in Ewing's sarcoma. *Clin Cancer Res* **16**, 3769-78, (2010).
- 9 Berghuis, D. *et al.* The CXCR4-CXCL12 axis in Ewing sarcoma: promotion of tumor growth rather than metastatic disease. *Clin Sarc Res* **2**, 24, (2012).
- 10 Sand, L. G. L. *et al.* CXCL14, CXCR7 expression and CXCR4 splice variant ratio associate with survival and metastases in Ewing sarcoma patients *Eur J Cancer* **51**, 2624-33, (2015).
- 11 van den Berg, H., Kroon, H. M., Slaar, A. & Hogendoorn, P. C. W. Incidence of biopsy-proven bone tumors in children: a report based on the Dutch pathology registration "PALGA". *J Pediatr Orthop* **28**, 29-35, (2008).
- 12 De Alava, E., Lessnick, S. L. & Sorensen, P. H. in *WHO Classification of Tumors of Soft Tissue and Bone* (eds C.D.M. Fletcher, J.A. Bridge, P. C. W. Hogendoorn, & F. Mertens) 306-9 (IARC, 2013).
- 13 Ladenstein, R. *et al.* Primary disseminated multifocal Ewing sarcoma: results of the Euro-EWING 99 trial. *J Clin Oncol* **28**, 3284-91, (2010).
- 14 Le Deley, M.-C. *et al.* Impact of EWS-ETS Fusion Type on Disease Progression in Ewing's sarcoma/peripheral primitive neuroectodermal tumor: Prospective Results From the Cooperative Euro-EWING 99

- Trial. *J Clin Oncol* **28**, 1982-8, (2010).
- 15 Na, I.-K. *et al.* Nuclear expression of CXCR4 in tumor cells of non-small cell lung cancer is correlated with lymph node metastasis. *Hum Pathol* **39**, 1751-5, (2008).
- 16 Brault, L. *et al.* CXCR4-SERINE339 regulates cellular adhesion, retention and mobilization, and is a marker for poor prognosis in acute myeloid leukemia. *Leukemia* **28**, 566-76, (2014).
- 17 Fischer, T., Nagel, F., Jacobs, S., Stumm, R. & Schulz, S. Reassessment of CXCR4 Chemokine Receptor Expression in Human Normal and Neoplastic Tissues Using the Novel Rabbit Monoclonal Antibody UMB-2. *PLoS One* **3**, e4069, (2008).
- 18 Kuil, J., Buckle, T. & van Leeuwen, F. W. B. Imaging agents for the chemokine receptor 4 (CXCR4). *Chem Soc Rev* **41**, 5239-61, (2012).
- 19 Tamamura, H. *et al.* A Low-Molecular-Weight Inhibitor against the Chemokine Receptor CXCR4: A Strong Anti-HIV Peptide T140. *Biochem Biophys Res Commun* **253**, 877-82, (1998).
- 20 Kuil, J. *et al.* Hybrid peptide dendrimers for imaging of CXCR4 expression. *Mol Pharm* **8**, 2444-53, (2011).
- 21 Hanaoka, H. *et al.* Development of a ¹¹¹In-labeled peptide derivative targeting a chemokine receptor, CXCR4, for imaging tumors. *Nucl Med Biol* **33**, 489-94, (2006).
- 22 van den Berg, N. S., Buckle, T., Kuil, J., Wesseling, J. & van Leeuwen, F. W. B. Immunohistochemical Detection of the CXCR4 Expression in Tumor Tissue Using the Fluorescent Peptide Antagonist Ac-TZ14011-FITC. *Transl Oncol* **4**, 234-40, (2011).
- 23 Boulais, P. E. *et al.* Photolabeling identifies transmembrane domain 4 of CXCR4 as a T140 binding site. *Biochem Pharmacol* **78**, 1382-90, (2009).
- 24 Buckle, T. *et al.* Use of a Single Hybrid Imaging Agent for Integration of Target Validation with *In Vivo* and *In Vivo* Imaging of Mouse Tumor Lesions Resembling Human DCIS. *PLoS One* **8**, e48324, (2013).
- 25 Szuhai, K., Ijszenga, M., Tanke, H. J., Rosenberg, C. & Hogendoorn, P. C. W. Molecular cytogenetic characterization of four previously established and two newly established Ewing sarcoma cell lines. *Cancer Genet Cytogenet* **166**, 173-9, (2006).
- 26 Ottaviano, L. *et al.* Molecular characterization of commonly used cell lines for bone tumor research: A trans-European EuroBoNet effort. *Genes Chromosomes Cancer* **49**, 40-51, (2010).
- 27 Nijmeijer, B. A. *et al.* Long-term culture of primary human lymphoblastic leukemia cells in the absence of serum or hematopoietic growth factors. *Exp Hematol* **37**, 376-85, (2009).
- 28 Luker, K. E., Gupta, M. & Luker, G. D. Bioluminescent CXCL12 Fusion Protein for Cellular Studies of CXCR4 and CXCR7. *Biotechniques* **47**, 625-32, (2009).
- 29 van Kuppeveld, F. J. *et al.* Genus- and species-specific identification of mycoplasmas by 16S rRNA amplification. *Appl Environ Microbiol* **58**, 2606-15, (1992).
- 30 Kuil, J., Velders, A. H. & van Leeuwen, F. W. B. Multimodal tumor-targeting peptides functionalized with both a radio- and a fluorescent label. *Bioconjug Chem* **21**, 1709-19, (2010).
- 31 Pelekanos, R. A. *et al.* Intracellular trafficking and endocytosis of CXCR4 in fetal mesenchymal stromal cells. *BMC Cell Biol* **15**, 15-, (2014).
- 32 Krook, M. A. *et al.* Stress-Induced CXCR4 Promotes Migration and Invasion of Ewing sarcoma. *Mol Cancer Res* **12**, 953-64, (2014).
- 33 Burger, J. A. & Peled, A. CXCR4 antagonists: targeting the microenvironment in leukemia and other cancers. *Leukemia* **23**, 43-52, (2008).
- 34 Sand, L. G. L. *et al.* Novel splice variants of CXCR4 identified by transcriptome sequencing. *Biochem Biophys Res Commun* **466**, 89-94, (2015).
- 35 Ziarek, J. J. *et al.* Sulfopeptide Probes of the CXCR4/CXCL12 Interface Reveal Oligomer-Specific Contacts and Chemokine Allostery. *ACS Chem Biol* **8**, 1955-63, (2013).
- 36 Rapp, C., Snow, S., Laufer, T. & McClendon, C. L. The role of tyrosine sulfation in the dimerization of the CXCR4:SDF-1 complex. *Protein Sci* **22**, 1025-36, (2013).
- 37 Zhou, N. *et al.* Structural and Functional Characterization of Human CXCR4 as a Chemokine Receptor and HIV-1 Co-receptor by Mutagenesis and Molecular Modeling Studies. *J Biol Chem* **276**, 42826-33, (2001).
- 38 Wang, J. *et al.* N-linked glycosylation in the CXCR4 N-terminus inhibits binding to HIV-1 envelope glycoproteins. *Virology* **324**, 140-50, (2004).

SUPPLEMENTARY FIGURES

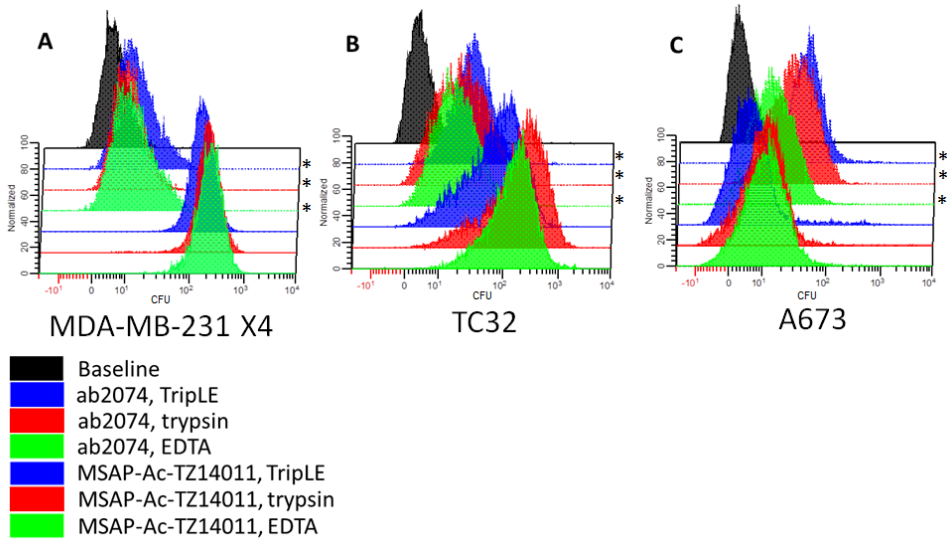


Figure S1: Validation to show the effect of cell harvesting procedure on detected MSAP-Ac-TZ14011 and ab2074 signal intensities. The effect of 10 μ M EDTA (green), TripLE (red) and 0.025% trypsin (blue) treatment on the fluorescence of ab2074 (*) and MSAP-Ac-TZ14011 staining were tested on (A) MDA-MB-231 X4, (B) TC32 and (C) A673. As representative baseline (black), the result of TripLE treatment without additional staining was used. No significant difference in fluorescence was observed. The Y-axis represents the normalized number of cell counts (n=1).

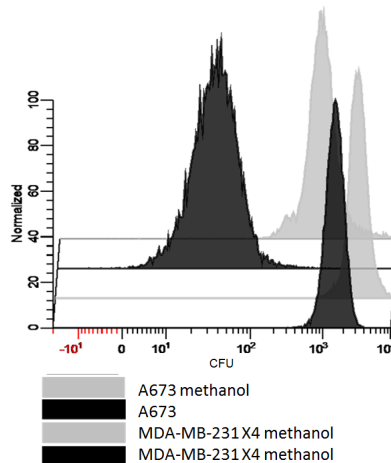


Figure S2: Influence of methanol fixation after MSAP-Ac-TZ14011 staining. EWS cell line A673 and MDA-MB-231 X4 were stained with MSAP-Ac-TZ14011 and subsequently were (black) or were not (gray) fixed with methanol. Methanol fixation of the cells lead to increased fluorescence levels. The Y-axis represents the normalized number of cell counts (n=1).

Chapter 7

Evaluation of CXCR4 specific endocytosis using an activatable peptide

**L.G.L. Sand, S. van der Wal, P.C.W. Hogendoorn, C.M. Korne, K. Szuhai, F.W.B. van
Leeuwen, T. Buckle**

In preparation

ABSTRACT

For many tumors the membrane-bound chemokine receptor CXCR4 is an important factor in tumor progression and metastasis. Upon binding of its dominant ligand CXCL12/stromal derived factor 1 (SDF-1), CXCR4 is internalized via endocytosis and degraded or recycled. To specifically study the endocytosis process, we have synthesized the receptor specific and redox sensitive/thiol-activatable Cy5-S-S-Cy3-Ac-TZ14011 peptide. In vitro analysis demonstrated that Foster Resonance Energy Transfer (FRET) with Cy5 quenched the Cy3 emission in the disulfide-containing label, while cleavage of this disulfide bond resulted in a fluorescently active Cy3-Ac-TZ14011 peptide. Real-time evaluation of receptor internalization in Ewing sarcoma cell lines demonstrated both a qualitative and quantitative increase in Cy3 intensity when CXCR4 was expressed at “high” levels. This method enables studying of CXCR4 dynamics at the live cell level and can discriminate between internalized and non-internalized receptors. This principle might be transferred to other receptor endocytosis studies.

KEYWORDS

FRET, internalization, fluorescence, sarcoma, chemokines, Ewing sarcoma

INTRODUCTION

CXCR4 is of major importance for a number of processes in the tumor microenvironment [1-3], for example in Ewing sarcoma (EWS), an aggressive, highly metastatic and well vascularized bone tumor [4]. It has been associated with the level of angiogenesis, metastasis and survival [5-9]. A complex network of regulation processes allows CXCR4 to perform its tumorigenic functions. One of these processes is the CXCR4 trafficking to and from the membrane and the availability on the membrane [10,11]. This process is cell/tissue-type dependent [10,12]. The general view is that newly synthesized CXCR4 receptors are directed towards the cell surface. Upon extracellular binding of its dominant ligand CXCL12 also known as stromal derived factor 1, the receptor then internalizes and is subsequently degraded by lysosomes or is recycled to the cell membrane [13]. The endocytosis process of CXCR4 is influenced by different tracks, including dynamin-dependent and clathrin-dependent endocytosis, lipid rafts or macropinocytosis [12,14,15].

To image CXCR4 *in vitro* and *in vivo* a variety of agents have been developed [16]. Especially fluorescent and hybrid (both fluorescent and radioactive) analogues of the antagonistic CXCR4 targeting peptide T140 showed great potential in flow cytometry, microscopy and non-invasive SPECT imaging [17-19]. However, these agents can only image and track CXCR4 and cannot on its own be used to discriminate between intracellular and extracellular CXCR4.

General the principle of an activatable peptide, a peptide active upon cleavage, has dominantly been used for enzymatic activity [20]. As an imaging agent this principle opens the possibility to use two tissue characteristics. For example, by combining a pH sensitive bond with a receptor targeting peptide, only in an acidic environment with the present receptor the signal after cleavage would appear [21]. This principle with an Iridium-Cy5 FRET pair for long luminescence lifetime has recently been reported [22].

When coupled to a receptor targeting agent, the activatable peptide principle can be also used to study the endocytosis dynamics and intracellular trafficking of receptors in live cells

when the receptor is internalized upon binding of the activatable peptide which is intracellularly cleaved [23]. Thereby, it can distinguish the internalized fraction of the studied receptor from the rest. To study the CXCR4 endocytosis dynamics we coupled an activatable Cy5-S-S-Cy3 label, to the CXCR4 binding and internalizing peptide Ac-TZ14011 [16,18,19]. Cy3 and Cy5 are a well-known Förster Resonance Energy Transfer (FRET) pair [24,25]. We reasoned that upon binding and cellular internalization of Cy5-S-S-Cy3-Ac-TZ14011, the disulfide bond between the two dyes will be reduced in the reducing intracellular environment. This will result in a change in fluorescence emitted by the peptide from 680 nm to 580 nm when excited at the 550 nm (**Figure 1**). This effect was studied in high and low CXCR4 RNA expressing EWS cell lines to validate the activatable CXCR4 targeting compound as receptor specific endocytosis tracer.

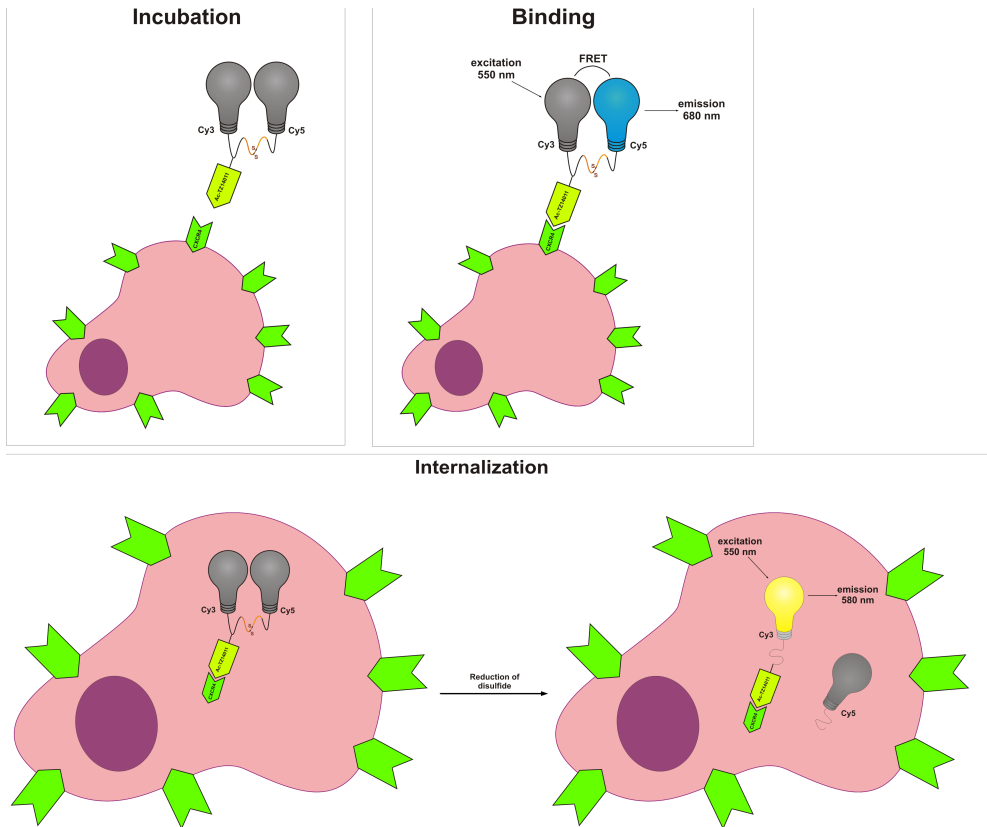


Figure 1: Principle of receptor targeted activatable imaging agents. The Cy3-Cy5 FRET label, with a disulfide bond between the dyes (depicted in orange), coupled to the CXCR4 targeting peptide Ac-TZ14011 is administrated to live cells. When the peptide (Cy5-S-S-Cy3-Ac-TZ14011) is excited at 550 nm the Cy3 transfers the energy to Cy5 which emits light of 680 nm. Upon binding, the Cy5-S-S-Cy3-Ac-TZ14011-CXCR4 complex is internalized and the disulfide bond between Cy3 and Cy5 is reduced in a reducing intracellular environment. When the reduced peptide is excited at 550 nm, Cy3 cannot transfer the energy to Cy5 and emits light at a wavelength of 580 nm.

MATERIAL & METHODS

Chemical synthesis, purification and characterization

All chemicals were obtained from commercial sources and used without further purification. Semi-preparative HPLC was performed on a Waters HPLC system using a 1525EF pump, a 2489 dual wavelength absorbance detector (Waters Chromatography, Etten-Leur, the Netherlands) and a flow rate of 6 mL/min using a gradient of 5 % to 95 % acetonitrile in water with 0.1 % TFA of 100 min (Dr. Maisch Reprosil-Pur C18-AQ, 10 μm (250 \times 10 mm) column) (Dr. Maisch High Performance LC, Ammerbuch-Entringen, Germany). Analytical HPLC was performed using a flow rate of 1 mL/min using a gradient of 5 % to 95 % acetonitrile in water with 0.1 % TFA of 40 min (Dr. Maisch Reprosil-Pur C18-AQ 5 μm , (250 \times 4.60 mm) column) (Dr. Maisch High Performance LC). A Waters Acquity UPLC-ESI-MS system using a Acquity UPLC photodiode array detector, an SQ Detector mass spectrometer and a flow rate of 0.5 mL/min (Waters BEH C18 130 \AA 1.7 μm (100 \times 2.1 mm) column) (all from Waters Chromatography) was used for ESI-MS analysis. MALDI-TOF analysis was performed on a Bruker Microflex (Bruker Daltonics, MA, US) using a matrix of α -cyano-4-hydroxycinnamic acid and a reference of Granuliberin R ($[\text{M}+\text{H}]^+ = 1423.7$ Da). Freeze-drying was performed by dissolution or dilution of the compound in *tert*-butanol/ H_2O (1:1 v/v) and freeze-drying in a Christ Alpha RVC equipped with a Mitsubishi VaCo 2 condenser (Christ, Osterode am Harz, Germany).

Synthesis of Boc-Cys(S- CH_2CH_2 - NH_2)-OH (1)

Boc-Cys(Npys)-OH (187 mg, 0.5 mmol) (Sigma-Aldrich GmbH, Steinheim am Albuch, Germany), and cysteamine hydrochloride (45 mg, 0.4 mmol) were dissolved in THF/ H_2O (1:1 v/v, 5 mL). *N*-methyl morpholine (NMM, 20 μL , 0.2 mmol) was subsequently added and the reaction mixture was stirred overnight. Disappearance of the cysteamine starting material from the now orange reaction mixture was confirmed by TLC (10% MeOH/ CH_2Cl_2 , staining with ninhydrin) and ESI-MS indicated a mass of 297.1 Da, corresponding to the $[\text{M}+\text{H}]^+$ of the product (calculated mass 297.1 Da). In addition, two other masses corresponding to 3-nitro-2-pyridine thiol (156.8 Da) and excess Boc-Cys(Npys)-OH (375.9 Da) were also found. This crude material was used directly in the next synthesis.

Synthesis of Boc-Cys(S- CH_2CH_2 -NH-Cy5)-OH (2)

To 0.5 mL of the reaction mixture of compound 1 (40 μmol), NMM (10 μL , 100 μmol) was added to adjust to pH to \sim 8. Cy5-OSu [26] (5 mg, 5.4 μmol) was added and stirred for 2.5 h. Hereafter the mixture was diluted with 4 mL H_2O and purified by semi-preparative HPLC (elution time: $t_R = 33$ min). The fraction containing the product was freeze-dried to yield a blue fluffy solid (0.8 mg, 0.7 μmol). MALDI-TOF: $[\text{M}]^+$ found 1043.96 Da, calculated 1043.29 Da. The Boc group was found to be partially removed during storage in the TFA buffer: mass $[\text{M}]^+$ found was 943.83 Da, calculated mass was 943.24 Da.

Synthesis of Cy3-Cys(S- CH_2 - CH_2 -NH-Cy5)-OH (Cy5-S-S-Cy3, 3)

The Boc-group was completely removed from compound 2 (0.4 mg, 0.35 μmol) by addition of trifluoroacetic acid (TFA, 1 mL) and stirring for 1 h. The TFA was removed by concentration *in vacuo* and the residue was co-evaporated with chloroform twice, after which it was lyophilized. The dry compound was dissolved in phosphate buffer (1 mL, 100 mM, pH 8.3), followed by the addition of Cy3-TFP ester [27] (3 mg, 3 μmol) in DMF (200

μL). The reaction mixture was allowed to stir for 3 h and was diluted with 4 mL H_2O . After acidification with 10 μL AcOH. The product was purified by semi-preparative HPLC ($t_R = 26$ min). This fraction was freeze-dried to yield a purplish blue fluffy solid (0.4 mg, 0.21 μmol) with an analytical HPLC $t_R = 23.9$ min. Mass $[\text{M}-\text{H}]^+$ found was 1664.46 Da, calculated mass was 1663.43 Da (**Figure S1**). Mass $[\text{M}-2\text{H}+\text{Na}]^+$ found was 1686.45 Da, calculated mass was 1685.41 Da. Some disulfide cleavage induced by the ionization process was also observed generating ions of 824.67 Da and 842.66 Da [28].

Synthesis of Cy3-Cys(S-CH₂-CH₂-NH-Cy5)-[Ac-TZ14011] (Cy-S-S-Cy3-Ac-TZ14011, 4)

Compound 3 (0.2 mg, 0.1 μmol), PyBOP (2 mg, 4 μmol), Ac-TZ14011 [29] (2 mg, 0.3 μmol) and NMM (10 μL , 100 μmol) were dissolved in DMF (400 μL) and stirred for 2 h, after which water was added and the reaction was allowed to continue for another 30 min. The reaction mixture was diluted with 4 ml water, acidified with AcOH (10 μL) and purified by semi-preparative HPLC ($t_R = 32$ min). The fraction containing the product was freeze-dried to yield a purplish blue fluffy solid that was dissolved in 1 mL water. The concentration was determined by spectroscopy using a molar extinction coefficient of $2.4 \cdot 10^5$ [30] and was found to be 2.4 μM . The resulting stock solution was used for all further experiments. MALDI-TOF Mass $[\text{M}]^+$ found a mass of 3752.36 Da, calculated mass was 3751.49 Da ($t_R = 26.1$ min on analytical HPLC) (**Figure S2**).

Photophysical properties of the Cy3-Cy5 FRET labelling

Compound 3 was dissolved in PBS (3 mL, 3 μM final volume and concentration) and absorbance was measured in a quartz cuvette on a Ultraspec 3000 (Amersham Pharmacia Biotech, Munich, Germany) subtracting a PBS blank. Fluorescence properties were analyzed on a Perkin-Elmer LS-55 spectrofluorometer (Perkin-Elmer, Waltham, MA, US). After excitation at 520 nm, the emission spectrum was obtained between 530-750 nm. A 2D excitation/emission scan was obtained while exciting between 450-750 nm with 5 nm increments with emission recorded at 450-750 nm for each scan. Results were incorporated into 2D and 3D representations using MatLab (Mathworks Inc., Massachusetts, USA) software using the surf(x,y,z) command. A DTT solution was subsequently added (50 mM stock, 60 μL) to the cuvette for a final concentration of 1 mM. After mixing, the cuvette was allowed to incubate for 140 min, after which fluorescence was measured every 5 min after excitation at 520 nm. When the compound was completely reduced, a 2D and 3D representation was recorded similar to the one described above.

Cell culture

EWS cell line TC32, having a high CXCR4 RNA expression, was obtained from the EuroBoNeT consortium collection (Institute of Pathology, University Medical Center, Düsseldorf, Germany) [31]; A673, having a low CXCR4 RNA expression, was obtained from the ATCC. TC32 and A673 were cultured in Iscove's modified Dulbecco's medium (IMDM) containing GlutaMAX supplement under standard culture conditions. Both media were supplemented with 1% streptomycin/penicillin and 10% heat-inactivated FCS (all were obtained from Life Technologies, Bleiswijk, The Netherlands).

Confocal imaging

Cells were plated on a glass bottom culture dish (MatTek corporation, Ashland, Ma, USA) 24 h before imaging to let the cells attach to the bottom. Hoechst 33258 and lysotracker DND-

26 (Life Technologies) were added at a final concentration of 1 $\mu\text{g}/\text{mL}$ for 1 h and excess was washed away prior to imaging. Cy-S-S-Cy3-Ac-TZ14011 was sonicated (1 min) and added to the dish at a final concentration of 4 μM and present in media during first 3 h of imaging. Live cell imaging was performed on SP8 with a white light laser and a UV laser by sequential imaging at the dye its optimal excitation wavelength and measured in their specific emission range at a 63 times magnification under standard culture conditions with a HC PL APO CS2 63x/1.40 OIL lens (Leica, Eindhoven, The Netherlands) (**Table 1**). Imaging was performed during 3 h. After 3 h imaging cells were washed incubated standard culture conditions to be measured at 24 h and 72 h.

Table 1: Excitation and emission wavelength ranges of the different fluorophores used during imaging

| Fluorophore | Excitation | Emission detection range |
|-------------|-------------------|--------------------------|
| Hoechst | 405 nm (UV diode) | 415-509 nm |
| DND-26 | 504 nm | 510-530 nm |
| Cy3 | 552 nm | 558-593 nm |
| Cy5 | 631 nm | 652-709 nm |
| FRET | 552 nm | 652-709 nm |

Image analysis

Quantitative fluorescence intensity levels of multiple images (minimal 3 per measurement) were obtained using LASX software by calculating the mean intensity of the cell covered area (Leica) and each image was background-corrected by the analyzed the fluorescence intensity levels of the nuclei present in the analyzed area (observed by Hoechst 33528 staining). As controls, images were made before adding Cy-S-S-Cy3-Ac-TZ14011 and after adding Ac-TZ14011-MSAP [17], which contains a Cy5 but no Cy3 fluorophore, was used as control for FRET fluorescence when exciting at 552 nm and measuring at 652-709 nm. All fluorescence images collected at different wavelengths are shown separately in **Figure S3 and S4**.

RESULTS

Synthesis and in vitro validation of activatable Cy-S-S-Cy3-Ac-TZ14011

As presented in **Figure 2**, the CXCR4 endocytosis tracer is generated by linking the synthesized Cy5-S-S-Cy3 FRET label to Ac-TZ14011 by using its carboxylic acid. FRET-label synthesis was started using Boc-Cys(Npys)-OH as a straightforward platform for a asymmetric disulfide bond (**Figure 2**, compound 1). Crude material 1 was used for conjugation with an activated ester of sulfonated Cy5 to afford compound 2. After purification of compound 2, the Boc protecting group was removed and the activated ester of sulfonated Cy3 was added under aqueous conditions yielding Cy5-S-S-Cy3 (3). Ultimately, conjugation of Cy5-S-S-Cy3 (3) with the targeting peptide Ac-TZ14011 yielded the activatable CXCR4 tracer Cy5-S-S-Cy3-Ac-TZ14011 (4).

The photophysical properties of compound 3 were analyzed *in vitro* by measuring the absorbance and FRET efficiency (**Figure 3 and S3A**). The absorbance demonstrated a pattern matching the Cy3 and Cy5 absorbance peaks. As a result of a difference in their extinction coefficients, the Cy5 signal intensity was higher than that of the Cy3 signal. The FRET efficiency was assayed in PBS and showed low Cy3 fluorescence upon excitation at 520 nm but a high

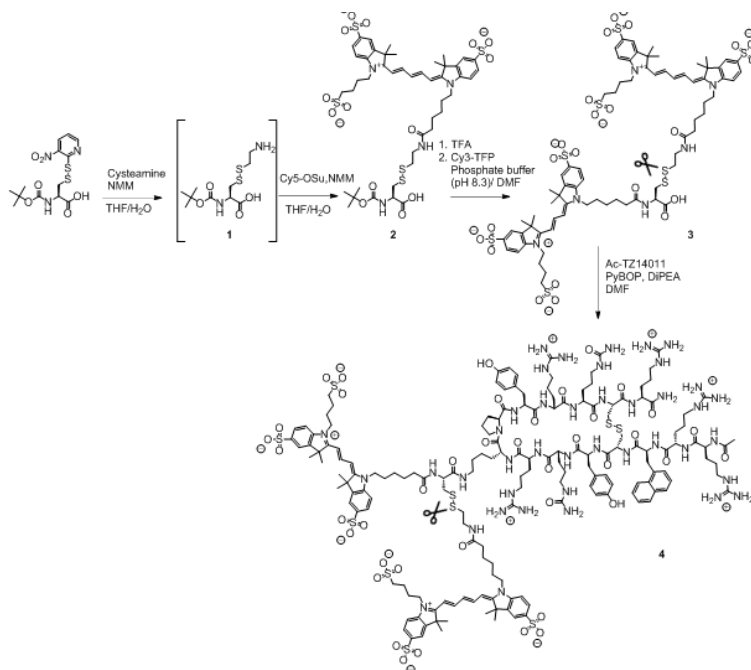


Figure 2: Synthesis of Cy-S-S-Cy3-Ac-TZ14011.

Synthesis was started with Boc-Cys(Npys)-OH which contains a disulfide bond. This is transformed to compound 1 with an asymmetrical disulfide bond as result and compound 1 is subsequently coupled to sulfonated Cy5, resulting in compound 2. By adding Cy3-TFP, Cy3 can be linked to generate compound 3, the Cy3-Cy5 FRET dimer. Ac-TZ14011 is coupled to compound 3 at the carboxylic acid group to generate compound 4, the CXCR4 endocytosis peptide (Cy5-S-S-Cy3-Ac-TZ14011). The scissors appoint the cleavage site.

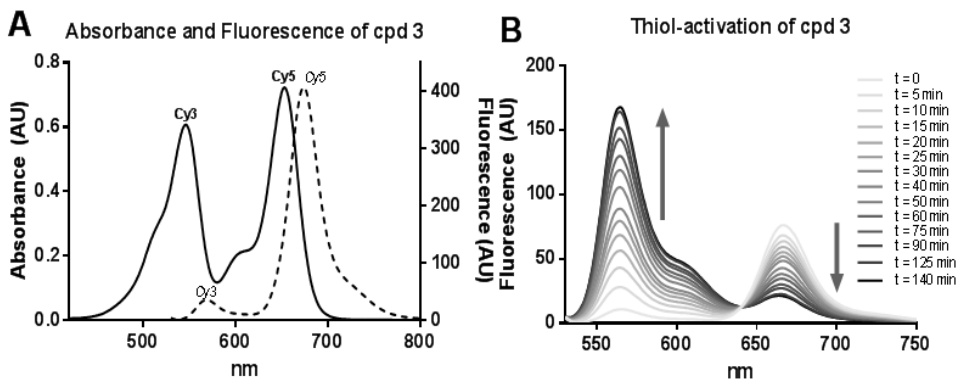


Figure 3: Photophysical properties of the Cy3-Cy5 FRET labelling. A) Absorbance and fluorescence spectra of compound 3 (3 μ M in PBS) in solid line, with the fluorescence spectrum upon excitation of Cy3 at 520 nm depicted in dotted line. B) Fluorescence spectra of the time-dependent disulfide reduction of 3 with DTT at various time points upon excitation at 520 nm. Increase in Cy3 fluorescence at 570 nm was found to be 20-fold, demonstrating *in vitro* functionality of compound 3.

Cy5 fluorescence (Figure 3A and S3A).

To test the cleavage of the FRET-pair and thereby the reactivation of the Cy3 signal, the strong disulfide reducing agent dithiothreitol (DTT) was used. Fluorescence spectrometric analysis during 140min (Figure 3B) revealed a gradual reduction in Cy5 fluorescence and increase in Cy3 fluorescence; after 140 min a 20-fold increase in Cy3-fluorescence was obtained. This suggests a \sim 95% FRET efficiency of compound 3 (Figure S5). Cy-S-S-Cy3-Ac-TZ14011 (4) was also examined by fluorescence spectroscopy prior to- and after DTT reduction. Herein a threefold increase in Cy3 fluorescence was observed between non-reduced and reduced state (data not shown).

***In vitro* validation of Cy-S-S-Cy3-Ac-TZ14011 by measuring CXCR4 endocytosis in EWS cell lines**

Further *in vitro* validation of Cy-S-S-Cy3-Ac-TZ14011 was performed using EWS cell lines TC32 and A673. Directly after Cy-S-S-Cy3-Ac-TZ14011 administration, a staining was observed which was consistent with previous observations; a strong cell membrane staining in TC32 and some membrane staining in A673 (**Figure S3A and S4A**). After 1 h, in both cell lines, a clustered staining which partly overlapped with the lysosome tracker DND-26 staining. Over time the Cy5 and FRET fluorescence signal decreased in both cell lines and only TC32 demonstrated an overall increase in Cy3 fluorescence signal (**Figure S3 and S4**). No clear membrane staining of the Cy3 signal like the Cy5 signal has been observed in both cell lines.

Quantitative analysis of the mean fluorescence intensity demonstrated similar trends; in both cell lines a decreasing trend in Cy5 and FRET signal was observed and in TC32 an increasing trend of Cy3 signal was observed which was significant after 72 h ($P < 0.03$) (**Figure 4**). In A673 no trend in Cy3 signal was observed.

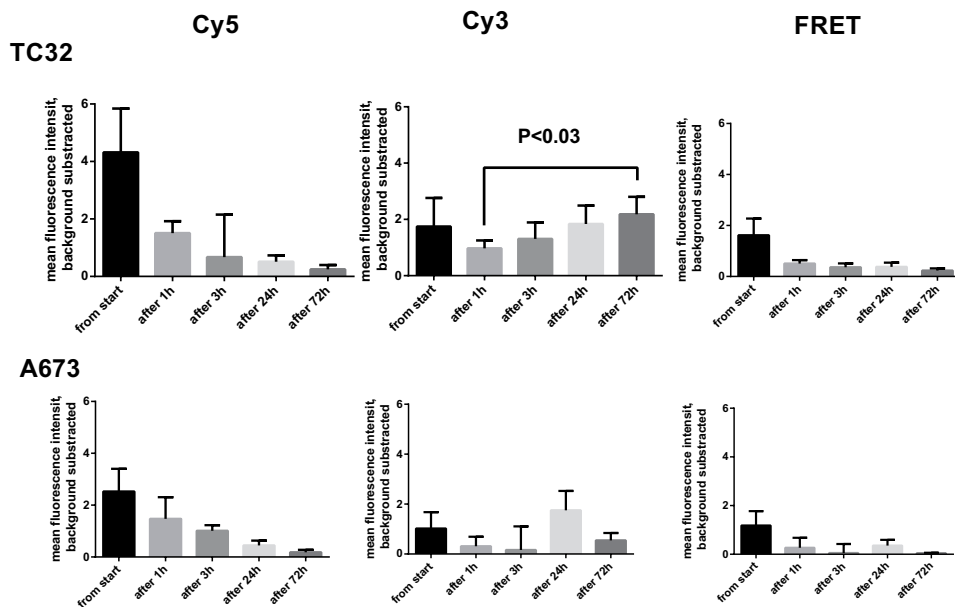


Figure 4: Mean fluorescence intensities over time in EWS cell lines TC32 and A673. After addition of Cy5-S-S-Cy3-Ac-TZ14011 confocal images of EWS cell line TC32, high *CXCR4* RNA expression, and EWS cell line A673, low *CXCR4* RNA expression, taken at five time points were analyzed with LASX software by calculating the mean fluorescence intensity. Mean with SEM of at least $n=3$ is demonstrated. A decreasing trend in Cy5 fluorescence and FRET fluorescence was observed in both cell lines. Only in TC32 an increase in Cy3 fluorescence was observed which was significant 72 h after Cy5-S-S-Cy3-Ac-TZ14011 addition compared to the Cy3 fluorescence 1 h after addition. This quantitatively validates the functionality of Cy5-S-S-Cy3-Ac-TZ14011 in a cellular environment.

DISCUSSION

Previously we demonstrated that the CXCR4 targeting peptide Ac-TZ14011-FITC was internalized over time [18]. These data, however, did not allow us to differentiate between CXCR4 that was originally residing on the surface during the labeling process and labeled-CXCR4 that might have recycled back to the surface [32,33]. This prompted us to study the live cell dynamics of CXCR4 internalization with an activatable CXCR4 endocytosis tracer (Cy5-S-S-Cy3-Ac-TZ14011) based on a disulfide-based Cy3-Cy5 FRET label linked to Ac-TZ14011. Upon cellular internalization the disulfide bond in the FRET-label was disrupted by reduction, leading to an increase in Cy3 fluorescence (**Figure 1**). Synthesis of Cy5-S-S-Cy3-Ac-TZ14011 was relatively straightforward, however solubility issues due to the charges on the dyes resulted in a low yield of the end product (**Figure 2**). The use of alternative (cyanine) dyes may improve the yield. Photophysical analyses of the unconjugated label (compound 3) demonstrated a ~95% FRET efficiency. This is consistent with expectations of FRET based on the close proximity of the two dyes ($\ll 6$ nm) compared with a R_0 distance of 6 nm reported for the Cy3-Cy5 FRET pair at which FRET efficiency is 50% [34]. The diminished increase in Cy3 signal observed when the complete tracer Cy5-S-S-Cy3-Ac-TZ14011 was reduced compared to the FRET label alone could stem from a higher initial Cy3 signal. This could be caused by minor reduction of the Cy5-S-S-Cy3-Ac-TZ14011 during coupling conditions which could not be fully removed by preparative HPLC or could be caused by leakage of the Cy3 fluorescence. The higher initial Cy3 signal was observed as well during live cell imaging at the start when a high Cy5 and FRET fluorescence of the Cy5-S-S-Cy3-Ac-TZ14011 were detected, suggesting leakage might partially be a cause (**Figure 4**). Moreover, similar FRETs earlier reported by us and others had comparable FRET efficiencies despite high purity [22,23]. During live cell evaluation of Cy5-S-S-Cy3-Ac-TZ14011, like during the synthesis, aggregates were observed but could partially be reduced by sonication of Cy5-S-S-Cy3-Ac-TZ14011 before addition to the cells. The internalization-dependent Cy3 fluorescence of Cy5-S-S-Cy3-Ac-TZ14011 shortly after internalization implies Cy5-S-S-Cy3-Ac-TZ14011 is functional and potentially suited to detect recycling of internalized CXCR4 to the cell membrane (**Figure 4, S3 and S4**). This is strengthened by the increasing trend of Cy3 signal observed in the high CXCR4 expressing EWS cell line TC32 which reached significance after 72 h compared to the Cy3 signal after 1 h. No trend in Cy3 signal was observed in the low CXCR4 expressing EWS cell line A673 [6]. This is consistent with earlier reported observation of CXCR4 expression in A673 [8]. The absence of clear membrane staining after internalization of CXCR4 and dominant overlap of Cy3 signal with the lysotracker signal suggest that in these EWS cell lines majority of the receptor is not recycled back to the membrane after internalization. However, that some receptors do relocate to the cell membrane after internalization cannot be excluded.

The principle of live cell imaging of receptor dynamics is especially for GPCRs an interesting method to study the dynamics per cell/tissue-type as without any further labeling needed and one is able to distinguish the internalized part of the studied receptor from the others. CXCR4 and other GPCRs were reported to be recycled back to the cell membrane after internalization [32,33,35]. By using Cy5-S-S-Cy3-Ac-TZ14011 it is possible to study this process. The observed absence of toxicity of Cy5-S-S-Cy3-Ac-TZ14011 might open new routes to study compound-receptor complex endocytosis. The gained insight in the CXCR4 endocytosis can be used for optimization of targeting CXCR4 in Ewing sarcoma by inhibitors which are based on Ac-TZ14011. In addition, the principle could be used to target both the CXCR4 receptor and to internalize chemotherapeutic agent carriers which can release their chemotherapeutics

in an reducing environment inside the cell which would increase their effect [36].

In conclusion, we present here a method to study live cell CXCR4 endocytosis by an activatable receptor targeting peptide Cy5-S-S-Cy3-Ac-TZ14011. Live cell evaluation in EWS cell lines confirmed the functionality of the peptide with a significant increase in Cy3 signal in a high CXCR4 expressing EWS cell line and not in a low expressing CXCR4 EWS cell line and provided insight in the cell biology of these cell lines which might lead to improved anti-CXCR4 therapy in EWS patients. The same concept may also proof to be of value for coming studies regarding (CXCR4) receptor dynamics.

ACKNOWLEDGEMENTS

This study was supported by National organization for Scientific Research (NWO) Grant NWO-TOP GO 854.10.012, by a Koningin Wilhelmina Fonds (KWF) translational research award (Grant No. PGF 2009-4344), a Netherlands Organization for Scientific Research VIDI grant (Grant No. STW BGT11272), and the 2015-2016 Post-Doctoral Molecular Imaging Scholar Program Grant granted by the Society of Nuclear Medicine and Molecular imaging (SNMMI) and the Education and Research Foundation for Nuclear Medicine and Molecular Imaging.

REFERENCES

- 1 Nagasawa, T. CXCL12/SDF-1 and CXCR4. *Front Immunol* **6**, 301, (2015).
- 2 Guo, F. *et al.* CXCL12/CXCR4: a symbiotic bridge linking cancer cells and their stromal neighbors in oncogenic communication networks. *Oncogene*, (2015).
- 3 Lippitz, B. E. Cytokine patterns in patients with cancer: a systematic review. *Lancet Oncol* **14**, e218-e28, (2013).
- 4 Sand, L. G. L., Szuhai, K. & Hogendoorn, P. C. W. Sequencing overview of Ewing sarcoma: a journey across genomic, epigenomic and transcriptomic landscapes. *Int J Mol Sci* **16**, 16176-215, (2015).
- 5 De Alava, E., Lessnick, S. L. & Sorensen, P. H. in *WHO Classification of Tumors of Soft Tissue and Bone* (eds C.D.M. Fletcher, J.A. Bridge, P. C. W. Hogendoorn, & F. Mertens) 306-9 (IARC, 2013).
- 6 Sand, L. G. L. *et al.* CXCL14, CXCR7 expression and CXCR4 splice variant ratio associate with survival and metastases in Ewing sarcoma patients *Eur J Cancer*, (2015).
- 7 Bennani-Baiti, I. M. *et al.* Intercohort Gene Expression Co-Analysis Reveals Chemokine Receptors as Prognostic Indicators in Ewing's sarcoma. *Clin Cancer Res* **16**, 3769-78, (2010).
- 8 Krook, M. A. *et al.* Stress-Induced CXCR4 Promotes Migration and Invasion of Ewing sarcoma. *Mol Cancer Res* **12**, 953-64, (2014).
- 9 Reddy, K. *et al.* Stromal cell-derived factor-1 stimulates vasculogenesis and enhances Ewing's sarcoma tumor growth in the absence of vascular endothelial growth factor. *Int J Cancer* **123**, 831-7, (2008).
- 10 Pelekanos, R. A. *et al.* Intracellular trafficking and endocytosis of CXCR4 in fetal mesenchymal stem/stromal cells. *BMC Cell Biol* **15**, 15-, (2014).
- 11 Marchese, A. Endocytic trafficking of chemokine receptors. *Curr Opin Cell Biol* **27**, 72-7, (2014).
- 12 Cepeda, E. B. *et al.* Mechanisms regulating cell membrane localization of the chemokine receptor CXCR4 in human hepatocarcinoma cells. *BBA-Mol Cell Res* **1853**, 1205-18, (2015).
- 13 Busillo, J. M. & Benovic, J. L. Regulation of CXCR4 Signaling. *Biochim Biophys Acta* **1768**, 952-63, (2007).
- 14 van Buul, J. D. *et al.* Leukocyte-Endothelium Interaction Promotes SDF-1-dependent Polarization of CXCR4. *J Biol Chem* **278**, 30302-10, (2003).
- 15 Orsini, M. J., Parent, J.-L., Mundell, S. J. & Benovic, J. L. Trafficking of the HIV coreceptor CXCR4: role of arrestins and identification of residues in the c-terminal tail that mediate receptor internalization. *J Biol Chem* **274**, 31076-86, (1999).
- 16 Kuil, J., Buckle, T. & van Leeuwen, F. W. B. Imaging agents for the chemokine receptor 4 (CXCR4). *Chem Soc Rev* **41**, 5239-61, (2012).
- 17 Kuil, J., Velders, A. H. & van Leeuwen, F. W. B. Multimodal tumor-targeting peptides functionalized with Both a Radio- and a Fluorescent Label. *Bioconjug Chem* **21**, 1709-19, (2010).
- 18 van den Berg, N. S., Buckle, T., Kuil, J., Wesseling, J. & van Leeuwen, F. W. B. Immunohistochemical

- Detection of the CXCR4 Expression in Tumor Tissue Using the Fluorescent Peptide Antagonist Ac-TZ14011-FITC. *Transl Oncol* **4**, 234-40, (2011).
- 19 Buckle, T. *et al.* Use of a Single Hybrid imaging agent for integration of target validation with *in vivo* and
ex vivo imaging of mouse tumor lesions resembling human DCIS. *PLoS One* **8**, e48324, (2013).
- 20 Ni, Q., Titov, D. V. & Zhang, J. Analyzing protein kinase dynamics in living cells with FRET reporters.
Methods **40**, 279-86, (2006).
- 21 Urano, Y. Novel live imaging techniques of cellular functions and *in vivo* tumors based on precise design
of small molecule-based 'Activatable' fluorescence probes. *Curr Opin Chem Biol* **16**, 602-8, (2012).
- 22 Rood, M. T. M. *et al.* An activatable, polarity dependent, dual-luminescent imaging agent with a long
luminescence lifetime. *Chemical Communications* **50**, 9733-6, (2014).
- 23 Yang, J., Chen, H., Vlahov, I. R., Cheng, J.-X. & Low, P. S. Evaluation of disulfide reduction during recep-
tor-mediated endocytosis by using FRET imaging. *Proceedings of the National Academy of Sciences* **103**,
13872-7, (2006).
- 24 Roy, R., Hohng, S. & Ha, T. A practical guide to single-molecule FRET. *Nat Meth* **5**, 507-16, (2008).
- 25 Iqbal, A. *et al.* Orientation dependence in fluorescent energy transfer between Cy3 and Cy5 terminally
attached to double-stranded nucleic acids. *Proceedings of the National Academy of Sciences* **105**, 11176-81,
(2008).
- 26 KleinJan, G. *et al.* Fluorescent Lectins for Local *in Vivo* Visualization of Peripheral Nerves. *Molecules* **19**,
9876, (2014).
- 27 Spa, S. J. *et al.* Orthogonal Functionalization of Ferritin via Supramolecular Re-Assembly. *Eur J Inorg*
Chem, n/a-n/a, (2015).
- 28 Patterson, S. D. & Katta, V. Prompt Fragmentation of Disulfide-Linked Peptides during Matrix-Assisted
Laser Desorption Ionization Mass Spectrometry. *Anal Chem* **66**, 3727-32, (1994).
- 29 Hanaoka, H. *et al.* Development of a ¹¹¹In-labeled peptide derivative targeting a chemokine receptor,
CXCR4, for imaging tumors. *Nucl Med Biol* **33**, 489-94, (2006).
- 30 Mujumdar, R. B., Ernst, L. A., Mujumdar, S. R., Lewis, C. J. & Waggoner, A. S. Cyanine dye labeling re-
agents: Sulfoindocyanine succinimidyl esters. *Bioconjug Chem* **4**, 105-11, (1993).
- 31 Ottaviano, L. *et al.* Molecular characterization of commonly used cell lines for bone tumor research: A
trans-European EuroBoNet effort. *Genes Chromosomes Cancer* **49**, 40-51, (2010).
- 32 Förster, R. *et al.* Intracellular and Surface Expression of the HIV-1 Coreceptor CXCR4/Fusin on Various
Leukocyte Subsets: Rapid Internalization and Recycling Upon Activation. *The Journal of Immunology*
160, 1522-31, (1998).
- 33 Patrussi, L. *et al.* Enhanced Chemokine Receptor Recycling and Impaired S1P1 Expression Promote Leu-
kemic Cell Infiltration of Lymph Nodes in Chronic Lymphocytic Leukemia. *Cancer Res* **75**, 4153-63,
(2015).
- 34 Ha, T. *et al.* Initiation and re-initiation of DNA unwinding by the Escherichia coli Rep helicase. *Nature*
419, 638-41, (2002).
- 35 David, R. Endocytosis: Sorting the recycling. *Nat Rev Mol Cell Biol* **12**, 3-, (2011).
- 36 Mei, L. *et al.* Enhanced antitumor and anti-metastasis efficiency via combined treatment with CXCR4
antagonist and liposomal doxorubicin. *J Control Release* **196**, 324-31, (2014).

SUPPLEMENTARY FIGURES

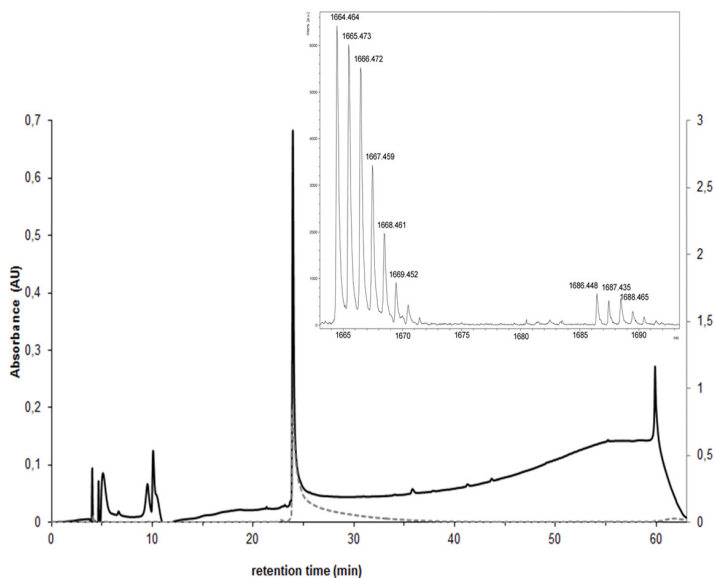


Figure S1: HPLC trace with inset MALDI-TOF of compound 3 injected in PBS with 220 nm absorbance in black and 650 nm absorbance in grey. A mass of 1664.46 Da was measured for compound 3 which is corresponding to the calculated mass of 1685.41 Da.

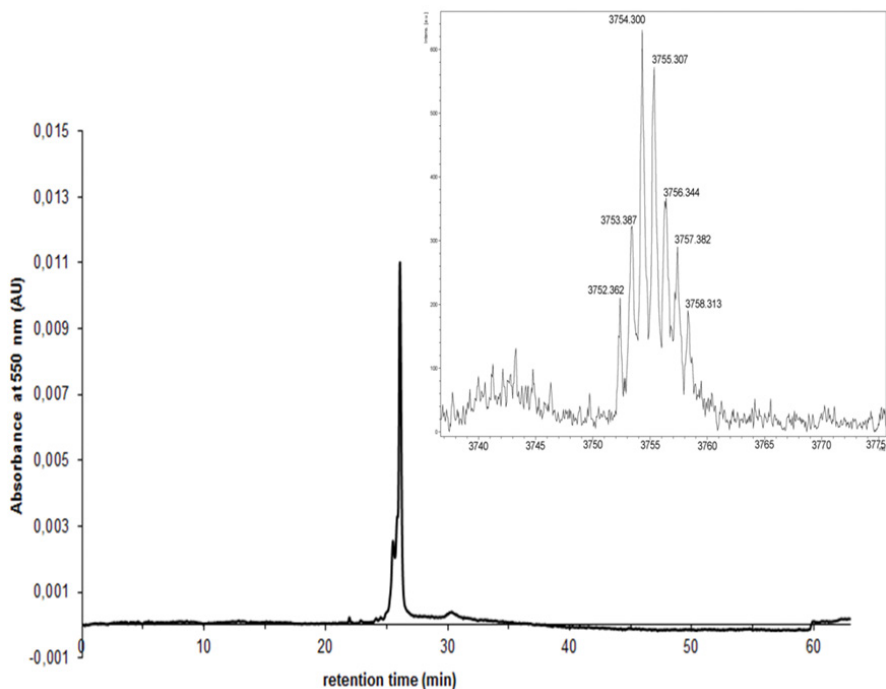


Figure S2: HPLC trace with inset MALDI-TOF of compound 4 (*Cy-S-S-Cy3-Ac-TZ14011*) injected in PBS. The measured mass of *Cy-S-S-Cy3-Ac-TZ14011* was 3752.36 Da which was corresponding to the calculated mass of 3751.49 Da

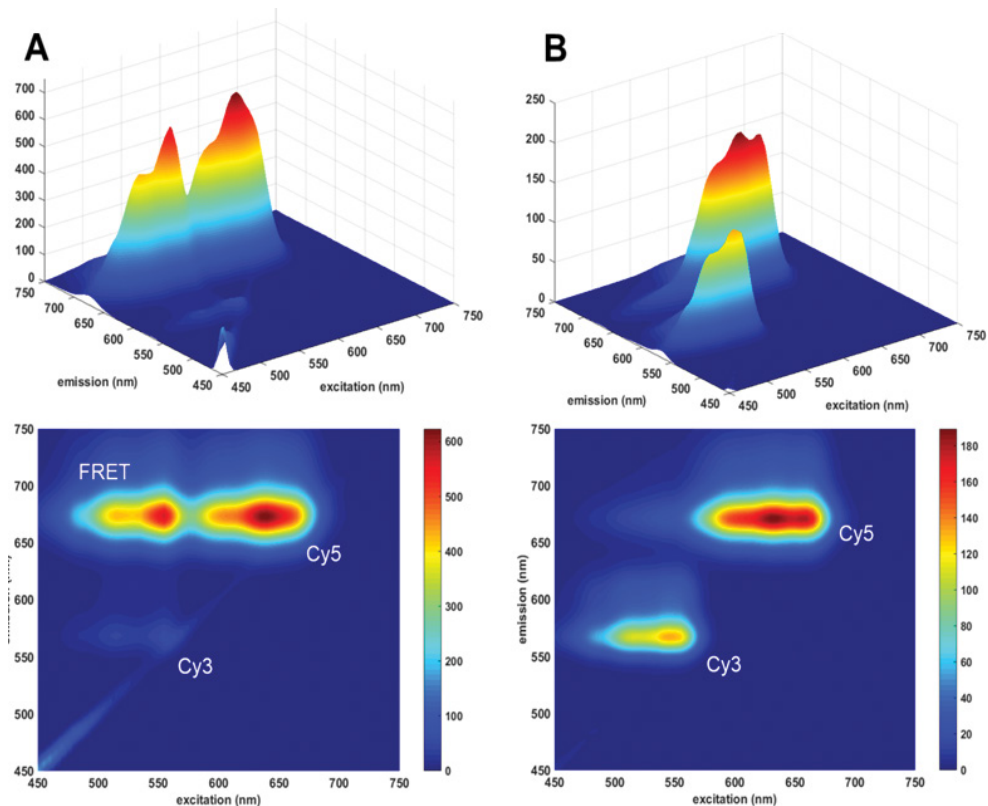
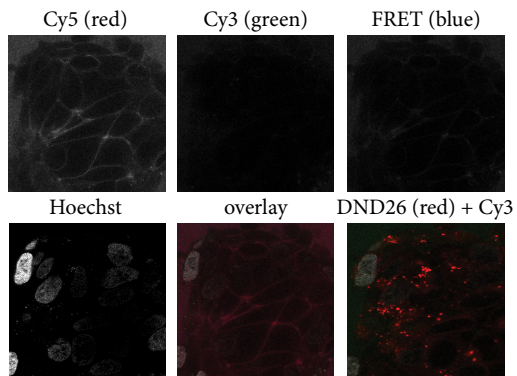


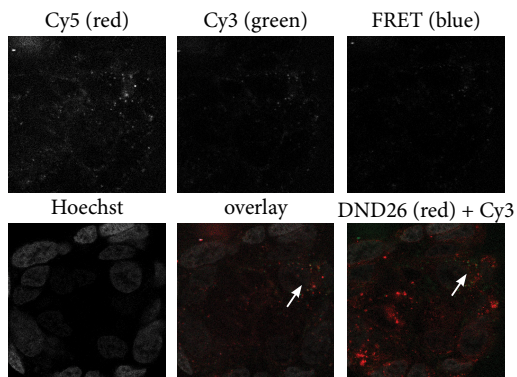
Figure S5: 2D and 3D representation of the excitation/emission spectrum of compound 3 ($3\mu\text{M}$ in PBS) prior to (A) and after DTT incubation (B) 140min. The photophysical properties of compound 3 (Cy5-S-S-Cy3) were determined by spectrofluorometry. **A)** Prior to reduction of the disulfide bond, compound 3 showed high FRET fluorescence (excitation between 500-570 nm and emission between 650-700 nm) and some Cy3 fluorescence (excitation between 500-570 nm and emission between 550-600 nm). **B)** After reduction of the disulfide bond by DTT the FRET fluorescence was almost completely reduced and the Cy3 fluorescence was highly increased. This demonstrates the in vitro functionality of compound 3 and its emission specificity. The gain of the spectrometer was reduced in the spectrum B to avoid oversaturation.

Figure S4 TC32

A: from start



B: after 1 h



C: after 3 h

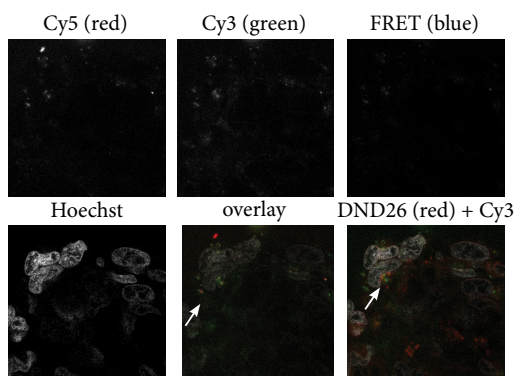
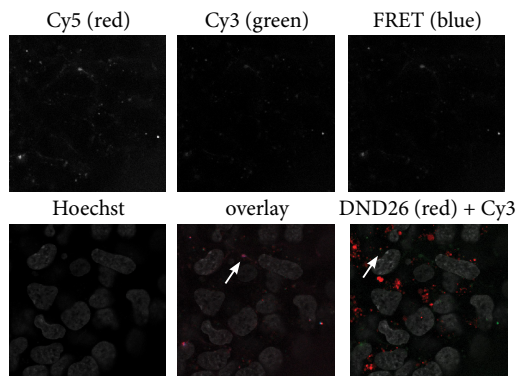
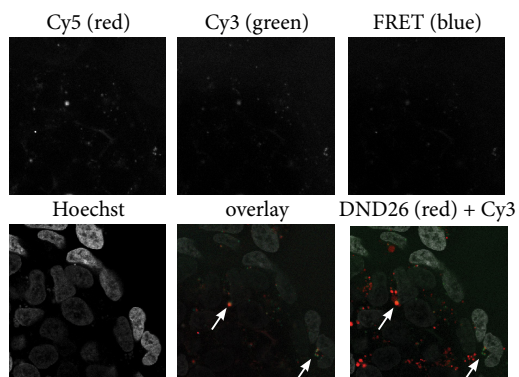


Figure S5 A673

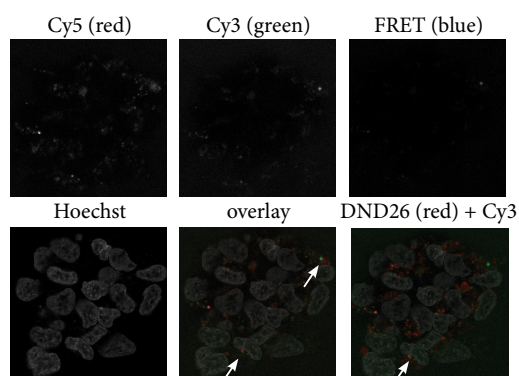
A: from start

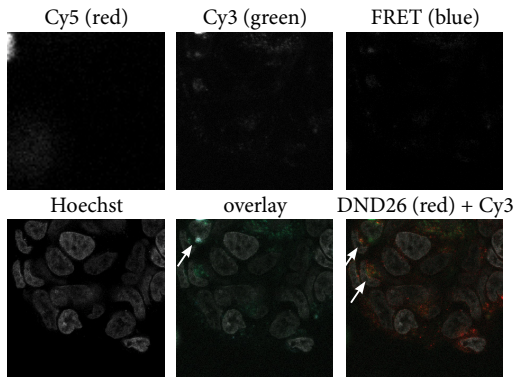
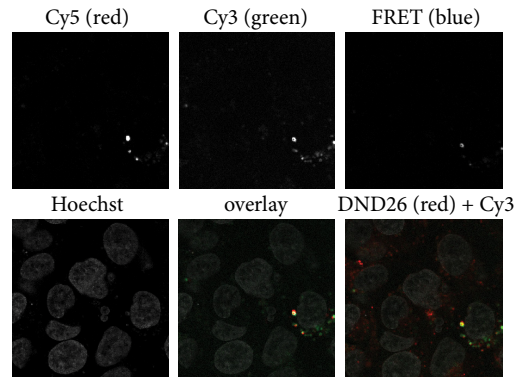
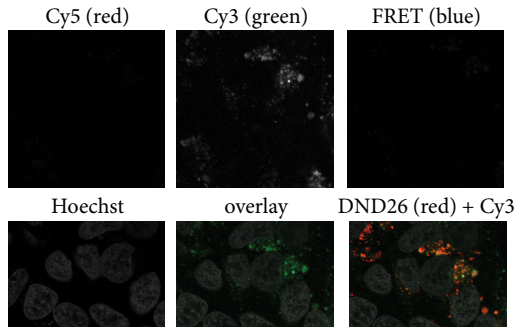
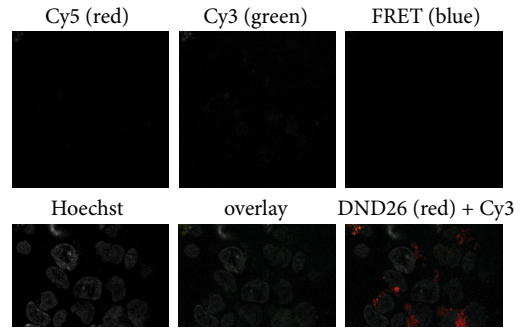


B: after 1 h



C: after 3 h



D: after 24 h

D: after 24 h

E: after 72 h

E: after 72 h


Supplementary description Figure S3 and S4: Representative images ($n > 3$) were collected during live cell imaging of high CXCR4 expressing EWS cell line TC32 (S4) and low CXCR4 expressing EWS cell line A673 (S5). Hoechst, lysotracker DND-26 and the Cy5, FRET, Cy3 signals emitted by Cy-S-S-Cy3-Ac-TZ14011 were excited, and emission was detected at the wavelengths described in **Table 1**. Color labels of the signals in the overlay are stated brackets. After addition of Cy-S-S-Cy3-Ac-TZ14011 a cell membrane staining pattern was shown in TC32 by the Cy5 and FRET signals (S4a). In A673 this was less pronounced (S5a). No Cy3 signal was observed in TC32 and only at a few sites in A673 (arrow). After 1 h, especially in TC32, the Cy5 signal was more clustered (S4b and S5b). Internalized peptide is observed in both cell lines, indicated by the overlap with the DND26 signal (arrow at DND26 + Cy3). This overlap is present throughout the rest of the imaging process and was most present after 72 h in TC32. Overlap of all three the peptide emitted signals is demonstrated at some sites (arrows in overlays). This overlap suggests a combination of reduced and non-reduced of Cy-S-S-Cy3-Ac-TZ14011 at the same position. Overall decrease of Cy5 and the FRET signals over time was observed in both TC32 and A673 and was almost absent at 72 h. Increase of Cy3 signal over time could only be observed in TC32. This implies that Cy-S-S-Cy3-Ac-TZ14011 is functional in an cellular environment and that the CXCR4 bound by Cy-S-S-Cy3-Ac-TZ14011 is directed to the lysosomes in TC32 upon internalization over a time course of at least 72 h.

Chapter 8

Summary and future perspectives

Nederlandse samenvatting

Curriculum Vitae

List of publications

SUMMARY AND FUTURE PROSPECTIVE

Ewing sarcoma (EWS) is an aggressive primary malignant bone tumor with high degree of tumor vascularization, to the extent that it was originally supposed to be of vascular origin [1]. High vascularization is often a result of an intensive interaction between the tumor and its microenvironment. For the understanding of its interactions within the microenvironment detailed characterization of EWS at the molecular level is needed. This thesis focusses on chemokine signaling. In addition, characterization of EWS at the genome, epigenome and transcriptome levels may potentially help to identify new druggable targets and prognostic markers. In **Chapter 2** results of so far published large sequencing studies were combined to provide a comprehensive overview that can facilitate the use of large datasets generated from EWS. At genome level, besides the characteristic *EWSR1-ETS* translocation, no frequently recurring structural rearrangements were identified to be present in EWS. The number of gene mutations detected in EWS was very low and only two gene mutations, *TP53* and *STAG2*, were frequently observed in multiple studies with frequencies of 5.2-7% and 9-21.5%, respectively [2-4]. The distribution of these mutations across the gene sequence showed an interesting pattern. The most frequent *TP53* mutation in EWS -c.527G>T (p. C176F)- was not listed as hot spot mutation in the *TP53* mutation database of the IARC, which collects mutations from many types of cancer [5]. It may be speculated that these *TP53* mutations are appearing due to or are related to the EWS-ETS fusion protein [6]. One clear hot spot mutation c.646C>T (p.R216X) was identified in *STAG2*, which was present in 25% of the analyzed cases. These mutations together with structural alterations including 1q gain, are clinically relevant as they can be used as prognostic markers for survival [2,7-9]. In addition, *CDKN2A/CDKN2B* locus deletion, observed in 12% of the analyzed cases was not associated with survival which is conflicting with the results of earlier studies [2,3,7]. The overall low number of mutations in EWS suggests that the cell death pathways, in contrast to most other tumors, are not genetically but rather functionally defective. Intracellular or extracellular reactivation of these pathways by the DNA damage recognition system or immune cells, respectively, might be feasible, creating additional opportunities for chemo- and immunotherapy (**Chapter 2**) [10].

The impact of the EWSR1-ETS fusion protein on cellular processes was observed both at epigenome and transcriptome level. EWS specific epigenetic patterns were observed at distant enhancer and super-enhancers sites [11]. In addition, EWSR1-ETS binds at specific GGAA satellites and requires interactions with various epigenetic modifiers to be able to bind and act as oncogenic driver [12]. These epigenetic modifiers would be therefore be ideal therapeutic targets for EWSR1-ETS specific treatment [13]. The blocking of the interaction sites of EWSR1-ETS or of the epigenetic modifiers which are involved epigenetic regulation are both plausible therapies that have been investigated; YK-4-279 as blocking agent for EWSR1-ETS, and HCl2509 as reversible blocking agent for lysine-specific histone demethylase 1 (LSD1) [13,14].

At transcriptome level -besides a specific Ewing sarcoma gene expression pattern- a specific non-coding RNA expression pattern and alternative splicing events were identified, all influenced by the EWSR1-ETS fusion protein. The fusion protein up- and downregulates several cellular processes. For the studies presented in this thesis, downregulation of extracellular signaling, including chemokines and chemokine receptors signaling was highly relevant and investigated in more detail.

The downregulation of specific chemokines and their receptors might be used as a treatment option for EWS. In **Chapter 3** the lack of chemokine CCL21 and CCR7 expression in

EWS cells makes this tumor a prime candidate for CCL21 activation-based immunotherapy. The CCL21-CCR7 axis is often activated by the immune system that improves the anti-tumor immune response. However, it has been reported that when tumor cells express CCL21 and/or its receptor CCR7, a pro-tumorigenic response can occur upon CCL21 immunotherapy with an adverse effect. *CCL21*, in addition, might be used as a prognostic marker in EWS since increased RNA expression of *CCL21* was associated with decreased event free survival and overall survival in therapy-naïve primary EWS samples and inversely correlated with CD4⁺/CD8⁺ T-cell ratio (**Chapter 3**).

Although most chemokines and chemokine receptors are downregulated in EWS, upregulation of CXCR4 has been described in EWS [15]. CXCR4 is involved in all the major processes of the tumor microenvironment: angiogenesis, tumor growth, metastasis and immune surveillance [16]. In EWS its expression has been examined at RNA and protein level with conflicting results [17,18]. At the RNA level high CXCR4 expression was associated with metastasis, but at the protein level no expression in metastasis was observed. By studying the *CXCR4-CXCR7* axis in two patient cohorts we investigated the role of CXCR4 in EWS in broader perspective and demonstrated a role for the chemokine factors that inhibit CXCR4 activation, namely chemokine receptor CXCR7 and chemokine CXCL14 (**Chapter 4**). Increased expression of these factors showed a negative correlation/association with the development of metastases and with improved overall survival in one cohort (**Chapter 4**). These data confirmed the importance of CXCR4 activity in EWS and in its microenvironment.

CXCR4 expression and activity are regulated at various levels, including alternative splicing, post-translational modifications, dimerization and cellular localization. Previously, two *CXCR4* splice variants had been reported (*CXCR4-1* and *CXCR4-2*) but their role in the tumor microenvironment was undetermined. The balance between splice variants is known to be important in protein function [19,20]. In **Chapter 4** we demonstrated that the *CXCR4-1/CXCR4-2* ratio is increased in tumor samples compared to cell lines and this increased ratio was associated with an improved patient survival. CXCR4 can form dimers or even oligomers. We propose that a heterodimer formed by CXCR4-2 and CXCR4-1 isoforms might influence activation of CXCR4-2 [21]. Besides these two known splice variants, we have identified two novel splice variants (annotated as *CXCR4-3*, *CXCR4-4*) in EWS cell lines by using whole transcriptome sequencing (**Chapter 5**). Interestingly, all identified CXCR4 splice variants showed variations only at the N-terminal end of CXCR4 implying an important role for this N-terminal region in signaling. For the *CXCR4-2* variant, this role has been confirmed by modeling experiments [22]. The expression of these, novel splice variants were detected in both other tumor and normal tissue samples, indicating that their expression is not EWS specific but they are regular splice variants. Further validation at protein and functional level revealed that ectopic expression resulted in a dominantly unstable intracellular protein. However, the *CXCR4-3* isoform in the T7 transformed human embryonic kidney cell line HEK293T demonstrated some cell membrane localization and activity upon CXCL12a stimulation.

CXCR4 receptor activation by CXCL12 ligand binding is dependent on the subcellular localization of the receptor and its highly regulated cellular trafficking. Only cell membrane located CXCR4 receptor is accessible for ligand binding and the cell membrane expression levels have been associated with a degree of metastasis [23]. As in EWS conflicting CXCR4 protein and RNA expression levels are reported, a peptide-based staining method was applied and compared with antibody-based staining method (**Chapter 6**). The peptide-based method could qualitatively and quantitatively detect the CXCR4 cell membrane expression and was linearly correlated to the *CXCR4* RNA expression levels where the antibody-based method de-

tected the same cell membrane expression levels in EWS cell lines with varying RNA expression levels. In addition, the CXCR4 receptor internalized upon binding of the used peptide Ac-TZ14011-Cy5. Upon CXCL12 binding the intracellular domains of the transmembrane receptor are modified by ubiquitination and phosphorylation leading to CXCR4 internalization [24]. Receptor internalization and intracellular trafficking is a complex process achieved via multiple pathways and has been shown to be a cell/tissue specific process [25,26]. Since binding of the previous used peptide Ac-TZ14011-Cy5 to CXCR4 resulted in internalization of the receptor-peptide complex, this peptide was used as chemical backbone for the synthesis of an activatable CXCR4 endocytosis tracer to study intracellular trafficking. The tracer contained, besides the Ac-TZ14011 peptide, a double fluorescence labeling that is appropriate for Förster resonance energy transfer (FRET) analysis. The disulfide bond between the two fluorophores enabled to measure the endocytosis process as a function of the reducing environment (**Chapter 7**). *In vivo* validation of the tracer revealed that the peptide internalized with the receptor and could be used to measure the internalized CXCR4 qualitatively and quantitatively. The development of such novel tracers will allow to further study the role and regulation of CXCR4 in different tumor types.

In conclusion, this thesis illustrates the importance of chemokines in EWS tumor cells and its tumor microenvironment. *CCL21*, *CXCL14*, *CXCR7* and the ratio between *CXCR4-1* and *CXCR4-2* have been identified as candidate prognostic markers, *CCL21* immunotherapy as potential therapy and CXCR4 as potential therapeutic target in EWS. In addition, the presented peptide-based life cell imaging methods improve the ability to study CXCR4 cell membrane expression and dynamics qualitatively and quantitatively. This approach might be helpful for the measurement of anti-CXCR4 therapy efficacy. This work identified specific chemokine signaling pathways that can be used to target Ewing sarcoma and its tumor microenvironment.

The present EWS treatment regimen with surgery and intense chemotherapy has led to a survival of around 70% when EWS is localized but worse for patients with a metastatic disease at diagnosis or relapse. In addition, the regimen results in severe long-term effects on the health of these patients [27]. To stratify patients in the clinic only classic prognostic markers are used. The inclusion of targeted - and immunotherapy in the EWS treatment regime, such as YK-4-279 and *CCL21* dendritic cell therapy, and inclusion of genetics and tumor-microenvironment related markers, such as TP53 and *CXCL14* could lead to an increase in overall survival. Especially the combined analysis of these different kinds of markers could further help to improve patient stratification and survival prediction. To measure the expression and spatial-temporal activity of these markers new methods are needed. Examples of these methods are described in this thesis. Further development for successful application of these techniques will require a multi-disciplinary approach involving multiple fields of expertise such as radiology, (molecular) pathology and molecular biology.

EWS is a EWSR1-ETS driven tumor with low number of additional mutations and in which almost all pro-inflammatory chemokines are downregulated. Due to these characteristics, activation-immunotherapy may have great potential as additional treatment for EWS and could have a long lasting effect. Earlier lymphocyte recovery, high number of infiltrating CD8+ T-cells and high expression of *CCL21* are all associated with favorable overall survival in EWS patients (Chapter 3)[28,29]. The ideal target would be the EWSR1-ETS protein. However, its native peptides are poor immunogenic, MHC class I cell membrane expression is lacking in advanced-stage EWS and reactive cytotoxic T-cells which are present in EWS

tumors are exhausted [30-32]. For the optimal response a active immune microenvironment in combination with a high MHC class I expression and immunogenic EWSR1-ETS peptides to prime the T-cells would be required.

The tumor microenvironment is of key importance for understanding the behavior of the tumor, predicting its reaction on therapeutics and for predicting patients' survival. This thesis has shown that not only the targeted receptor but the complete interaction network should be considered. Although, next generation sequencing and proteomics have identified several new DNA, RNA and protein variants, like the novel CXCR4 RNA splice variants presented in this thesis, tools to study their biological relevance in the complex tumor microenvironment are lacking. Ex vivo model systems that allow recapitulation of the tumor microenvironmental conditions in patients might improve our knowledge of the interaction network between the tumor and its microenvironment. Next generation sequencing and proteomics could be used to monitor changes in these ex vivo models if certain conditions were changed, for example altering pH, metabolic products or bringing in additional cell types or (novel) therapeutics. At last, these ex vivo systems could provide a platform to validate molecular markers which were obtained by retrospective research, like the novel markers presented in this thesis, at a cell biological level to understand their predictive value.

Research on the tumor microenvironment of EWS has been performed in a multicenter approach (NWO TOP GO 854.10.012) and presented in this thesis hopefully leading to a stronger scientific basis for development of immunotherapy based strategies for the high-risk and relapsed patient groups.

REFERENCES

- 1 Ewing, J. Diffuse endothelioma of bone *Proc New York Path Soc* **21**, 17-24, (1921).
- 2 Tirode, F. *et al.* Genomic Landscape of Ewing sarcoma Defines an Aggressive Subtype with Co-Association of STAG2 and TP53 Mutations. *Cancer Discov* **4**, 1342-53, (2014).
- 3 Brohl, A. S. *et al.* The Genomic Landscape of the Ewing sarcoma Family of Tumors Reveals Recurrent STAG2 Mutation. *PLoS Genet* **10**, e1004475, (2014).
- 4 Crompton, B. D. *et al.* The Genomic Landscape of Pediatric Ewing sarcoma. *Cancer Discov* **4**, 1326-41, (2014).
- 5 Olivier, M., Hollstein, M. & Hainaut, P. TP53 Mutations in Human Cancers: Origins, Consequences, and Clinical Use. *Cold Spring Harb Perspect Biol* **2**, a001008, (2010).
- 6 Ban, J. *et al.* Suppression of Deacetylase SIRT1 Mediates Tumor-Suppressive NOTCH Response and Offers a Novel Treatment Option in Metastatic Ewing sarcoma. *Cancer Res* **74**, 6578-88, (2014).
- 7 Huang, H.-Y. *et al.* Ewing sarcomas with p53 mutation or p16/p14ARF homozygous deletion: a highly lethal subset associated with poor chemoresponse. *J Clin Oncol* **23**, 548-58, (2005).
- 8 Hattinger, C. M. *et al.* Prognostic impact of chromosomal aberrations in Ewing tumours. *Br J Cancer* **86**, 1763-9, (2002).
- 9 Mackintosh, C. *et al.* 1q gain and CDT2 overexpression underlie an aggressive and highly proliferative form of Ewing sarcoma. *Oncogene* **31**, 1287-98, (2012).
- 10 de Hooge, A. S. K. *et al.* Expression of cellular FLICE inhibitory protein, caspase-8, and protease inhibitor-9 in Ewing sarcoma and implications for susceptibility to cytotoxic pathways. *Clin Cancer Res* **13**, 206-14, (2007).
- 11 Tomazou, E. M. *et al.* Epigenome Mapping Reveals Distinct Modes of Gene Regulation and Widespread Enhancer Reprogramming by the Oncogenic Fusion Protein EWS-FLI1. *Cell Rep* **10**, 1082-95, (2015).
- 12 Riggi, N. *et al.* EWS-FLI1 Utilizes Divergent Chromatin Remodeling Mechanisms to Directly Activate or Repress Enhancer Elements in Ewing sarcoma. *Cancer Cell* **26**, 668-81, (2014).
- 13 Sankar, S. *et al.* Reversible LSD1 inhibition interferes with global EWS/ETS transcriptional activity and impedes Ewing sarcoma tumor growth. *Clin Cancer Res* **20**, 4584-97, (2014).
- 14 Tosso, P. N. *et al.* Synthesis and Structure-Activity Relationship Studies of Small Molecule Disruptors of EWS-FLI1 Interactions in Ewing's sarcoma. *J Med Chem* **57**, 10290-303, (2014).
- 15 Marques Howarth, M. *et al.* Long noncoding RNA EWSAT1-mediated gene repression facilitates Ewing

- sarcoma oncogenesis. *J Clin Invest* **124**, 5275-90, (2014).
- 16 Guo, F. *et al.* CXCL12/CXCR4: a symbiotic bridge linking cancer cells and their stromal neighbors in oncogenic communication networks. *Oncogene*, (2015).
- 17 Bennani-Baiti, I. M. *et al.* Intercohort Gene Expression Co-Analysis Reveals Chemokine Receptors as Prognostic Indicators in Ewing's sarcoma. *Clin Cancer Res* **16**, 3769-78, (2010).
- 18 Berghuis, D. *et al.* The CXCR4-CXCL12 axis in Ewing sarcoma: promotion of tumor growth rather than metastatic disease. *Clin Sarc Res* **2**, 24, (2012).
- 19 Huang, G., Zhou, Z., Wang, H. & Kleinerman, E. S. CAPER- α alternative splicing regulates the expression of vascular endothelial growth factor165 in Ewing sarcoma cells. *Cancer* **118**, 2106-16, (2012).
- 20 Sanchez, G., Delattre, O., Auboeuf, D. & Dutertre, M. Coupled alteration of transcription and splicing by a single oncogene: Boosting the effect on cyclin D1 activity. *Cell Cycle* **7**, 2299-305, (2008).
- 21 Rapp, C., Snow, S., Laufer, T. & McClendon, C. L. The role of tyrosine sulfation in the dimerization of the CXCR4:SDF-1 complex. *Protein Sci* **22**, 1025-36, (2013).
- 22 Tamamis, P. & Floudas, C. A. Elucidating a Key Component of Cancer Metastasis: CXCL12 (SDF-1 α) Binding to CXCR4. *J Chem Inf Model* **54**, 1174-88, (2014).
- 23 Buckle, T. *et al.* Use of a Single Hybrid Imaging Agent for Integration of Target Validation with *In Vivo* Imaging of Mouse Tumor Lesions Resembling Human DCIS. *PLoS One* **8**, e48324, (2013).
- 24 Pelekanos, R. A. *et al.* Intracellular trafficking and endocytosis of CXCR4 in fetal mesenchymal stem/stromal cells. *BMC Cell Biol* **15**, 15-, (2014).
- 25 Verma, R. & Marchese, A. The Endosomal Sorting Complex Required for Transport Pathway Mediates Chemokine Receptor CXCR4 Promoted Lysosomal Degradation of the mTOR Antagonist DEPTOR. *J Biol Chem*, (2015).
- 26 Cepeda, E. B. *et al.* Mechanisms regulating cell membrane localization of the chemokine receptor CXCR4 in human hepatocarcinoma cells. *BBA-Mol Cell Res* **1853**, 1205-18, (2015).
- 27 Ginsberg, J. P. *et al.* Long-term Survivors of Childhood Ewing sarcoma: Report From the Childhood Cancer Survivor Study. *J Natl Cancer Inst* **102**, 1272-83, (2010).
- 28 De Angulo, G. *et al.* Early lymphocyte recovery as a prognostic indicator for high-risk Ewing sarcoma. *J Pediatr Hematol Oncol* **29**, 48-52, (2007).
- 29 Berghuis, D. *et al.* Pro-inflammatory chemokine-chemokine receptor interactions within the Ewing sarcoma microenvironment determine CD8+ T-lymphocyte infiltration and affect tumour progression. *J Pathol* **223**, 347-57, (2011).
- 30 Evans, C. H. *et al.* EWS-FLI-1-targeted cytotoxic T-cell killing of multiple tumor types belonging to the Ewing sarcoma family of tumors. *Clin Cancer Res* **18**, 5341-51, (2012).
- 31 Berghuis, D. *et al.* Reduced human leukocyte antigen expression in advanced-stage Ewing sarcoma: implications for immune recognition. *J Pathol* **218**, 222-31, (2009).
- 32 Pahl, J. W. *et al.* Antibody-dependent cell lysis by NK cells is preserved after sarcoma-induced inhibition of NK cell cytotoxicity. *Cancer Immunol Immunother* **62**, 1235-47, (2013).

NEDERLANDSE SAMENVATTING

Het Ewing-sarcoom is een agressieve primair maligne bottumor met een hoge graad van tumor vascularisatie. Zelfs in zo'n hoge mate dat het oorspronkelijk was verondersteld dat het een vasculaire oorsprong had. Voor dit soort uitgebreide vascularisatie is een intensieve interactie en samenspel tussen de tumor en zijn micro-omgeving nodig. Om die interacties binnen de tumormicro-omgeving te begrijpen is gedetailleerde karakterisering op moleculair niveau van het Ewing-sarcoom geboden. In dit proefschrift is binnen de tumormicro-omgeving gefocuseerd op de chemokine signalering. Een gedetailleerde karakterisering van het Ewing-sarcoom op genomisch, epigenomisch en transcriptomisch niveau kan daarnaast mogelijk helpen om nieuwe behandelbare doelwitten en voorspellende factor te identificeren. In **Hoofdstuk 2** zijn de resultaten van de tot nu toe gepubliceerde grote sequentie analyse studies samengevoegd tot een overkoepelend overzicht die het gebruik van deze grote, Ewing-sarcoom specifieke, datasets kan vergemakkelijken. Op genomisch niveau zijn in het Ewing-sarcoom, naast de karakteristieke *EWSR1-ETS* translocatie, geen andere meermaals terugkerende structurele herschikkingen geïdentificeerd. Het totaal aantal genmutaties gedetecteerd in het Ewing-sarcoom was erg laag en slechts twee genmutaties, *TP53* en *STAG2*, zijn meerdere keren waargenomen in verschillende studies met frequenties van respectievelijk 5.2-7% en 9-21,5%. De verdeling van deze mutaties over de twee genen resulteerde een interessant patroon in beide gevallen. De meest voorkomende *TP53* mutatie in Ewing-sarcoom -c.527G > T (p. C176F)- is niet vermeld als hotspotmutatie in de *TP53* mutatie databank van het internationaal agentschap voor onderzoek naar kanker, het IARC, waarin de *TP53* mutaties van vele soorten kanker zijn opgenomen. Deze resultaten zouden te maken kunnen hebben met het *EWSR1-ETS* fusie-eiwit en zijn effect op de functie van het *TP53* eiwit. In *STAG2*, was een duidelijke hotspotmutatie -c.646C > T (p.R216X)- geïdentificeerd en was goed voor 25% van de *STAG2* mutaties. De *STAG2* en *TP53* mutaties zijn beiden klinisch relevant en kunnen dienen als voorstellende factoren voor de prognose van de patiënt. Het algeheel lage aantal mutaties in het Ewing-sarcoom suggereert dat de celdood signaleringcascades, in tegenstelling tot in de meeste andere tumoren, niet genetisch defect zijn. Intracellulaire of extracellulaire activatie van deze signaleringcascades door respectievelijk het DNA beschadiging herkenningssysteem en immune cellen zou hierdoor mogelijk zijn. Dit biedt grote kansen voor effectiviteit van chemo- en immunotherapie (**Hoofdstuk 2**).

Het effect van het *EWSR1-ETS* fusie-eiwit op de cellulaire processen is zowel op epigenoom als transcriptoom gebied duidelijk zichtbaar. Het Ewing-sarcoom heeft zijn eigen epigenetische patronen bij sommige ver gelegen versterker en superversterker gebieden. Daarnaast bindt *EWSR1-ETS* op specifieke GGAA satelliet sequenties wat belangrijke factor is in het functioneren als oncogen⁸. Om te kunnen binden is het afhankelijk van interacties met verschillende epigenetische modifierende eiwitten en deze eiwitten en het interactiegebied zijn daarom ideale therapeutische doelen voor een specifieke *EWSR1-ETS* behandeling.

Op transcriptoom gebied -naast een Ewing-sarcoom specifiek gen expressie patroon- zijn er Ewing-sarcoom specifieke niet-coderende RNA expressie patronen en alternatieve splicing gebeurtenis geïdentificeerd. Dit alles komt grotendeels door het *EWSR1-ETS* fusie-eiwit. Het verhoogt en verlaagt de activiteit verscheidene cellulaire processen. Voor de studies gepresenteerd in dit proefschrift was de verlaging van de extracellulaire signalering -met name de chemokines en chemokinerceptoren signalering- relevant en in meer detail onderzocht.

De gereguleerde expressieverlaging van chemokines en hun receptoren kan ook juist in het voordeel zijn voor de behandeling van de EWS. Het in **Hoofdstuk 3** besproken ontbreken van

chemokine CCL21 en CCR7 expressie in Ewing-sarcoom cellen maakt deze tumor een uitstekende kandidaat voor actieve immunotherapie met CCL21. De CCL21-CCR7 signalering wordt namelijk vaak geactiveerd door het immuunsysteem en dat verbetert de anti-tumor immuunrespons. Echter, wanneer tumorcellen CCL21 en/of CCR7 tot expressie brengen kan er een pro-tumor respons optreden bij een CCL21 immunotherapie met een ongunstig effect van dien. *CCL21* RNA expressie kan tevens mogelijk gebruikt worden als een prognostische marker in het Ewing-sarcoom omdat verhoogde RNA expressie van *CCL21* in therapie-naïeve primaire tumormonsters retrospectief geassocieerd was aan een langere levensduur en omgekeerd gecorreleerd met verhouding tussen CD4⁺ en CD8⁺ T-cellen (**Hoofdstuk 3**).

In tegenstelling tot de meeste chemokines en chemokinereceptoren receptoren, is verhoging van expressie van CXCR4 in het Ewing-sarcoom beschreven. CXCR4 is betrokken bij alle belangrijke processen van de tumormicro-omgeving: angiogenese, tumorgroei, uitzaaiing op afstand en immuunsurveillance. Op het gebied van associatie van CXCR4 expressie met deze processen zijn er in het Ewing-sarcoom tegenstrijdige resultaten gevonden op RNA en eiwit niveau. Hoge RNA expressie was geassocieerd met uitzaaiingen, hoge eiwit was geassocieerd met groei en geen aanwezigheid van metastase was waargenomen. Door het bestuderen van de *CXCR4-CXCR7* -as op RNA niveau in twee patiënt cohorten hebben we de rol van CXCR4 in het Ewing-sarcoom in een breder perspectief onderzocht. In deze studie hebben we een rol aangetoond voor de chemokine receptor CXCR7 en chemokine CXCL14 die beiden een remmende werking hebben op CXCR4 activering (**Hoofdstuk 4**). Verhoogde genexpressie van deze factoren bleek een negatieve correlatie/associatie met de ontwikkeling van uitzaaiingen in beide cohorten en met verbeterde overleving in één cohort en bekrachtigt het belang van CXCR4 activiteit in de tumormicro-omgeving van het Ewing-sarcoom (**Hoofdstuk 4**).

CXCR4 wordt op vele niveaus gereguleerd, inclusief alternatieve splicing, post-translationele modificaties, dimerisatie en cellulaire lokalisatie. In het verleden zijn er twee *CXCR4* splice varianten gerapporteerd (*CXCR4-1* en *CXCR4-2*), maar hun rol in de tumormicro-omgeving was onbekend. Het is bekend dat het evenwicht tussen splice varianten van belang zijn voor functie van een eiwit. In **Hoofdstuk 4** is gedemonstreerd dat de *CXCR4-1/CXCR4-2* verhouding verhoogd was in weefselmonsters van de tumor ten opzichte van cellijnen en deze verhoogde ratio was geassocieerd met een betere overleving. Wanneer CXCR4 kan dimeriseren of zelfs oligomeriseren stellen wij voor dat er een CXCR4-2 en CXCR4-1 heterodimer gevormd kan worden deze de activering van CXCR4-2 kan beïnvloeden. Naast deze twee bekende splice varianten, we hebben met behulp van transcriptoom sequentieanalyse twee nieuwe splice varianten (geannoteerd als *CXCR4-3*, *CXCR4-4*) in Ewing-sarcoomcellijnen (**Hoofdstuk 5**) gevonden. Deze varianten kwamen ook tot expressie in andere tumor en normale weefselmonsters en hieruit blijkt dat hun expressie niet Ewing-sarcoom specifiek is. Validatie op eiwit en functioneel niveau openbaarde dat ectopische expressie in een overwegend onstabiel intracellulaire eiwit resulteerde. De CXCR4-3 isovorm in HEK293T-cel lijn bleek echter gedeeltelijk gelokaliseerd te zijn op het celmembraan en actief wanneer gestimuleerd werd met CXCL12a. Interessant is dat alle geïdentificeerde CXCR4 splice varianten alleen variëren in het N-terminale eind van CXCR4 en dit impliceert een belangrijke rol voor dit N-terminale gebied in de CXCR4 signaaltransductie. Voor de CXCR4-2 variant is deze rol al bevestigd door model-experimenten.

CXCR4 activatie door zijn ligand CXCL12 is afhankelijk van de subcellulaire lokalisatie van de receptor en zijn sterk gereguleerde cellulaire transportatie. Alleen celmembraan gelokaliseerd CXCR4 is toegankelijk voor ligand binding en de celmembraanexpressie niveaus zijn geassocieerd met de vorming van metastases. Sinds in het Ewing-sarcoom conflicterende

CXCR4 RNA en eiwit expressie is gerapporteerd is een op peptide-gebaseerde kleuring gebruikt en vergeleken met een antilichaam-gebaseerde kleuring (**Hoofdstuk 6**). De peptide-gebaseerde kleuring kon zowel kwalitatief als kwantitatief CXCR4 celmembraanexpressie detecteren en deze was in Ewing-sarcoomcellijnen lineair gecorreleerd met de CXCR4 RNA expressie niveaus. Bij de antilichaam-gebaseerde kleuring werd daarentegen geen verschil in celmembraanexpressie gedetecteerd in dezelfde Ewing-sarcoomcellijnen. Daarbij werd CXCR4 als gevolg van binding het gebruikte peptide Ac-TZ14011-Cy5 geïnternaliseerd. Na CXCL12 binding worden de intracellulaire domeinen van CXCR4 gemodificeerd door ubiquitinatie en fosforylering wat leidt tot internalisering van CXCR4. Receptor internalisering en intracellulair transport is een complex proces waarbij meerdere signaaltransductiepaden betrokken zijn en het is aangetoond cel/weefsel specifiek te zijn. Binding van het peptide Ac-TZ14011-Cy5 leidde tot internalisatie van het CXCR4-peptide complex en was daarom gebruikt als chemische basis voor de synthese van een CXCR4 endocytose tracer dat als techniek kan helpen bij de bestudering van CXCR4 intracellulair transportatie. De tracer bestond naast het Ac-TZ14011 peptide uit twee fluorophores verbonden door middel van een zwavelbrug en deze dimeer was geschikt voor Förster resonance energie transfer (FRET) (**Hoofdstuk 7**). Deze zwavelbrug maakte het mogelijk om de endocytose te meten op gebied van fluorescentie omdat deze zwavelbrug verbroken wordt in een reducerend milieu. Internalisatie van de tracer was *in vivo* geobserveerd in Ewing-sarcoomcellijnen. Dit kon zowel kwalitatief als kwantitatief bepaald worden. Deze methode zou kunnen helpen bij de verdere studies naar de rol en de regulering van CXCR4 in andere tumortypes.

Concluderend, illustreert dit proefschrift het belang van chemokines in het Ewing-sarcoom en haar tumormicro-omgeving. *CCL21 CXCL14, CXCR7* en de verhouding tussen *CXCR4-1* en *CXCR4-2* zijn retrospectief geïdentificeerd als prognostische markers, *CCL21* immunotherapie als potentiële therapie en *CXCR4* als potentieel therapeutisch doel in het Ewing-sarcoom. De twee gepresenteerde methodes, peptide-gebaseerde CXCR4 celmembraankleuring en CXCR4 endocytose tracer, kunnen helpen bij de experimentele validatie van de anti-CXCR4 therapie in het Ewing-sarcoom en andere tumoren. Dit proefschrift biedt een perspectief voor aanpakken van de tumormicro-omgeving van het Ewing-sarcoom en handvaten voor verbeterde stratificatie van Ewing-sarcoom patiënten wat misschien kan resulteren in betere prognose voor de patiënten op korte en lange termijn.

CURRICULUM VITAE

Laurens Gerard Leo Sand was born on February 13, 1988 in Breda, the Netherlands. After graduating at the secondary school Mencia de Mendoza in Breda with a broad subject cluster, he started his Bachelor program Life Science & Technology at Technical University of Delft in 2006. During his Bachelor program he did his internship at the Medical Pharmacology Department of the Leiden Amsterdam Center for Drug Research (LACDR) and received his Bachelor degree in 2009. Directly thereafter he started the Research master program Life Science & Technology in Leiden University and followed subjects at multiple institutes, including the Kluyver Center, LACDR and LUMC. His first research internship was at the Department of Medicinal Chemistry of the LACDR on G protein-couple receptor NIACR1 affinity studies. The second internship was in Basel at the Biologics department of the Novartis Institutes of BioMedical Research (NIBR) on antibody display in *Saccharomyces cerevisiae*. He accomplished his Master program with honor in 2011 and started in 2011 with his PhD at the Department of Pathology under supervision of Dr. Karoly Szuhai and Prof. Pancras C.W. Hogendoorn. Results obtained during this PhD are described in this thesis. Currently, he is pursuing a career in research & development at Janssen Infection Disease and Vaccines.

LIST OF PUBLICATIONS

Pahl JHW, Santos SJ, Kuijjer ML, Boerman GH, Sand LGL, Szuhai K, Cleton-Janssen AM, Egeler RM, Bovée JVMG, Schilham MW and Lankester AC. Expression of the immune regulation antigen CD70 in osteosarcoma. *Cancer Cell International* 2015, 15:31

Sand LGL, Scotlandi K, Berghuis D, Snaar-Jagalska BE, Picci P, Schmidt T, Szuhai K and Hogendoorn PCW. CXCL14, CXCR7 expression and CXCR4 splice variant ratio associate with survival and metastases in Ewing sarcoma patients. *Eur. J. Cancer* 2015, 51(17), 2624-2633

Sand LGL, Szuhai K and Hogendoorn PCW. Sequencing overview of Ewing sarcoma: a journey across genomic, epigenomic and transcriptomic landscapes. *Int. J. Mol. Sci.* 2015, 16(7), 16176-16215

Sand LGL, Berghuis D, Szuhai K and Hogendoorn PCW. Expression of CCL21 in Ewing sarcoma is associated with development of metastases and a candidate target for immunotherapy. *Cancer Immunol. Immunother.* 2016, 65(8), 995-1002

Sand LGL, Jochemsen AG, Beletkaia E, Schmidt T, Hogendoorn PCW and Szuhai K. Novel isoforms CXCR4-3 and CXCR4-4 identified by transcriptome sequencing in Ewing cell lines and functional validated. *Biochem. Biophys. Res. Commun.* 2015, 466(1), 89-94

Sand LGL, Buckle T, van Leeuwen FWB, Corver WE, Kruisselbrink AB, Hogendoorn PCW and Szuhai K. Fluorescently labeled CXCR4 targeting peptide as alternative to antibody staining in Ewing sarcoma. *Submitted*

Sand LGL, Van der Wal S, Hogendoorn PCW, Korne CM, Szuhai K, van Leeuwen FWB and Buckle T. Evaluation of CXCR4 specific endocytosis using an activatable peptide. *In preparation*

ABBREVIATIONS:

| | |
|-----------|--|
| EWS | Ewing sarcoma |
| PNET | peripheral primitive neuroectodermal tumor |
| RMS | Rhabdomyosarcoma |
| MSC | Mesenchymal stem cell |
| EWRS1-ETS | Fusion gene/protein consisting of Ewing sarcoma breakpoint region-1 and a member of the erythroblast transformation-specific family of transcription factors |
| miRNA | micro-RNA |
| lncRNA | Long non-coding RNA |
| NGS | Next generation sequencing |
| SNP | Single nucleotide polymorphism |
| SNV | Single Nucleotide Variant |
| LOH | Loss of heterozygosity |
| DSB | double-strand break |
| GPCR | G-protein coupled receptor |
| NK | Natural killer |
| OS | Overall survival |
| EFS | Event free survival |
| MHC | major histocompatibility complex |
| WGBS | whole-genome bisulfite sequencing |
| ChIP-seq | chromatin immunoprecipitation sequencing |
| MeDIP-seq | methylated DNA immunoprecipitation sequencing |
| ChIP-exo | chromatin immunoprecipitation-exonuclease |
| UTR | Untranslated region |
| RT-Q-PCR | real-time quantitative-reverse transcriptase PCR |
| FISH | Fluorescence in situ hybridization |
| FRET | Förster resonance energy transfer |
| FFPE | Formalin fixed paraffin embedded |
| IHC | Immunohistochemistry |
| CFU | Central flow cytometry fluorescence units |
| PBA | PBS 5% BSA |
| SPECT | Single-photon emission computed tomography |

